2012

FABRICATION OF SWNTs FOR WATER DESALINATION AND MULTILAYER STRUCTURE FOR DNA SEQUENCING

Jingyuan Yao
University of Kentucky, jingyuanyao@gmail.com

STUDENT AGREEMENT:

I represent that my thesis or dissertation and abstract are my original work. Proper attribution has been given to all outside sources. I understand that I am solely responsible for obtaining any needed copyright permissions. I have obtained needed written permission statement(s) from the owner(s) of each third-party copyrighted matter to be included in my work, allowing electronic distribution (if such use is not permitted by the fair use doctrine) which will be submitted to UKnowledge as Additional File.

I hereby grant to The University of Kentucky and its agents the irrevocable, non-exclusive, and royalty-free license to archive and make accessible my work in whole or in part in all forms of media, now or hereafter known. I agree that the document mentioned above may be made available immediately for worldwide access unless an embargo applies.

I retain all other ownership rights to the copyright of my work. I also retain the right to use in future works (such as articles or books) all or part of my work. I understand that I am free to register the copyright to my work.

REVIEW, APPROVAL AND ACCEPTANCE

The document mentioned above has been reviewed and accepted by the student's advisor, on behalf of the advisory committee, and by the Director of Graduate Studies (DGS), on behalf of the program; we verify that this is the final, approved version of the student's thesis including all changes required by the advisory committee. The undersigned agree to abide by the statements above.

Jingyuan Yao, Student

Dr. Bruce J. Hinds, Major Professor

Dr. Fuqian Yang, Director of Graduate Studies

FABRICATION OF SWNTs FOR WATER DESALINATION AND MULTILAYER STRUCTURE FOR DNA SEQUENCING

THESIS

A thesis submitted in partial fulfillment of the
requirements for the degree of Master of Science in Materials Engineering
in the College of Engineering
at the University of Kentucky

By

Jingyuan Yao

Lexington, Kentucky

Directors: Dr. Bruce J. Hinds, Professor of Materials Engineering Department

Lexington, Kentucky

2012

ABSTRACT OF THESIS

FABRICATION OF SWNTs FOR WATER DESALINATION AND MULTILAYER STRUCTURE FOR DNA SEQUENCING

0.7nm single wall carbon nanotubes have been synthesized within VPI-5 zeolite channels with sucrose as carbon precursor. VPI-5 molecular sieves are synthesized hydrothermally under conventional heating. X-ray powder diffraction, micro raman, scanning electron microscope (SEM), transmission electron microscope (TEM), Thermogravimetric analysis have been used to investigate the structure of zeolite and thermal decoposition process of carbon precursors. 0.4nm single wall carbon nanotubes have also been fabricated within $AlPO_4$-5 nanopores. A key challenge is to produce high yield single wall carbon nanotubes with uniform diameter. In order to improve the carbon nanotube yield, different organic precursors are employed. Although the problem is still the repetition and low yield of CNTs, it is still an improvement for 0.7nm SWNTs synthesis with the new template prolysis method.

The novel multilayer conductor/insulator/conductor structures have been fabricated. This structure might find potential application in DNA sequential reactions because each layer might be individually addressed with voltage. When bias is applied to the conductive layer, it can be chemically functionalized, which leads to membrane pore with multiple reaction sequences when the molecule traverses the membrane reactor. In this thesis, Carbon/polymer/carbon system and copper/polymer system will be introduced. O_2 RIE was used to expose the edge of carbon/polymer/carbon structure. However, the conductivity of carbon layer is not high enough for electroplating. Copper pores etched by $FeCl_3$ solution shows good conductivity, and can be electroplated with metal nanoparticles.

KEYWORDS: Single wall carbon nanotube, Zeolite, water desalination, Multilayer, DNA sequencing.

Jingyuan Yao

06/05/2012

FABRICATION OF SWNTs FOR WATER DESALINATION AND MULTILAYER STRUCTURE FOR DNA SEQUENCING

By

Jingyuan Yao

Dr. Bruce Hinds

Director of Thesis

Dr. Fuqian Yang

Director of Graduate Studies

July 18, 2012

Dedicated to my parents who always guide and support me in my whole life

ACKNOWLEDGEMENTS

I would like to thank my advisor Dr. Bruce J. Hinds, for continuous support of my graduate study, excellent guidance in my research work, and dissertation preparation. I am thankful to DARPA and NSF for funding this dissertation work.

I would like to express my appreciation to my advisory committee members, Dr. Fuqian Yang, and Dr. Jeffrey Todd Hastings, for showing interest in my research work and for their advice.

I also would like to thank Dr. Chuck May and Brian Wajdyk for training me. Help in electron microscopy work by Larry Rice and Dr. Jia Ye is also appreciated. Thanks for Dr. Eitel, Dr. Naresh Shah, Dr. John P. Selegue, Jin Luo, Mahendra K. Sreeramoju, Borgohain, Rituraj and Abhijit Bhagavatula helping me with TGA experiment. Thanks for Dr. Eric Munson, xiaoda yuan, Rodica McCoy and Chandrashekhar help me with micro raman measurement.

I express my thanks to my lab mate, Dr. Bing Hu, for training me all the equipments and his valuable discussion. I also would like to thank for my lab mates' kind help from Dr. Ji Wu, Dr. Xinhua Sun, Dr. Xin Su, Xin Zhan, Karen Gerstandt, and Zhiqiang Chen.

TABLE OF CONTENTS

LIST OF TABLES

LIST OF FIGURES

Chapter 1 Introduction

The high cost of DNA sequencing and the shortage of fresh water are two very diverse world problems that can be solved with breakthroughs in membrane technology. The human genome project is very important because it could help the treatment of human disease by designing drugs that are tailored to the individual and predicting risk factors. US National Human Genome Research Institute (NHGRI) are trying to reduce the cost of genome sequencing to ~$1,000 by 2014 [1]. Nowadays, the price for DNA sequencing is $48,000 [2], which is much lower than $300 million of Human Genome Project completed nine years ago. The ideal DNA decoder would have a specific voltage pulsed corresponding to each sequence as a DNA strand passed through a pore with nm-scale electrodes.

Fresh Water is very important to human, agriculture and industry. Water is an abundant natural resource, which covers more than 70% of the earth's surface. However, only about 3% is fresh water, with the majority of that in polar regions and inaccessible lakes.[3] Therefore, it is necessary to find a way to improve the effectiveness and efficiency of water purification. Reverse osmosis is the primary method to desalinate water however has very large capital and energy costs. Large capital costs are due to the large surface area required for water to 'diffuse' through the 50nm thick membrane skin layer and the energy consumed for sustaining large area cross-flow to reduce concentration polarization. Ideal would be to have a membrane with pores that are small enough to exclude ions but allow the fast flow, approaching that of aquaporin protein channels, of water.

The controlled passage of ions through nanopore membrane has attracted great interest in biochemistry, biophysics, and chemistry fields. It has gained popularity because these membranes with uniform pore diameter and good mechanical property may find potential applications in water desalination, molecules separation, DNA translocation and other fields.

1.1 Multilayer nanopore structure for DNA translocation

In recent years, scientists are using nanopore structure for individual molecule sensing, which can make DNA sequencing at high speed and low cost. It is possible for such molecule sensing if the diameter of the nanopore is similar as the molecule. When the nanopore is put into a solution and potential is applied, a detectable ionic current change can be observed due to ions passing through the nanopore.

Various methods have been employed for single molecule sensing. Natural protein pores, organic polymer pores or inorganic materials such as silicon nitride, silicon dioxide, graphene, and nanotube pores are fabricated.

1.1.1 Bio-nanopore

Biological nanopore sensor has a single transmembrane protein imbedded in a lipid bilayer (Fig.1.1). The most widely used protein is a-hemolysin (αHL). The mushroom shaped pore of αHL consists of a 14 stranded β-barrel with its narrowest part of 1.4nm in

diameter[4], [5]. When a molecule enters the nanopore, it causes temporary current blockades, and when the molecule exits, the current is restored. [5]

1.1.2 Nanopores in silicons

Because the lipid membrane is very fragile, solid-state nanopores have been fabricated to solve this problem. Two methods have been used to fabricate nanometer scale channels within inorganic materials. One is ion beam sculpting and the other is wet etching. Each of these methods is briefly introduced here.

1.1.2.1 Ion beam sculpting

Golovchenko's group [6-9] use two-step ion-beam sculpting process to fabricate solid-state nanopores as shown in Figure 1.2. The first step is to make a 50-100 nm bowl-shaped cavity at the backside of the Si_3N_4 membrane using focused ion beam (FIB). In the next step, the pore was opened with feedback controlled Ar^+ ion beam sculpting. Atomic layer deposition (ALD) of Al_2O_3 can also be used to decrease nanopore diameter [10]. Dekker's group[11, 12] reported using electron beam of transmission electron microscopy (TEM) to shrink the pore size. The advantage of this method is that in situ process can be observed from the microscope. Therefore, the process can be stopped as soon as the desired pore dimension is reached.

1.1.2.2 Etching

The feedback electrochemical etching is used to obtain nanopores (Fig.1.3) [13]. When the pore is etched through by KOH solution, the electronic current increases sharply. It

allows the etching process to be stopped promptly and prevent over-etching. The diameter of the pores could be further reduced by thermal oxidation. (Fig.1.3d) This method avoids of using ion beam, which reduces the cost of drilling a hole and make it more accessible.

1.1.3 Polymer nanopores by the track-etching method

Polymer nanopores can be obtained by track-etching technique, which has been widely used in polymer materials such as polycarbonate and polyimide. The polymer film is firstly bombarded with heavy ions beam, which create tracks on the polymer. Then it is chemically etched along the tracks by immersion into an etchant. Siwy's group [14-18] fabricates conically shaped nanopores in polymer films by track-etching method. To obtain the conical stucture, they use the asymmetrical etching process with etchant placed on one side of the membrane and stop solution on the other side (Fig.1.4). They also indicate that a conical nanopore shows nonlinear current-voltage curves as nanofluidic diode. Martin and co-workers [19-21] found that the shape of conical pores produced by the track-etching technique was related to the etch time, temperature and percentage of ethanol in the etching solution.

1.1.4 CNT membrane

The pore length of the track-etched membrane is not uniform due to different track tilt angle, and its pore surface is rough. [22] Carbon nanotube has uniform pore diameter and atomically smooth inner wall. Crooks et al. [22, 23] fabricate a nanopore membrane with a single multiwall carbon nanotube (i.d ~100nm) in it. The carbon nanotube is firstly

mounted on a TEM grid then embedded in epoxy matrix, microtome cut, and subsequently mounted onto a Si_3N_4 wafer. Liu et al. [24] fabricated a device with one single-walled carbon nanotube spanning cross two reservoirs, which generates a large ionic current increase by DNA translocating through the nanotube.

1.1.5 Graphene Nanopore

Graphene is an atomically thin sheet with sp^2 bonded carbon atoms that are packed in two dimensional (2D) honeycomb crystal lattice. [25] Because of its atomic thinness, stability and electronic conductivity, graphene has attracted great attention in DNA translocation.[26-30]. The atomic thick property makes graphene to be an ideally high resolution device. Golovchenko's group fabricated a detector by drilling a single nanopore in graphene membrane. [26] Recently, multilayered graphene- Al_2O_3 structure[30] has been fabricated by sequentially depositing layers of graphene and Al_2O_3, and the nanopores are obtained by electron beam sculpting process. However, they didn't address each layer with voltage and functionalize the graphene layer with charged groups for better selectivity.

1.1.6 Pore functionalization

Pore functionalization can modify pore properties and improve ion selectivity by grafting different chemical groups. Different surfaces modified with various chemicals are presented here.

SiN nanopore can be chemically modified by negatively charged silanol groups.[31] It shows that the negatively charged dye is excluded from the pores by electrostatic forces, and only the positive one can pass through.

Martin's group[32] deposits Au nanowires in polymer nanopores using electroless plating method. Firstly, Sn^{2+} adheres to the membrane which is coated with poly (viny1pyrrolidone) (PVP) on its surface. Secondly, the polymer is deposited with Ag. Finally, Ag is replaced with Au. The gold surface can be further modified with a variety of molecules by Au- thiol chemistry.

Siwy et al. [17, 18] reported the formation of nanofluidic diode by modifying nanopores with carboxyl groups and amino groups. Carboxyl groups can be transformed into amino groups by 1-ethyl-3-[3(dimethylamino) propyl] carbodiimide hydrochloride (EDC) coupling agent, and reverse process can be done by succinic anhydride.

Electrochemical reduction of aryl diazonium salts has been applied to modify carbon nanotube surfaces [33-36]. As shown in Figure 1.5, the molecule covalently bonds to the carbon surface. This technique has been employed to other carbon materials, such as pyrolitic graphite and glassy carbon electrodes [37]. This chemistry has not yet been applied to DNA translocation.

1.1.7 Molecule translocation through the nanopore

Gradient in electrochemical potential μ and convection lead to mass transfer in solution. [38].

$$J = -\frac{cD}{RT}\frac{\partial \mu}{\partial x} + cv \quad (1)$$

The difference of μ over a distance changes because of a concentration gradient c or the change of potential gradient φ from the electric field. The flux can be calculated by diffusion, electrophoretic and convection. Then we get the Nernst- Plank equations [38], [39]

$$J = -\frac{cD}{RT}\left[\frac{\partial}{\partial x}(RTlnc) + \frac{\partial}{\partial x}(zF\varphi)\right] + cv \quad (2)$$

$$J = -D\left[\frac{\partial c}{\partial x} + \frac{zFc}{RT}\frac{\partial \varphi}{\partial x}\right] + cv \quad (3)$$

Where *c* is the concentration of the ion, *φ* the electric potential at any point *x* in the membrane, F the Faraday constant, R the gas constant, T the absolute temperature, D the diffusion coefficient, *z* the charge of the ion, *v* the average velocity of the solvent and *cv* the transport of permeant because of the convective solvent flow.

In capillary electrophoresis, convection is considered as absent, the velocity of the flow is given by [40]

$$v = \frac{|z|eE}{f} \quad (4)$$

where *f* is the hydrodynamic drag,

From the Stokes formula

$$f = 6\pi\eta r \quad (5)$$

Then electrophoretic velocity [19]

$$v = \frac{|z|eE}{6\pi\eta r} \quad (6)$$

where r is the radius of the ion, e is the electronic charge and η is the viscosity of the solution.

Electrophoretic mobility μ is defined as

$$\mu = \frac{v}{E} = \frac{|z|e}{6\pi\eta r} \quad (7)$$

1.1.8 molecule sensing

When a molecule travels through a single nanopore, it gives rise to a detectable ionic current change (Fig.1.6). Branton's group [10] found that the current blockage is equal to the current carried by solution which is replaced by the translocating molecule,

$$I_{block} = \rho \times A \times \frac{V_{bias}}{L_{pore}}$$

where ρ is the solution conductivity, V_{bias} the applied voltage, L_{pore} the effective pore length, and A the hydrodynamic cross section of the translocating molecule.

The dwell time of DNA in silicon oxide nanopores is related with the molecule length [12],[16] $t_{dwell} \approx L^{\alpha}$, α=1.26, where L is the DNA length.

1.1.9 Molecular separation

Various nanofabricated membranes have potential applications in molecular separations. For example, Martin's group[41] used gold nanotubules in polymeric membranes for small molecules separation because of size difference. This membrane shows high selectivity of methyl viologen (MV^{2+}) and Ru(II) tris(2,2'-bi-pyridine) [Ru $(bipy)_3^{2+}$].

Ultrathin (15nm thickness) porous nanocrystalline silicon (pnc-Si) membrane was reported for molecular separation(Fig.1.7) [42]. This membrane has excellent mechanical strength, and it can support 1 atm of differential pressure without plastic deformation. Silicon nitride membranes[43] with pore diameter less than 10nm also exhibit good mechanical, chemical and thermal properties. After functionalized by specific antibody, silica nanotubes [44] growth within AAO membrane is used to separate two enantiomers of a chiral drug.

1.1.10 Novel Design of nanopore for DNA sequencing

In this thesis, two system of conductor/insulator/conductor multilayer system and conductor/lipid bilayer system were chosen to produce the nanopore structure.

1.1.10.1 Conductive/Insulator/Conductive multilayer system

As shown in Figure 1.8, this multilayer nanopore device contains one nanometer-scale hole. Each layer is several nanometers thick and can be individually addressed with voltage. The conductive layer can be independently functionalized to control a DNA strand passing through the nanopore. The influence of electric field due to different voltage might trap DNA in the nanopore.[45-47] Copper nanoparticles are electroplated at the edge of the conductive layer to prove the conducting property. The tethered functional chemistry could affect the pore selectivity, which leads to membrane pore having multiple reaction sequences as the molecule translocating through the memebrane.

1.1.10.2 Conductive/Lipid bilayer system

Self-assembled bilayer lipid membranes (BLMs) in vitro were first reported in 1962. [48] The artificial lipid bilayers have been prepared at the edge of Teflon membrane similar as soap bubble.[49] It has also been reported that pore-spanning lipid membranes are formed over plasmonic nanopore arrays in a 200nm thick gold film for biosensing.[50] Here, we design to use electrochemistry to graft the edge of the conductive layer with long chain alkane primary amine molecule (i.e. $CH_3(CH_2)_{10}NH_2$) in order to make it hydrophobic. (Fig.1.9) This structure with single nanopore in the lipid bilayer might be a good platform for DNA translocation and biosensing. The advantage of imbedding protein in lipid bilyaer is its small pore size, and if different proteins are chosen, it can show different molecular specificity.

1.2 Water desalination

The requirement for excellent desalination membranes is not easily met. It requires high flux and salt rejections. In addtion of that, the membranes should be also resistant to fouling, cheap and mechanical stable.

Various methods have been employed for desalination, including distillation [51], reverse osmosis[52] and nanofiltration [53]. Among all these techniques, reverse osmosis is widely used because of energy saving. Ultrapure water can be produced by RO membranes from salt water such as seawater or brackish water. In order to force water flow from high to low concentration, the pressure required for this process should be

larger than the osmotic pressure. These RO membranes include cellulose acetate (CA) [54], poly amide [55], and so on.

Zeolite membranes have been studied for desalination application because of its chemical and thermal stability. MFI-type zeolite (pore size ~0.56nm) membranes have been used for water desalination.[56, 57] It is reported that NaA zeolite nanoparticles/ polyamide composite prepared by interfacial polymerization showed better permeability than pure polyamide films. [58]

Carbon nanotube (CNT) membranes may offer an exciting opportunity for water desalination due to its nearly ideal slip-boundary interface, which can greatly enhanced fluid flow. It is reported that fluid moves through hydrophobic SWNTs 4-5 orders of magnitude faster than in conventional materials.[59] In this way, it may dramatically save the energy needed for water desalination. Hummer and co workers[60] reported molecular dynamics simulations results of one-dimensional water in carbon nanotube leading to rapid transport of water. 1 to 2nm carbon nanotube membrane with negatively charged at its entrance shows high ion rejection which is greater than 90% exclusion for 1 mM $K_3Fe(CN)_6$. [61] A US patent reported carbon nanotubes embedded in a polymeric matrix demonstrated a higher salt rejection and water flux compared with the membrane without carbon nanotubes. [62]

However, a major challenge is the uniformity of carbon nanotube diameter. Nowadays, CNTs are usually synthesized by laser ablation [63], arc-discharge between electrodes

[64], and chemical vapor deposition (CVD). [65] In the CVD method, carbon nanotubes nucleate and grow on the Ni, Co, or Fe based catalyst. The diameter of CNT is determined by catalyst particles size. [66] Therefore, in order to control the carbon nanotube diameter, it is very important to control the catalyst size. However, the size control process is a challenge.

Zeolites have uniform pores, which can be a good size control substrate to confine the carbon nanotube growth inside their channels. Recently, Z.Tang's group reported the in-situ growth of SWNTs in the $AlPO_4$-5 (structure code AFI) zeolite pore by pyrolysis of the organic precursor tripropylamine (TPA). [67] The $AlPO_4$-5 consists of alternating tetrahedral $(AlO_4)^-$ and $(PO_4)^+$ with one dimensional hexagonal structure, and the inner diameter is about 0.73nm. These 4 angstrom carbon nanotubes exhibit supconductivity property. [68, 69] Various conditions have been investigated for producing higher loading density and better carbon nanotube quality. Synthesis with F^- and F^- free [70], with different carbon precursor molecules (triethylamine (TEA), TPA, tetrapropylammonium hydroxide (TPAOH), and tetrabutylammonium hydroxide (TBAOH)) [71] , different metal cations [72-74], e.g. Mn^{2+}, Mg^{2+}, Co^{2+}, Si^{4+}, etc. have been reported. 0.3nm (2,2) armchair SWNTs synthesized by pyrolyzing organic template molecules dipropylamine (DPA) in $AlPO_4$-11 nanochannels has also been reported.[75] However, the 0.3nm and 0.4nm SWNTs are too small for water desalination process, because a sodium ion has a radius of 0.3nm with a hydrated ion size of 0.7nm. [76]

The microporous aluminum phosphate VPI-5(Virginia Polytechnic Institute number 5)[77] has uniform 1.2nm pore diameter. As shown in Figure 1.10, VPI-5 has much larger pore diameter than $AlPO_4$-5 and $AlPO_4$-11.[78] In order to obtain larger diameter SWNTs, VPI-5 is employed as a hard template in our experiment.

1.2.1 Novel Design of 0.7nm SWNTs growth

Carbon nanotube membranes are attractive for water desalination for three reasons. First, the atomically flat graphitic planes allow fast fluid flow. Second, with the 0.7nm SWNTs, it is possible to separate water molecules and salt molecules by size difference. Third, the entrance of the nanotubes can be covalently functionalized with charged groups. Here, we try to fabricate membranes, which have uniform diameter (~0.7nm) SWCNT. To get the well defined diameter SWCNT, the carbon nanotube has been fabricated by pyrolysis of the carbon precursor inside the VPI-5 channel. The carbon nanotube will be embedded within a highly stable epoxy matrix. A membrane with 5μm thick SWCNTs is obtained from microtome dicing technique, which could greatly enhance reproducibility and reduce sample preparation time.

1.3 Challenges

Some critical problems have already been solved, such as the back etch, open nanopore structure, Cu electroplating, the vertical pore structure fabrication. However, challenges still remain.

A key challenge is how to fabricate uniform sized single wall carbon nanotube. The experiment results indicate that it might be achieved by using VPI-5 zeolite as the template to encapsulate carbon inside its channel. A continuing concern is that the carbon nanotube yield is too low, and its poor repeatability.

The second challenge is how to load the fragile lipid bilayer onto the nanopore structure. One possible solution is making the pore smaller because it is reported that lipid bilayer is very fragile across a large area. [49]

The third challenge is how to slow down DNA translocation speed, control its translocation and make it readable. It might be solved by binding the DNA strand to the functional group to slow down the DNA passing rate.

Although challenges remain, the progress toward the goal of inexpensive nanopore sequencing and uniform carbon nanotube is encouraging.

1.4 Conclusions

Nanopore sequencing and water desalination are attractive fields and they are growing areas in nanotechnology. Our goal is to fabricate conductor/insulator/conductor multilayer structure for the DNA sequence and synthesis of uniform diameter carbon nanotubes for water desalination. In Chapter 2, we present a method to fabricate 0.7nm SWCNT by pyrolysis of carbon precursor inside the VPI-5 zeolite channels. TEM images confirmed the exsistance of 0.7nm SWNTs obtained by carbonization of VPI-5/ sucrose

composite at 1000◦C at inert atmosphere. Different organic precursors are used to find the suitable condition for carbon nanotube growth. The challenge is the poor repeatability of the synthesis and low yield of carbon nanotubes.

In Chapter 3, we are trying to fabricate the multilayer pore structure. We will introduce two systems, one is carbon/polymer/carbon system and the other is metal/lipid bilayer system. In the first system, we have fabricated reproducible and controllable nanopore structure. 200nm vertical carbon/polymer multilayer pore structure has been prepared by RIE etching and pore edges are confirmed by SEM. Thin AAO membrane with 50nm pore diameter has been synthesized by one step anodization. However, the carbon layer is not so conductive, which is not good enough for voltage applying on it and electrochemistry functionalization. In the second system, metal/lipid bilayer system is established. Micrometer copper pores have been successfully etched by $FeCl_3$ solution and coated with metal particles by electroplating method. Ni layer serves as good protective layer during the RIE etching SiO_2 process, about 1.4μm thick SiO_2 pores are opened by C_4F_8/O_2 etching.

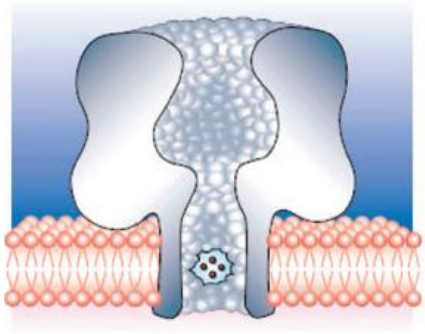

Figure 1.1 Detection of Metal ions by pore of αHL[4]. Reprinted with permission from ref.4. Copyright (2001) Nature Publishing Group.

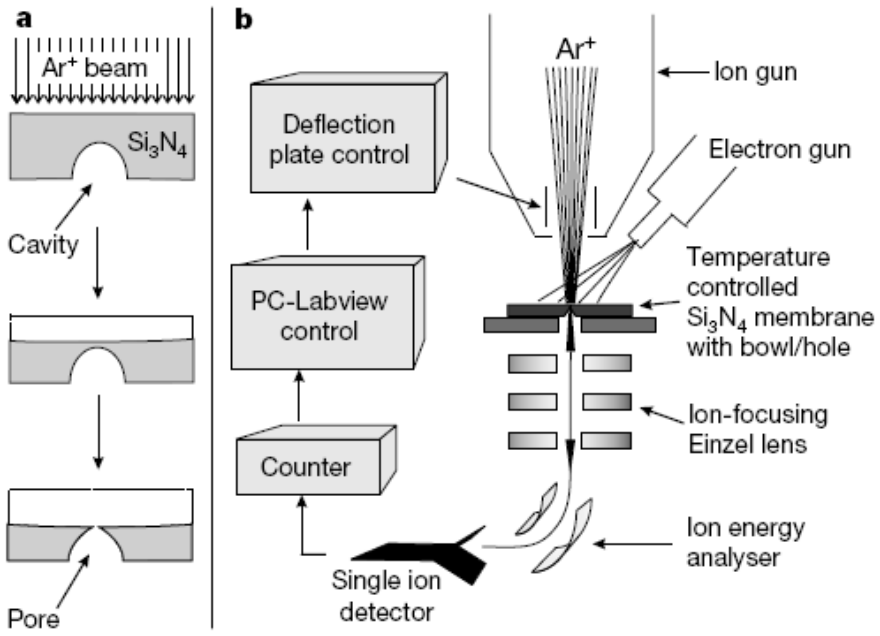

Figure 1.2 Strategy to make nanopores using ion-beam sculpting. [6] Reprinted with permission from ref.6. Copyright (2001) Nature Publishing Group.

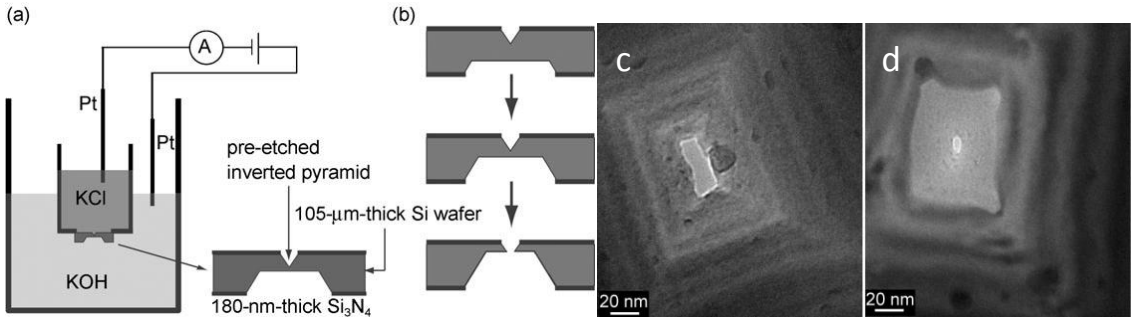

Figure 1.3 Fabrication of silicon nanopores with feedback electrochemical etching. (a) Schematic image of the experimental setup. (b) Schematic image of KOH etches through the tip of the inverted pyramid. TEM images showing the morphology of (c) an as-etched pore and (d) pore after oxidation. [13] Reprinted with permission from ref.13. Copyright (2007) WILEY-VCH Verlag GmbH&Co. KGaA

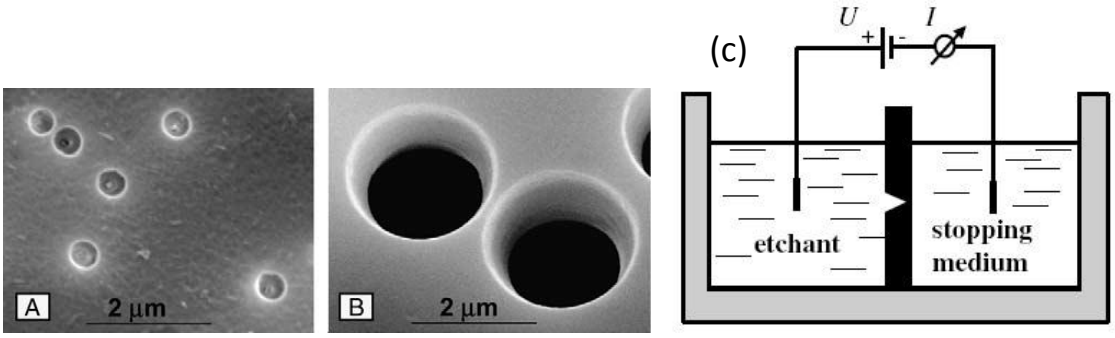

Figure 1.4 SEM images of the etched side of (A) a polyethylene terephthalate (PET) and (B) a polyimide foil. (C) Schematic image of the experimental setup. [14] Reprinted with permission from ref.14. Copyright (2003) Elsevier.

.

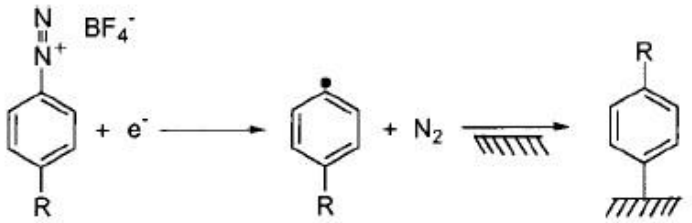

Figure 1.5 Electrochemical reduction of an aryl diazonium salt. [33] This figure is reproduced form ref.33. Reprinted with permission from ref.33. Copyright (2001) American Chemical Society.

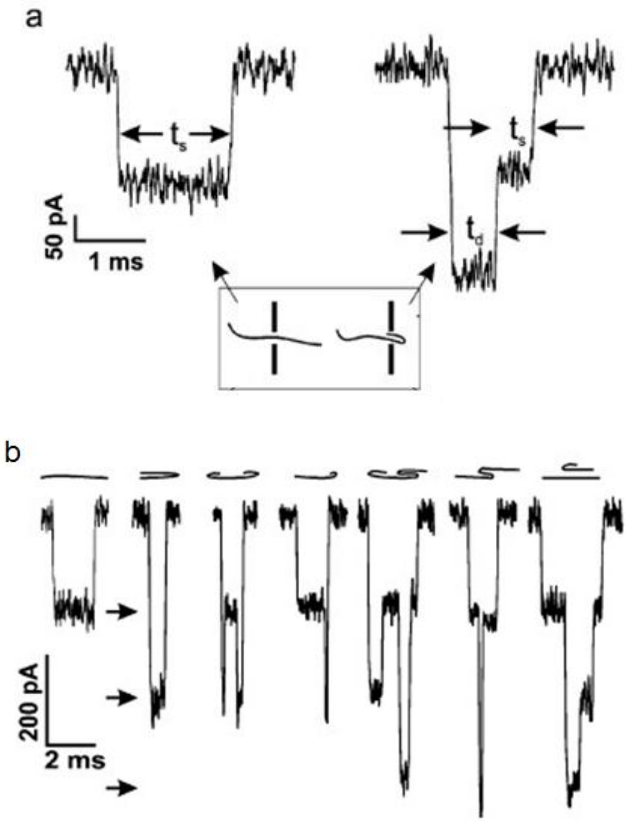

Figure 1.6 Translocation events. (a) DNA molecules translocating through a nanopore in strictly single-file (left) and folded one (right). (b) seven translocation events.[10] Reprinted with permission from ref.10. Copyright (2004) American Chemical Society.

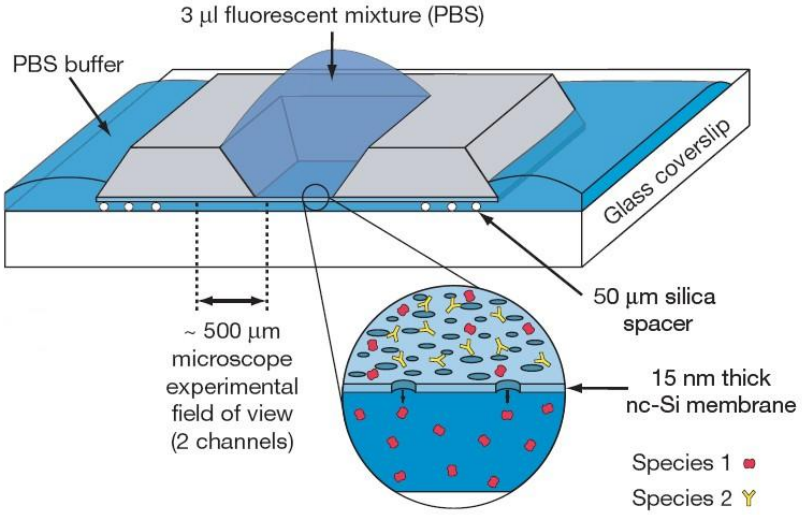

Figure 1.7 Molecular separation though pnc-Si membrane. [42] Reprinted with permission from ref.42. Copyright (2007) Nature Publishing Group.

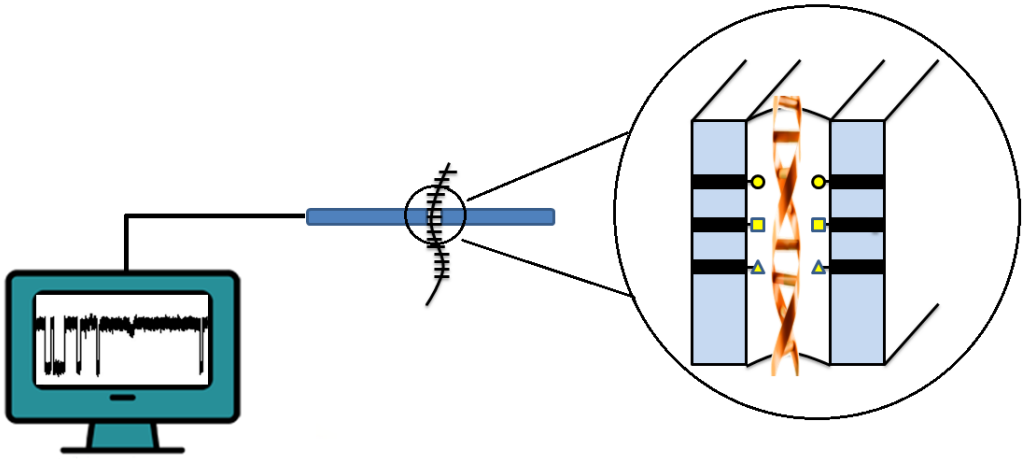

Figure 1.8 Proposed membrane device structure with independently functionalized multilayer nanoporefor DNA sequencing.

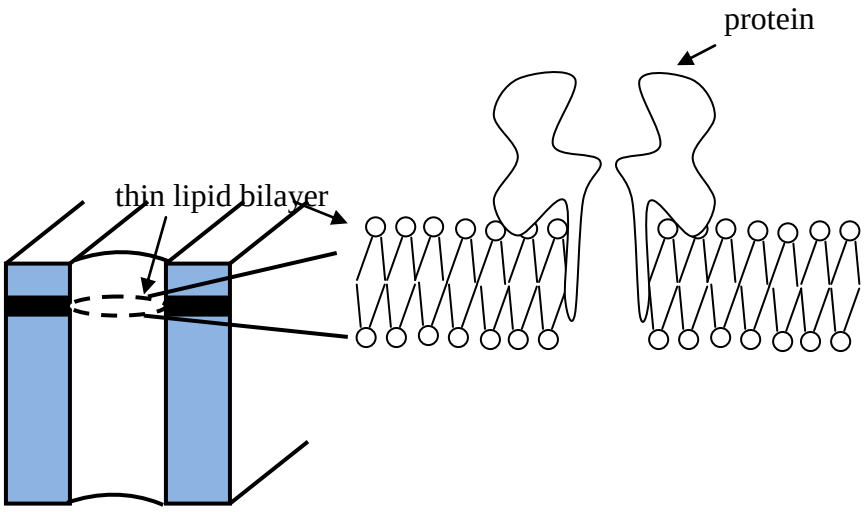

Figure 1.9 Schematic of protein embedded in lipid bilayer nanopore at a single layer.

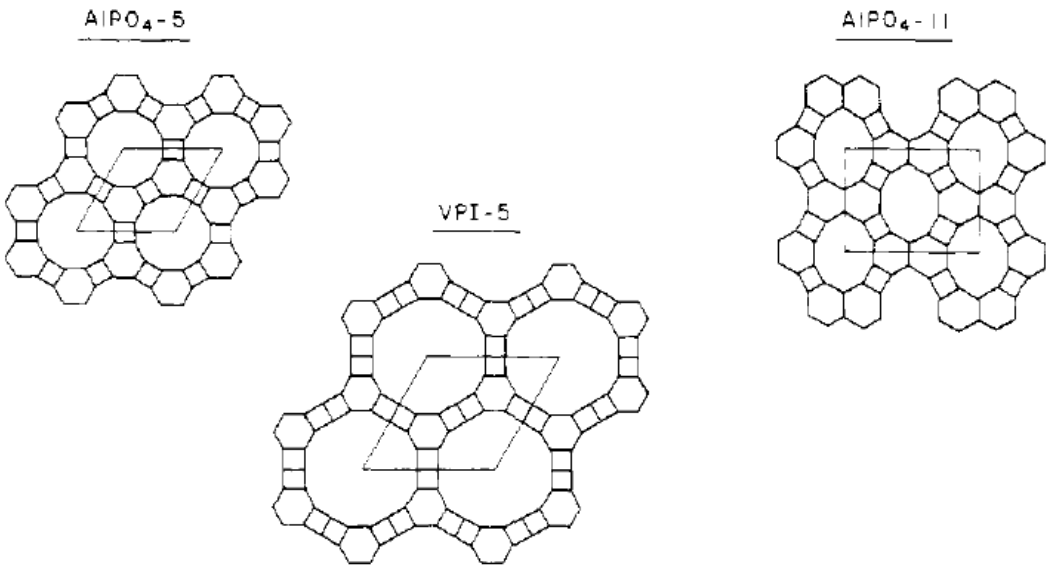

Figure 1.10 Framework [100] projections of $AlPO_4$-11, $AlPO_4$-5 and VPI-5. [78] Reprinted with permission from ref.78. Copyright (1989) American Chemical Society.

Chapter 2 Synthesis of single walled carbon nanotubes (SWCNTs) in zeolite template

2.1 Introduction

Since the first report of carbon nanotubes (CNTs) by Iijima in 1991 [81], many research work have been carried out because of their unique physical, chemical properties and potential applications.[59],[82] However, the lack of purity and uniformity in diameter has become a significant hindrance for its application.

Recently, highly ordered porous materials, such as anodic aluminum oxide (AAO), mesoporous silica and zeolite, have attracted great attention because of their crystalline structure and precisely controlled pore size, which can be used in hard template carbonization technique. Kyotani et al.[83] use AAO to fabricate carbon nanotubes in its one-dimensional channel. Various materials such as sucrose [84], phenolic resin[85], and meso-phase pitch [86] have been used as carbon precursor with mesoporous sieve template to produce ordered mesoporous carbon. The mesoporous carbon replica is obtained after the removal of template. It has also been reported that multi-walled carbon nanotubes were synthesized by a pyrolytic technique with MCM-41 (Mobil composite material-41) as template and sucrose as carbon precursor. [87] Other zeolite, like 13X [88] and Y-type high-silica zeolite [89], have been reported as the support for carbon nanotubes growth by CVD method. However, there are a noticeable amount of MWNTs mixed with SWNTs.

Z. Tang group reported that 0.4nm single walled carbon nanotubes have been synthesized from carbonization of template molecules of tripropylamine (TPA) in one-dimensional $AlPO_4$-5 zeolite template.[67] The framework of $AlPO_4$-5 has 12-ring hexagonal P6cc structure with inner diameter of 0.73nm. By considering the Van der Waals radius of carbon, the nanotubes diameter allowed in the channel is extremely small (0.39nm), which leads to the instability after removal from template. [90] Micro-Raman system is used to characterize the carbon nanotube structure, and G band located around 1600 cm^{-1} has been measured [91], [92]. Co^{2+}, Si^{4+} and other cations are introduced in order to enhance the adsorption on the channel walls, and they also play a catalytic role in carbonization of organic precursor [93],[72].

Extra large pore molecular sieve VPI-5(Virginia Polytechnic Institute number 5)[77] has uniform 1.2nm pore diameter, which might be a good template for larger diameter single wall carbon nanotubes synthesis. Large molecule as triisopropylbenzene (kinetic diameter=8.5Å) [77] and Iron-phthalocyanines (FePc) [94] have been reported loaded into VPI-5. One European patent reported formation of carbon nanostructures with phthalocyanine molecule in VPI-5 zeolite crystals. [95] However, they didn't provide the TEM image of the carbon nanostructure to show if it is carbon nanotube.

In this work, we first report the synthesis of 0.7nm single wall carbon nanotubes through VPI-5 templates by carbonization of sucrose in the presence of Co catalyst. Other organic precursors have also been used, but no carbon naotubes are found from their TEM images. Although the substantial challenge now is the repetition of carbon nanotube synthesis and

the low yield, the results from TEM images of uniform diameter (~0.7-0.8nm) single wall carbon nanotubes is an improvement, and future work is promising.

2.2 Experimental

2.2.1 Chemicals & Equipments

Table 2.1 Chemicals used and manufacturers

Chemical	Manufacturer
Aluminum tri- isopropoxide [$(iPrO)_3$ Al]	Aldrich (98%+)
Pseudoboehmite	SASOL (Catapal® B)
H_3PO_4 (85%)	EMD
Tri- tripropylamine (TPA)	Aldrich (≥ 98%)
di-n-propylamine (DPA)	Alfa Aesar (99%)
D-fructose	Amresco ®
sucrose	Domino®
1-aminopyrene	Aldrich
1-pyrenebutyric acid	Aldrich (97%)
$Co(CH_3COO)_2$▪ $4H_2O$	Alfa Aesar

Samples were pyrolyzed at a quartz boat in Lindberg/blue tube furnace (Figure 2.1). It has a microcomputer based programmable temperature controller. Therefore, temperature and time could be accurately controlled. Gas flows were controlled by the MKS Instruments 1179A flow controllers.

2.2.2 Materials Characterization

2.2.2.1 Scanning electron microscopy (SEM)

SEM was carried out on S-4300 HITACHI scanning electron microscopy. Samples were coated with gold before analysis.

2.2.2.2 XRD

Powder X-ray diffraction (XRD) patterns were recorded on a Siemens D500 system operating with Cu Kα radiation (λ = 1.5406 Å). A 2θ scan from 5 °to 50 °at a rate of 1.5 ° per minute was employed.

2.2.2.3 The transmission electron microscope (TEM)

High resolution transmission electron microscope (HRTEM) images were obtained using a JEOL 2010F microscope operating at 200 keV. Before TEM observations, the samples were prepared by dispersing the products in ethanol or water with an ultrasonic bath for 10-20 min and then one drop of the resulting suspension was placed on a copper grid. Samples were dried at vacuum oven overnight before measurement.

2.2.2.4 Micro Raman

Raman spectra were measured for SWCNTs at room temperature using a Dispersive Raman Spectrometer (Thermo Scientific) and 780nm laser excitation. Another one is Renishaw's invia micro raman and PL spectroscopy system, which is equipped with a 633 nm red laser.

2.2.2.5 TGA

Thermogravimetric analysis (TGA) was conducted on a NETZSCH STA449C simultaneous thermal instrument. The sample (about 15 mg) was heated at a heating rate of 20 ℃ min^{-1} from room temperature to 1000 ℃ under flowing nitrogen (20 ml min^{-1}), and then burn the carbon at 1000 ℃ under air (60 ml min^{-1}) for 20minutes. The other two TGA equipments were universal instruments 2950 TGA HR V5.4A and STA6000 from PerkinElmer.

2.2.3 Experimental details

2.2.3.1 Autoclave clean

Before starting the hydrothermal crystallization step, Teflon-lined autoclave (Parrinst Instrument company) is cleaned with 30% NaOH at 423K for 10-12h. Then it is washed with distilled water and dried at room temperature.

2.2.3.2 Synthesis of $AlPO_4$-5 in HF

The gel mixture consisted of the following composition $1.0Al_2O_3$: $1.0P_2O_5$: 1.2TPA: 0.8HF: $400H_2O$. A typical synthetic procedure involved the following steps: aluminum tri- isopropoxide was first hydrolyzed in water for 2h followed by addition of phosphoric acid with stirring for 30 minutes. Then TPA was dropwisely added into the mixture. After continuous stirring for 2h, HF acid was added into the gel to adjust PH value. The formed gel was sealed in a Teflon-lined stainless autoclave and heated at 453k under autogenous pressure for 24h. The obtained hexagonal shaped $AlPO_4$-5 crystals were filtered, washed with distilled water, and dried at 333k temperature.

2.2.3.3 Synthesis of $AlPO_4$-5 in H_2SO_4

A reaction mixture was prepared by combining $(iPrO)_3$ Al, phosphoric acid, TPA, H_2SO_4 and distilled water in the ratio $1.0Al_2O_3$: $1.0P_2O_5$: 1.4TPA: 0.5 H_2SO_4: $400H_2O$. We use similar procedure as the synthesis of $AlPO_4$-5 in HF.

2.2.3.4 Synthesis of CoAPO-5

We use similar procedure to synthesis CoAPO-5. It was synthesized by adding Co cations into the gel during the $AlPO_4$-5 crystals synthesis process. The composition of the gel is xCo: $1.0Al_2O_3$: $1.0P_2O_5$: 1.2TPA: 0.8HF: $800H_2O$, where x is the molar ratio of Co to phosphorus. The aluminum tri- isopropoxide was first hydrolyzed in water, and then $Co(CH_3COO)_2$▪ $4H_2O$, H_3PO_4, TPA, HF were added into the solution under stirring. The gel was sealed in an autoclave and heated at 453k for 24h. The products were filtered, washed with distilled water, and dried at 333k temperature.

2.2.3.5 Synthesis of $AlPO_4$-5 without HF

The gel mixture consisted of the following composition $1.0Al_2O_3$: $1.0P_2O_5$: 1.0TPA: $100H_2O$. A typical synthetic procedure involved the following steps: $(iPrO)_3$ Al was first slurred into water for 1h followed by addition phosphoric acid with stirring for another 30 minutes. Then TPA was dropwisely added into the mixture. After continuous stirring for 2h, the gel was sealed in a Teflon-lined stainless autoclave and heated at 363k under autogenous pressure for 24h, and then heated at 453k for 24h. The solid products were filtered, washed with distilled water, and dried at 333k temperature.

2.2.3.6 Synthesis of 0.4nm SWNTs

The crystals were uniformly put inside a quartz boat, which is placed in the central part of the tube furnace. Before heating, the chamber is vacuumed and purged with Ar flow for 5 cycles in order to remove the remained air. The samples were then treated in a range of temperatures between 20 ℃ and 1000 ℃, with a temperature increase rate of 20◦C /min in a steady flow of Argon gas (60 sccm). After maintaining the required temperature of synthesis (1000 ℃) for one hour, the tube cools down to room temperature in Argon. Then the zeolite framework was dissolved in 30% hydrochloride acid overnight to get the freestanding 0.4nm SWNTs.

2.2.3.7 Synthesis of $AlPO_4$-5 in 200nm AAO pores

A reaction mixture was prepared by $(iPrO)_3$ Al, phosphoric acid, TPA, and distilled water in the ratio $1.0Al_2O_3$: $1.0P_2O_5$: 1.0TPA: $100H_2O$. A synthetic procedure involved the following steps: $(iPrO)_3$ Al was suspended in H_2O with vigorous magnetic stirring, followed by addition of phosphoric acid with stirring. Then TPA was dropwisely added into the mixture. After continuous stirring, the gel was sealed in a Teflon-lined stainless autoclave and heated at 363k under autogenous pressure for 24h. The autoclave containing the gel was quenched under water, opened, and a commercial porous anodic alumina membrane (0.2 μm membrane discs by Whatman) was put at the surface of the liquid to let it filled with zeolite gel. The sample was then re-sealed in the autoclave and heated at 453k for another 24h.

2.2.3.8 Synthesis of VPI-5

The gel mixture consisted of the following composition $1.0Al_2O_3$: $1.0P_2O_5$: 1.0DPA: $40H_2O$. Pseudoboehmite and phosphoric acid are employed as sources for Al and P, respectively. Typical synthetic procedure involved the following steps: 1.436g pseudoboehmite was suspended into 4.52g water (2/3 of total water) for 1h.[96] 2.42g phosphoric acid along with the rest 2.26g H_2O was added dropwisely to the slurry, and continue stir for 1h. The resulting gel was aged at room temperature for 3h. Then 1.05g di-n-propylamine(DPA) was dropwisely added into the mixture. After continuous stirring for 1h, the stirring was stopped, and the gel was aged at room temperature for 20h. The gel was then sealed in a Teflon-lined stainless autoclave and put into a preheated conventional electric oven at 398k (in the range of ±5◦C) under autogenous pressure for 24h. The solid products were filtered, washed with distilled water and dried in vacuum oven overnight at room temperature.

2.2.3.9 Synthesis of 0.7nm SWNTs with sucrose

0.091gVPI-5 zeolite was immersed in a catalyst solution of 0.018g $Co(CH_3COO)_2$▪ $4H_2O$ and 2g ethanol for overnight. Precipitation of Co complex was seen in the EtOH solution. After filtration and washed with ethanol, the crystals were dried in a vacuum oven at room temperature. Carbon precursor solution of sugar and water (mixing of 0.05g sugar, 0.2g H_2O and 0.4g ethanol) was added dropwise to the crystals to fill the void pores. After overnight immersion, the product is filtered and washed with ethanol and dried at vacuum oven overnight. Before heating, the chamber is vacuumed and purged with Ar flow for 5 cycles in order to remove the remained air. Graphite felt and graphite piece are

used to completely remove the O_2. The sample is then treated in a range of temperatures between 300k and 1273k, with a temperature increase rate of 20◦C /min in Ar gas. After maintaining the required temperature of synthesis (1000 ℃) for one hour, the tube cools down to room temperature in Argon. Then the zeolite framework was dissolved by using 30% hydrochloride acid to get the freestanding 0.7nm SWNTs.

2.2.3.10 Synthesis of 0.7nm SWNTs with other organics

PEG sample: PEG didn't dissolve well in ethanol, but well dissolved in water. Carbon precursor solution of 0.1g PEG and water/ethanol mixture (1g H_2O and 1g ethanol) was added dropwise to 0.1g VPI-5 zeolite. After overnight immersion, the product is filtered and washed with ethanol and dried at vacuum oven overnight.

Triton X-100 sample: Carbon precursor solution of 0.1g Triton and 2g ethanol mixture was added dropwise to 0.1g VPI-5 zeolite. After overnight immersion, the product is filtered and washed with ethanol and dried at vacuum oven overnight.

Ni phthalocyanines sample: Carbon precursor solution of 0.1g Ni phthalocyanines and 2g ethanol mixture was added dropwise to 0.1g VPI-5 zeolite. After overnight immersion, the product is filtered and washed with ethanol and dried at vacuum oven overnight.

Ionic liquid (1-Buty1-2,3- dimethylimidazolium chloride) sample:

sample #1: 0.118g VPI-5 was mixed together with 0.33g ionic liquid and heated at 90℃ in the vacuum oven overnight. The product is filtered and washed with ethanol and dried at vacuum oven overnight.

Sample #2: 0.1g VPI-5 was mixed together with 0.255g ionic liquid and 0.005g $Fe(NO_3)_3$, followed by heating at 60℃ in the vacuum oven overnight. The product is filtered and washed with ethanol and dried at vacuum oven overnight.

Fructose sample:

sample #1: 0.62g VPI-5 zeolite was was immersed in 4g H_2O with 0.116g $Co(CH_3COO)_2 \cdot 4H_2O$ and 1g fructose. The product is filtered and washed with water and dried at vacuum oven for 4h at 60℃.

Sample #2: 0.126g VPI-5 zeolite was was immersed in 1.1g H_2O with 0.1g $Co(CH_3COO)_2 \cdot 4H_2O$ and 1g fructose. The product is filtered and washed with water and dried at vacuum oven overnight.

sample #3: 12g ethanol solution with 0.1g $Co(CH_3COO)_2 \cdot 4H_2O$ and 1g fructose is heated at 80℃ for 30min and then cool down. After heating, most fructose are dissolved. The clear solution is transferred to another beaker and 0.117g VPI-5 zeolite was immersed in the solution. After overnight immersion, the product is filtered and washed with ethanol and dried at vacuum oven overnight.

1-aminopyrene sample: 0.091g VPI-5 zeolite was mixed with 0.1g $Co(CH_3COO)_2 \cdot 4H_2O$ and 0.22g 1-aminopyrene. Because the melting point for 1-aminopyrene is 115◦C-118◦C, the sample is then put into tubefurnace and heated to 120℃ with a temperature increase

rate of 3◦C /min in Ar gas. After maintaining the temperature at 120 ℃ for one hour, the tube cools down to room temperature in Argon. Acetone is used to rinse the sample during filtration step. After filtration, the crystals were dried in a vacuum oven at room temperature.

1-pyrenebutyric acid sample: 0.069gVPI-5 zeolite was immersed in a 12g ethanol solution with 0.1g $Co(CH_3COO)_2$▪ $4H_2O$ in the solution. The product is filtered and washed with ethanol and dried at vacuum. Because the melting point for 1-pyrenebutyric acid is 184◦C, the sample is then put into tubefurnace and heated to 200 ℃ with a temperature increase rate of 10◦C /min in vacuum. After maintaining the temperature at 200 ℃ for one hour in Argon, the tube cools down to room temperature in Argon. Acetone is used to rinse the sample during filtration step. After filtration, the crystals were dried in a vacuum oven at room temperature.

2.3 Results and discussion

2.3.1 $AlPO_4$-5

2.3.1.1 XRD

Various methods have been reported for the synthesis of $AlPO_4$-5[97],[80],[98] employing different organic templates, aluminium precursors and different reaction conditions. The crystallinity of the as-synthesized AFI crystals with starting gel composition of $1.0Al_2O_3$: $1.0P_2O_5$: 1.0TPA: $100H_2O$ was checked by powder X-ray diffraction as shown in Figure 2.2. The XRD patterns of the $AlPO_4$-5 crystal correspond

well with the reported pattern of pure AFI structure[99], which means that high quality $AlPO_4$-5 crystals were synthesized.

2.3.1.2 Micro Raman data

The raman spectra of the 0.4nm SWNTs exhibit three features. The first mode is the radial-breathing modes (RBMs) (100-600cm^{-1}), which is due to tubular vibrations along the radial direction. The second mode is the D band (1200-1500cm^{-1}) due to disordered carbon structures. The third mode is the G band (1500-1620cm^{-1}), which is a characteristic feature of the graphitic layers and due to tangential vibration of carbon atoms.[72, 74] Figure 2.3 shows two peaks at 510 and 550cm^{-1}, which are attributed to the chiral (4, 2) nanotubes and zigzag (5, 0) nanotubes, respectively. [71],[74]

The RBM is very sensitive to the nanotube diameter, according to the equation

$$\omega(d_t)=\alpha/d_t \quad [90]$$

where d_t is the nanotube diameter, α is the proportional constant. From Fig.2.3, α can be estimated to be 223.9nm cm^{-1}, then

$$d_t= 223.9/550=0.407nm$$

Figure 2.3 also shows strong G band near 1600cm^{-1}, which indicates graphitic structure are formed.

2.3.1.3 TEM

To view the SWCNTs in TEM, AFI template was dissolved in 30% hydrochloric acid. From the TEM image (Fig. 2.4), by measuring the separation between the two parallel dark lines of SWCNT image, the diameter of CNT is around 0.42nm, which is in good

agreement with the micro raman data. It is reported that the SWNTs extracted from AFI template were not stable under electron beam radiation. It is because that strong bending of carbon bonds, size confinement, and the imperfection result in high energy regions in the ultra small CNTs. [67], [90]

2.3.1.4 TGA

To investigate the pyrolysis process of the carbon precursors in the channels, TGA technique is used. The $AlPO_4$-5 crystal containing TPA is transparent in microscope. After pyrolysis at 1000◦C in N_2, the crystal color turned to homogeneous black. Fig. 2.5 shows the measured TG curves. The TG curve contains three main parts: The weight loss of $AlPO_4$-5 crystals in the temperature region from 50◦C to 140◦C is due to the moisture desorption, the loss in the region from 200◦C to 650◦C is due to the decomposition of TPA, and weight loss of about 2% appearing at 1000 ℃ is because of carbon completely burnt out in air.

2.3.1.5 SEM images

2.3.1.5.1 Synthesis of $AlPO_4$-5 in H_2SO_4

Different dimensions of $AlPO_4$-5 crystal have been reported by addition with H_2SO_4 to adjust the PH value at 3.5.[97] Fig. 2.6 shows the SEM images of as synthesized $AlPO_4$-5 by with gel composition of $1.0Al_2O_3$: $1.0P_2O_5$: 1.4TPA: 0.5 H_2SO_4: $400H_2O$. Some crystals obtain perfect hexagonal shape, but most of the resulting products are in amorphous phase.

2.3.1.5.2 Synthesis of $AlPO_4$-5 in H_3PO_4

We also tried to use H_3PO_4 to adjust PH value between 3 and 4. Fig. 2.7 shows the SEM images of as synthesized $AlPO_4$-5 by with gel composition of $1.0Al_2O_3$: $1.4P_2O_5$: 1.4TPA: $450H_2O$. However, it seems that only very small crystal structure is formed. The as grown $AlPO_4$-5 crystals have a length of 1-2 μm, which is less than the 5 μm thick carbon nanotube membrane.

2.3.1.5.3 Synthesis of $AlPO_4$-5 in HF

The function of F^- is to make the starting gel favorable to get large-sized single crystal and improve the quality of the AFI crystals. [74] High quality $AlPO_4$-5 sample were synthesized with gel composition of $1.0Al_2O_3$: $1.0P_2O_5$: 1.2TPA: 0.8HF: $400H_2O$ as shown in Figure 2.8. The as synthesized $AlPO_4$-5 crystals have a typical dimension of 100 μm × 20 μm ×20 μm, with regular hexagonal cylinders in shape and good morphology.

2.3.1.5.4 Synthesis of $AlPO_4$-5 without HF

It is reported that the addition of F^- can affect the form of TPA, which may lead to different carbonization processes. The filling density of SWCNTs can be enhanced by pyrolysis of TPA precursor without F^- ions. [70] Therefore, we synthesized $AlPO_4$-5 crystals without the existent of F^- ions by a two steps heating process. Figure 2.9 shows images of $AlPO_4$-5 crystals with gel composition of $1.0Al_2O_3$: $1.0P_2O_5$: 1.0TPA: $100H_2O$. The AFI crystals have dimensions 5μm in cross-section diameter and 100 μm in length. As it can be seen, the F^- distinctly influences the size of the crystals.

2.3.1.5.5 CoAPO-5

When Al^{3+} is replaced by Co^{2+}, the framework is negatively charged. It leads to the formation of BrØnsted acid sites, which can enhance the adsorption and catalyze the pyrolysis of carbon precursor.[93] We synthesized CoAPO-5 crystals with two different gel compositions of $0.2Co:1.0Al_2O_3$: $1.0P_2O_5$: 1.2TPA: 0.8HF: $450H_2O$ and $0.07Co:1.0Al_2O_3$: $1.0P_2O_5$: 1.2TPA: 0.8HF: $800H_2O$, respectively. Both of the as grown CoAPO-5 crystals have an interesting pencil-like structure with a length of about 70 μm, as shown by the SEM image in Fig. 2.10. This similar pencil-like structure of $AlPO_4$-5 has also been reported.[100] From Figure 2.10, less Co^{2+} ions and more water sample showed better crystal structure, indicating that an increase of Co^{2+} ions might decrease the crystal morphology.

2.3.1.5.6 Synthesis of $AlPO_4$-5 in AAO membrane

Anodic alumina membrane has been reported as a host to grow aligned arrays of $AlPO_4$-5 within its nanochannels.[101] In our work, commercial whatman AAO membrane was used as the template. Figure 2.11 is the schematic illustration of $AlPO_4$-5 growth inside the channels of AAO membrane. These membranes had an average pore size of about 200 nm. The pores of these membranes may be large to allow the $AlPO_4$-5 to penetrate during crystallization. Figure 2.12 shows the AAO membrane was not added to the autoclave until after 90◦C treatment. After 90◦C hydrothermal step, PH value of the solution was about 7, which did not damage the AAO membrane in the solution. Although there are some AFI zeolites inside the AAO pores, the crystals do not cover all the pores of AAO membrane, which can't be used as desalination membrane. Figure 2.13

shows the sample of AAO membrane added to the autoclave at the beginning and heated at 453k for 24h. It shows hair like structure at the top surface of AAO membrane, which is due to the etching of H_3PO_4 acid.

2.3.1.5.7 Zeolite/epoxy membrane

Carbon nanotube membranes had been reported forming by microtoming a nanotube-epoxy composite mixture to a thickness of 5 μm [102]. Similar microtomed cut method is used in this paper trying to obtain zeolite/epoxy membrane. However, zeolite is easy to break during cutting, which creates lot of defects in the membrane.

Another possible method is spin coating thin layer of epoxy/zeolite on a glass slide. After dried at room temperature, the membrane can be peeled off from the glass slide and exposed to O_2 plasma to partially remove the residual epoxy on the tips of zeolite. Figure 2.14 shows the SEM images of membrane before and after etching. The epoxy can be easily removed by O_2 RIE method, and the etching rate is about 500nm/min. However, ionic current of the etched membrane is very large, indicating leak of the membrane.

2.3.2 VPI-5

2.3.2.1 XRD

The crystallinity was investigated by an X-ray powder diffractometer. Fig.2.15 presents the XRD pattern of VPI-5 with gel composition of $1.0Al_2O_3$: $1.0P_2O_5$: 1.0DPA: $40H_2O$. The XRD patterns of the VPI-5 crystal correspond well with the reported pattern of pure VPI-5 structure [77], [103], which means that high quality crystals were synthesized.

2.3.2.2 SEM of VPI-5

It is reported that the optimal crystallization time is 24h. Shorter crystallization time generates a lot of unreacted gel and longer time may increase the amount of impurity phases. [104] Our 24h crystalized VPI-5 samples have a dimension of $80\mu m \times 2\mu m \times 2\mu m$ as shown in Fig. 2.16, with regular hexagonal cylinders in shape and good morphology. In Fig.2.16 (c), needles structure is radiated from a central core, which is due to different nucleation rate from the central part and the outer surfaces. [104]

2.3.2.3 TEM

In VPI-5, the pores are one-dimensional channels, which have uniform inner diameter of about 12Å.[105] The effective pore size distribution from argon adsorption has a main peak at 10.5Å. [106] By considering the distance between the carbon atoms of carbon nanotubes and the oxygen atoms on the channel wall (0.34nm)[67], the diameter of SWCNTs allowed in the pores is about 7 to 8Å (10.5 ± 1Å - 3.4Å). Figure 2.17 shows high resolution transmission electron microscopy images of freestanding SWCNTs removed from VPI framework. The diameter of these carbon nanotubes are about 0.7nm.

2.3.2.4 Micro raman

From our micro raman measurement, it is very hard to prove the existence of carbon nanotubes and confirm the diameter of carbon nanotube. Figure 2.18 shows G band near $1600cm^{-1}$, which indicates graphitic structure are formed. However, in the RBM region, it shows very broad peak which is difficult to calculate the diameter of CNTs. Compared with the sample before pyrolysis, the broad peak may comes from the zeolite template. After removal of the template, there is no broad peak show in the RBM region.

2.3.2.5 TGA

The difference from VPI-5 and $AlPO_4$-5 is although DPA acts as the structure directing agent for the crystallization, the as-synthesized VPI-5 does not contain organic species inside the 18-ring channels, while water molecules fills in these channels. [106] The pore volume of 18-ring channels in VPI-5 is about 0.25cm^3/g, and the water content absorbed in VPI-5 is around 0.31g/g.[106] It is also reported that there are seven different water molecules present in the structure of VPI-5. [107] TGA curves of VPI-5 at heating rate of 20◦C/min in N_2 and air are shown in Figure 2.19. Both curves illustrated significant weight of 23% in the range of 30◦C-120◦C, which is caused by the removal of water. Because there is almost no difference between VPI-5 heated in N_2 and air oxidation, it indicates that there is no organic precursor (from templating agent) inside the channels of as synthesized VPI-5. If we are able to load the pores completely with an organic precursor with a density of 1.2g/cm^3 (assumed for many organics) we would expect a 23% loss of sample in the TGA with O_2 present. If the pore was lined with graphitic carbon (a SWCNT) we would expect a loss of 10% after introduction of O_2 into the TGA.

In the paper various carbonaceous precursors are used in order to grow uniform diameter carbon nanotube through template approaches. To study the adsorption effect of VPI-5 and pyrolysis behavior of the carbon precursor, we monitored the gravimetric change of VPI-5 during heating by the TGA. VPI-5 is reported can be partially transformed to $AlPO_4$-8 in the presence of moisture when heating above 100◦C [108], but thermally stable in the absence of moisture [109]. Therefore, before starting TGA measurements,

the samples are put into vacuum oven at room temperature overnight for maximum removal of the absorbed water.

Figure 2.20 shows the measured TGA curve of sucrose as the carbon precursor. The TG curve contains four main parts: The first weight loss step of VPI-5 crystals in the temperature range from 30◦C to 50◦C is due to the moisture desorption. The second loss of 8% in the range from 50◦C to 650◦C corresponds to the decomposition of sucrose. The third mass loss of 0.5% in region from 650◦C to 1000◦C may due to the continuous graphitization process. The final weight loss of about 1.5% appearing at 1000◦C is because of carbon completely burnt out in air. The zeolite samples are initially a pale blue from Co catalyst and uncolored organic precursor. After pyrolysis in N_2 or Ar they become black/dark grey indicating either a-C or CNT formation. After oxidation with O_2 at 1000◦C the samples are pale blue from catalyst color and removal of carbon.

2.3.2.6 TGA of other organic precursor

Because of the repetition problem of sucrose sample, we tried other organic precursors in order to improve the carbon nanotube yield. Long Chain polyethylene glycol (PEG) is used because if it can transport into pore structure, the carbon yield might be high. However, after pyrolysis, it did not show any weight loss of carbon at 1000◦C in air, which may due to the long chain structure not easy going into the nanochannel of VPI-5. Triton-100 is employed because it is a nonionic surfactant which might be easily bonded with the channel wall. After pyrolysis, there is also no weigh loss of carbon, which may because that the Triton molecule is too big for entering. Ionic liquid is a salt in liquid

state. We tried to use the ionic liquid to avoid evaporation of organic molecule during heating, which may increase the filling density of carbon and enhance the nanotube yield. For of 1-Buty1-2,3- dimethylimidazolium chloride, the melting point is 96-99◦C. The VPI-5 powders are mixed with 1-Buty1-2,3- dimethylimidazolium chloride and heated at vacuum oven till 100◦C for 30min. After cooling down, the sample is washed with DI water, and dried overnight. However, after pyrolysis, we still didn't obtain carbon. It may because that it is very hard for this molecule to enter into the pores. We use Ni phthalocyanines as precursor because Iron-phthalocyanines (FePc) [94] have been reported loaded into VPI-5. However, from the TGA data, we didn't obtain carbon yield. Fructose has smaller diameter than sugar, therefore, we expected it entering into the pores more easily. Although there showed about 6% carbon yield, we didn't see carbon nanotube from TEM images. It may because that most amorphous carbon is formed on the surface of zeolite rather than in the pores. For 1-aminopyrene and 1-pyrenebutyric acid, we used similar melting method, and their melting point are 115-117◦C and 184-186◦C, respectively. VPI-5 is mixed with the precursor and loaded into the tube furnace in vacuum to remove the gas absorbed in the pore channels. When it reached melting temperature, we switch the valve to Ar for pushing the precursors into the nanopores and keep for 1h. Finally, the sample is cooled down in Ar. From TGA measurement, there are 3% and 10% carbon yield for 1-aminopyrene and 1-pyrenebutyric acid, respectively. However, we didn't find carbon nanotubes from TEM images, but only some carbon onions. Maybe most carbon is formed on the outside surfaces of zeolite template.

Table 2.2 organic precursors

Organic precursor	Weight loss in N_2	structure	Carbon yield	method
PEG	22%	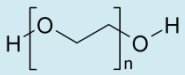	0	immersion
Triton	19%	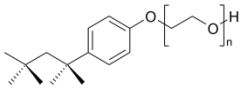	0	immersion
Ionic liquid-sample #1	26%	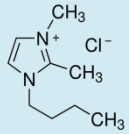	0	melting
Ionic liquid-sample #2	22%		0	melting
Ni phthalocyanines	23%	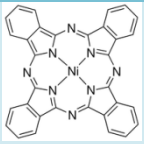	0	immersion
sugar	10%	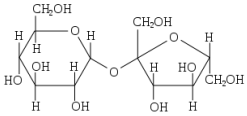	1.5%	immersion
fructose-sample#1	15%	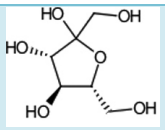	0.5%	immersion
fructose-sample#2	20%		1%	immersion
fructose-sample#3	30%		6%	immersion
1-aminopyrene	14%	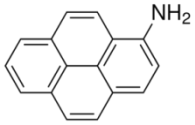	3%	melting
1-pyrenebutyric acid	25%	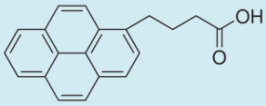	10%	melting

2.4 Conclusion

In summary, we have fabricated $AlPO_4$-5 zeolite with different PH value. Two step heating process is employed to obtain $AlPO_4$-5 in H_3PO_4 without HF acid. 0.4nm SWNTs are synthesized in $AlPO_4$-5 channel by pyrolysis TPA in AFI nanochannels. Raman measurement showed similar peaks as Z. Tang's group, which confirms the existing of carbon nanotubes.

VPI-5 is synthesized in order to fabrication larger diameter single wall carbon nanotubes for water desalination application. Different organic precursors are used in order to find the optimum condition for 0.7nm SWNTs growth in the nanopores of VPI-5. TGA, TEM and micro raman are employed to investigate the pyrolysis process and measure the final products. Only after the pyrolysis of sucrose/VPI-5 composite, 0.7nm SWNTs are found from its TEM image. However, we only once succeed with low yield and were unable to make membranes. The raman image shows the G peaks but only a very broad RBM peak, which makes it difficult to confirm the diameter of carbon nanotubes outside of the TEM observation area of the sample.

Tube furnace

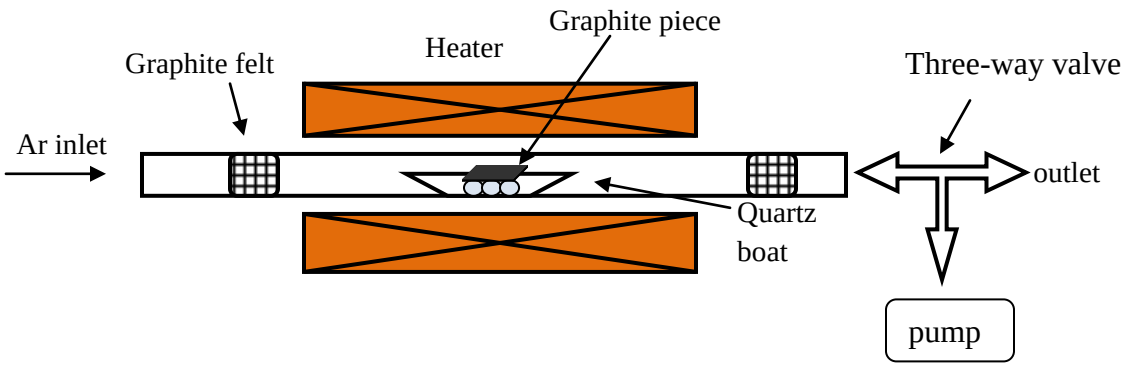

Figure 2.1 Schematic illustration of the SWCNTs pyrolysis in zeolite template

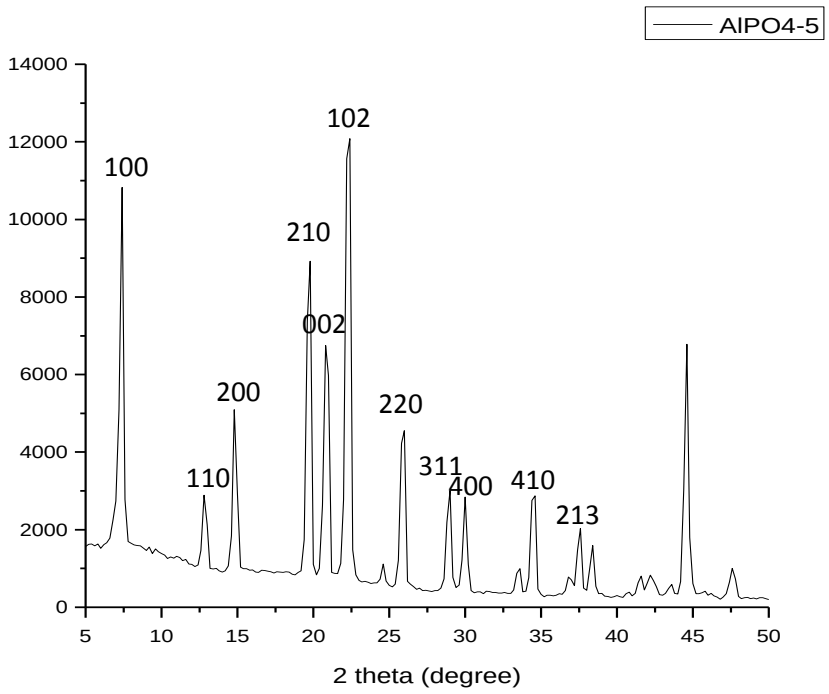

Figure 2.2 XRD pattern of the as-synthesized $AlPO_4$-5

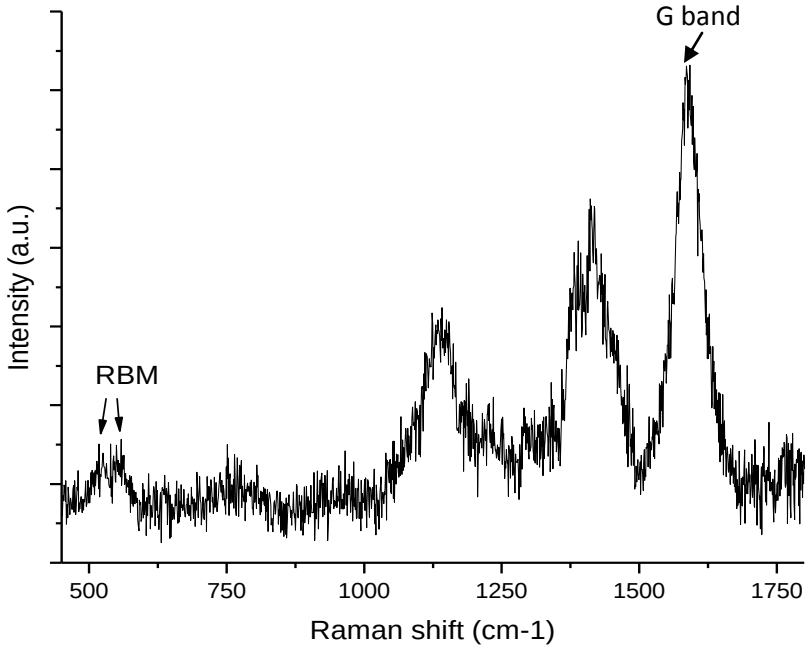

Figure 2.3 Raman spectra (after baseline correction) of the 0.4nm SWNTs formed inside the channels of $AlPO_4$-5 crystals excited using the Renishaw's invia micro raman 633nm laser line measured at room temperature.

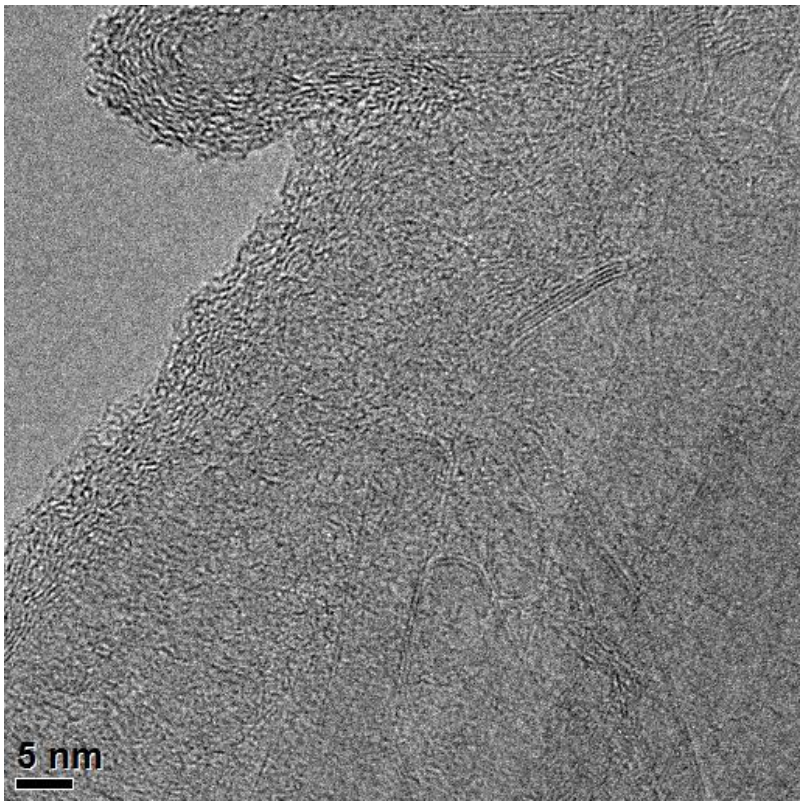

Figure 2.4 High resolution transmission electron microscope (TEM) image showing SWCNTs. The TEM image was taken after the AFI framework was removed by using HCl acid.

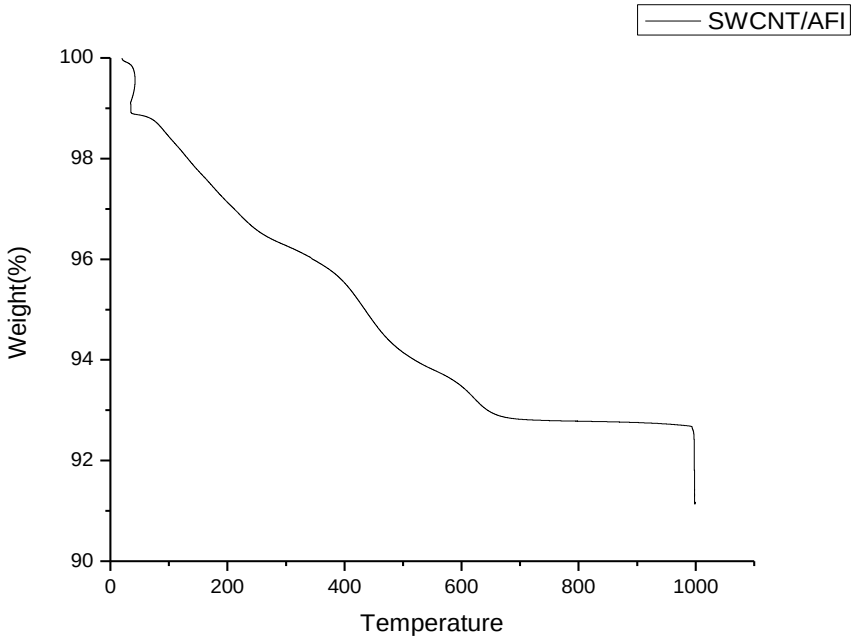

Figure 2.5 The TG curve measured at temperature ranging from 30◦C to 1000◦C of $AlPO_4$-5 crystal with TPA organic template inside the channels in N_2 gas. After pyrolysis in N_2, the sample is burnt at 1000 ℃ under air for 20minutes.

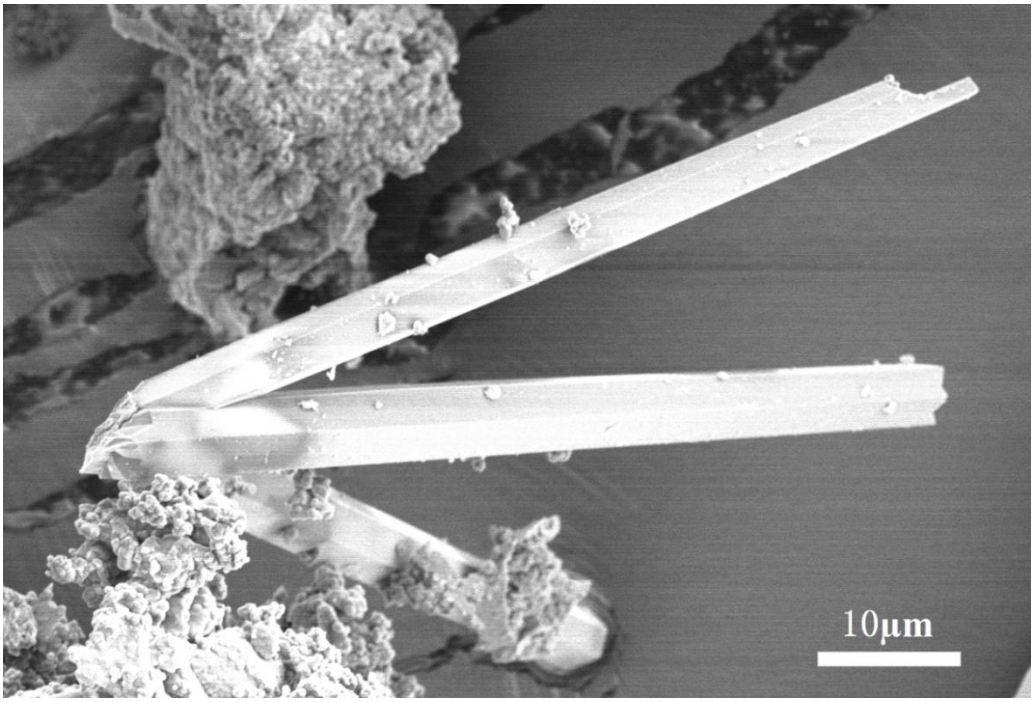

Figure 2.6 SEM image of $AlPO_4$-5 sample with gel composition of $1.0Al_2O_3$: $1.0P_2O_5$: 1.4TPA: 0.5 H_2SO_4: $400H_2O$

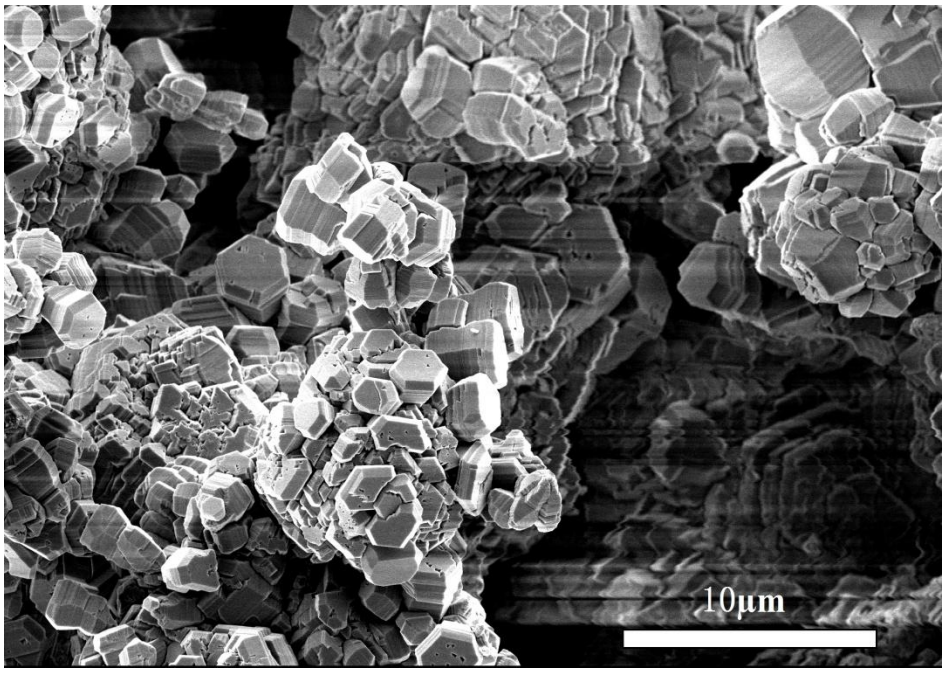

Figure 2.7 SEM image of $AlPO_4$-5 sample with gel composition of $1.0Al_2O_3$: $1.4P_2O_5$: 1.4TPA: $450H_2O$

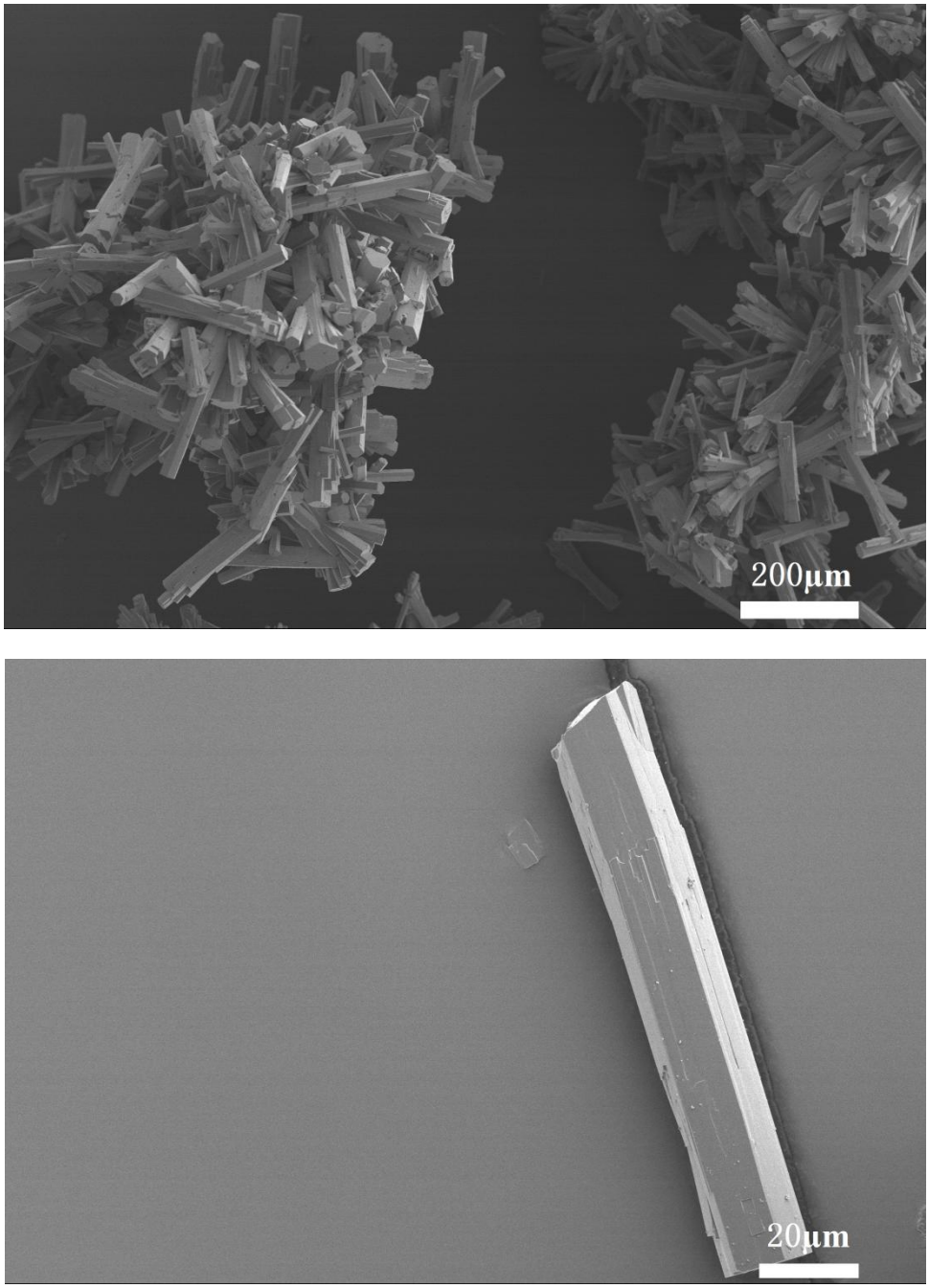

Figure 2.8 SEM image of $AlPO_4$-5 sample with gel composition of $1.0Al_2O_3$: $1.0P_2O_5$: 1.2TPA: 0.8HF: $400H_2O$

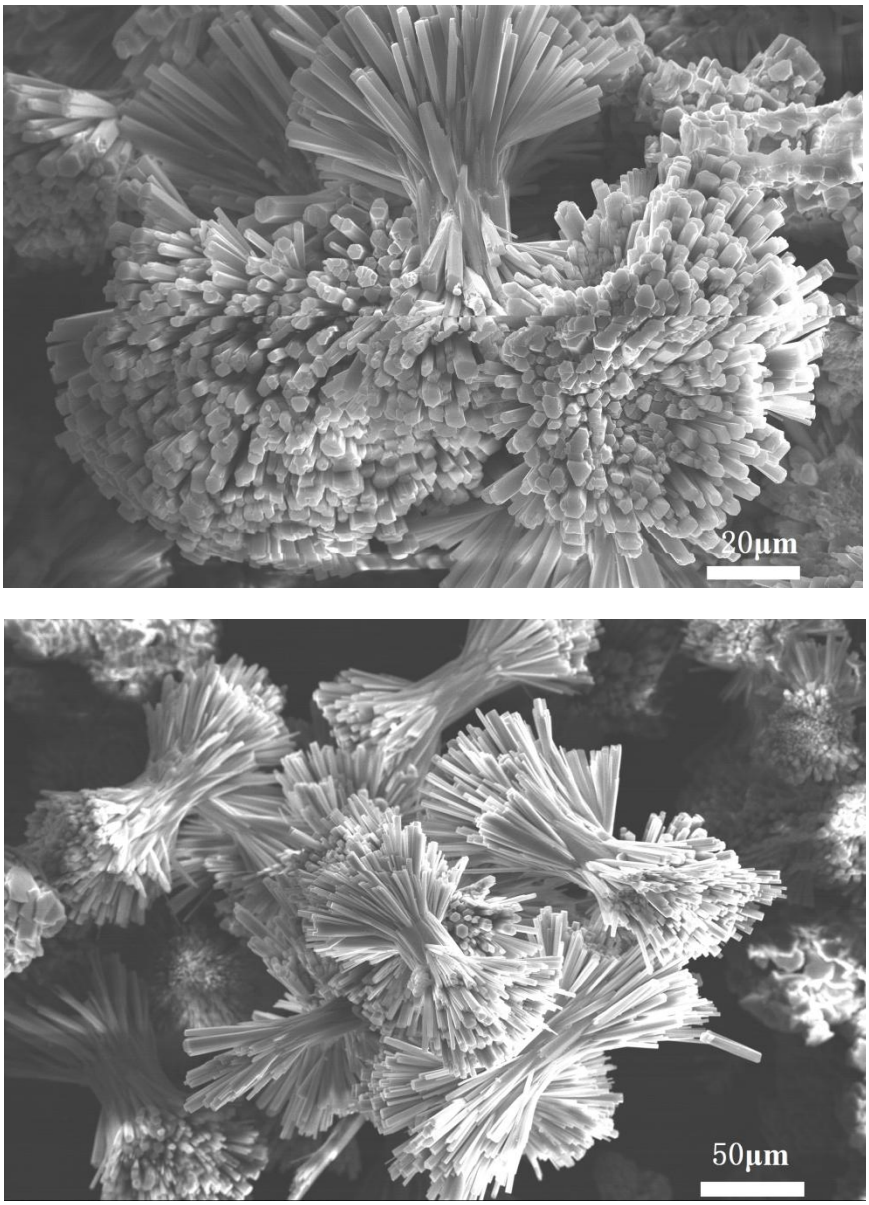

Figure 2.9 SEM images of $AlPO_4$-5 crystals with gel composition of $1.0Al_2O_3$: $1.0P_2O_5$: 1.0TPA: $100H_2O$ at different magnification

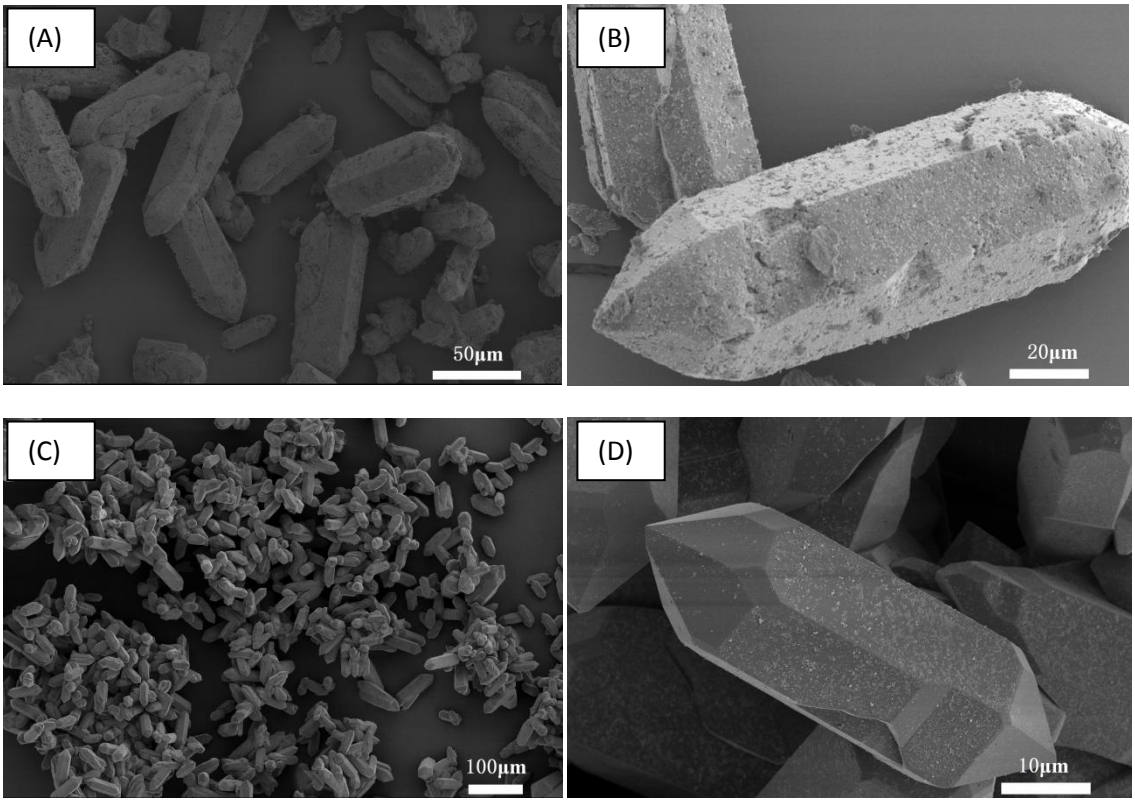

Figure 2.10 (a) and (b) SEM images of $AlPO_4$-5 crystals with gel composition of $0.2Co:1.0Al_2O_3: 1.0P_2O_5: 1.2TPA: 0.8HF: 450H_2O$; (c) and (d) SEM images of $AlPO_4$-5 crystals with gel composition of $0.07Co:1.0Al_2O_3: 1.0P_2O_5: 1.2TPA: 0.8HF: 800H_2O$

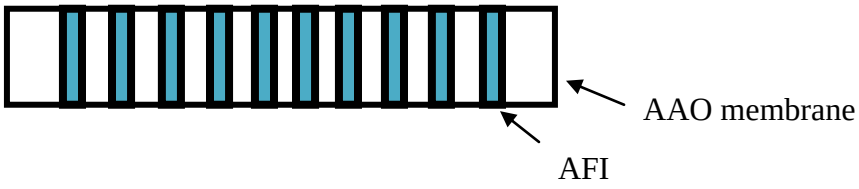

Figure 2.11 Schematic illustration of $AlPO_4$-5 growth inside the channels of AAO membrane

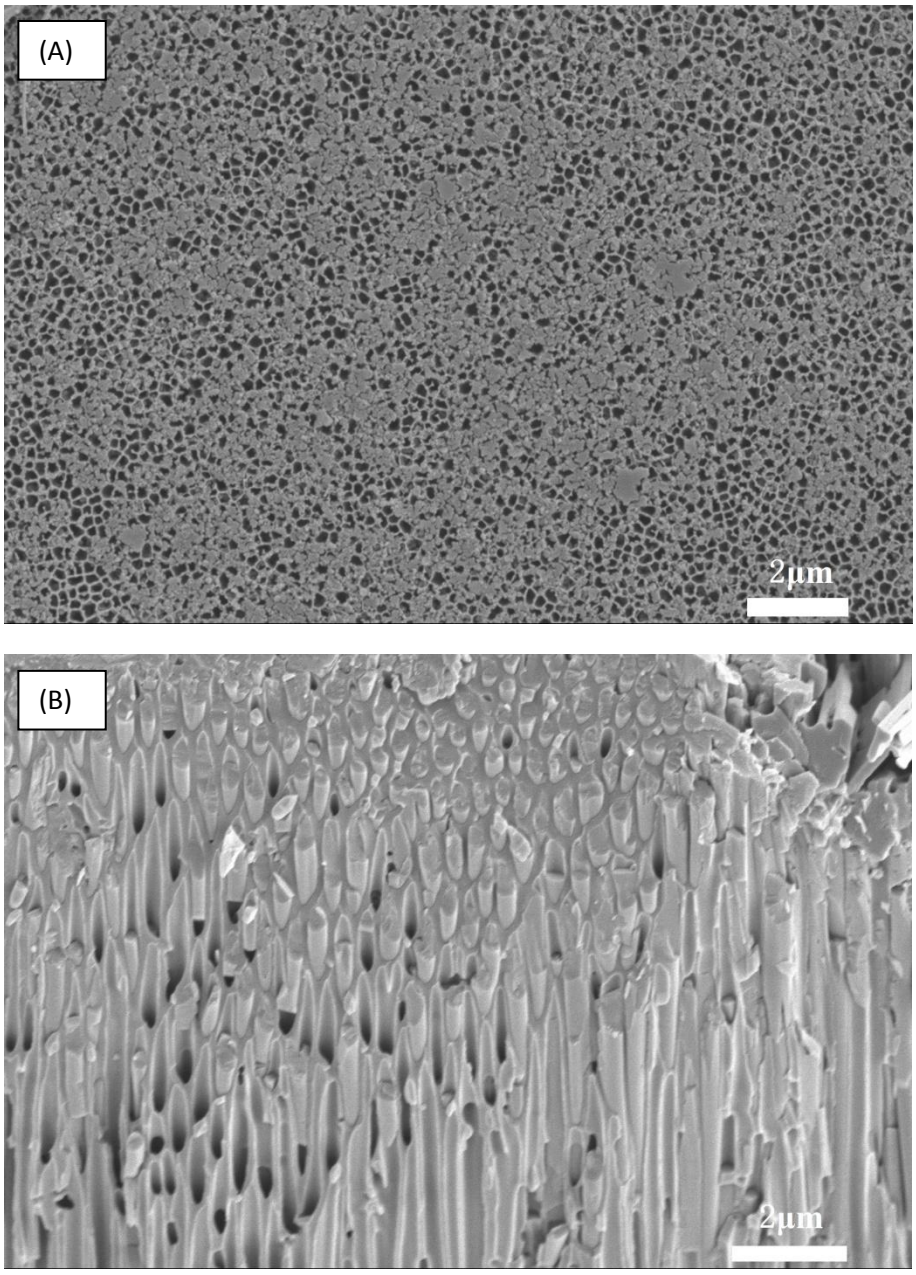

Figure 2.12 SEM images of $AlPO_4$-5 growth in AAO membrane. AAO membrane was not added to the autoclave until after 90◦C treatment. (A) top surface of the sample (B) A broken edge of $AlPO_4$-5 growth inside AAO membrane, showing crystal growth.

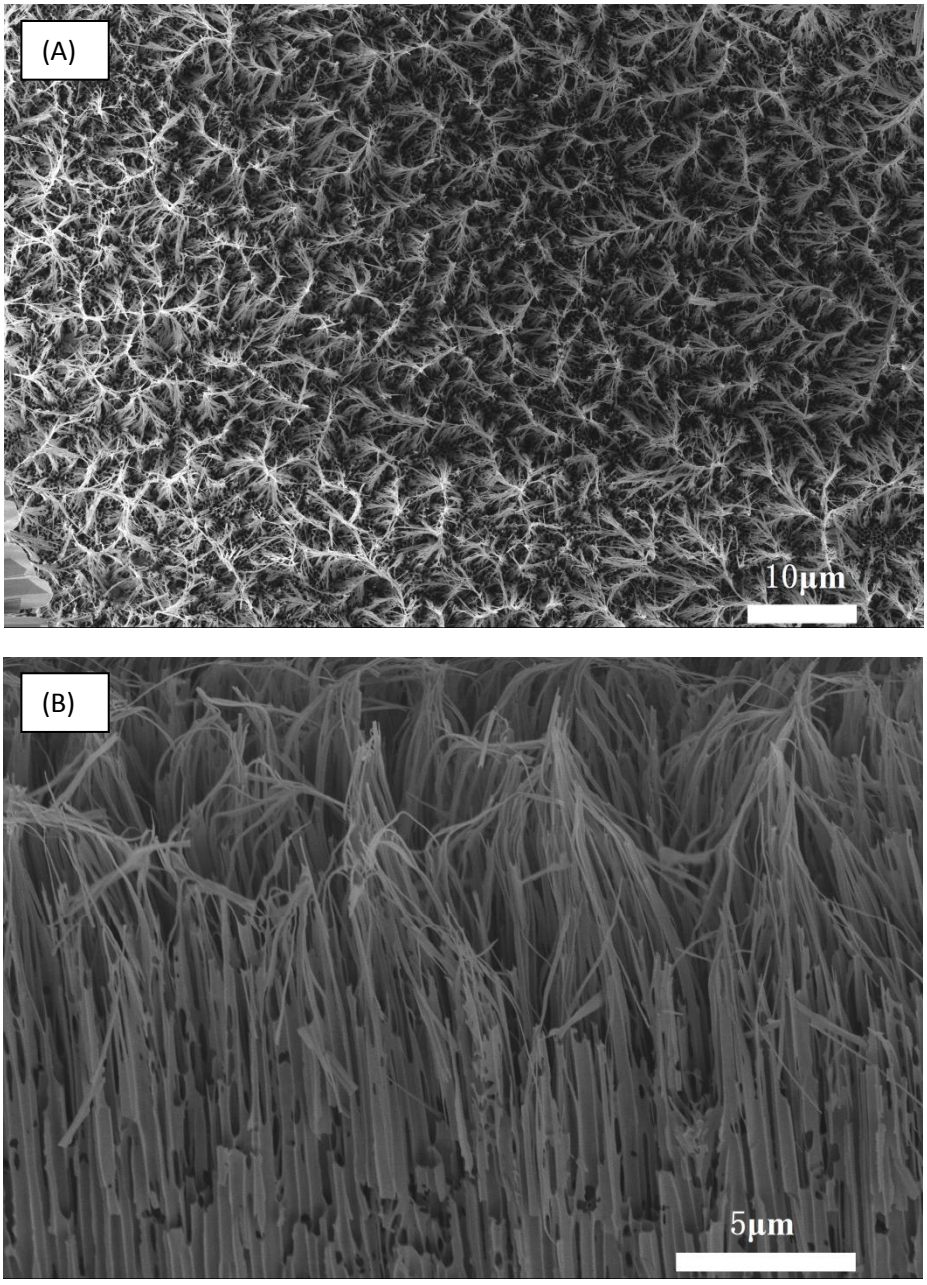

Figure 2.13 SEM images of $AlPO_4$-5 growth in AAO membrane. The AAO membrane added to the autoclave at the beginning and heated at 453k for 24h. It shows hair like structure of AAO membrane. (A) top surface of the sample (B) A broken edge of AAO membrane.

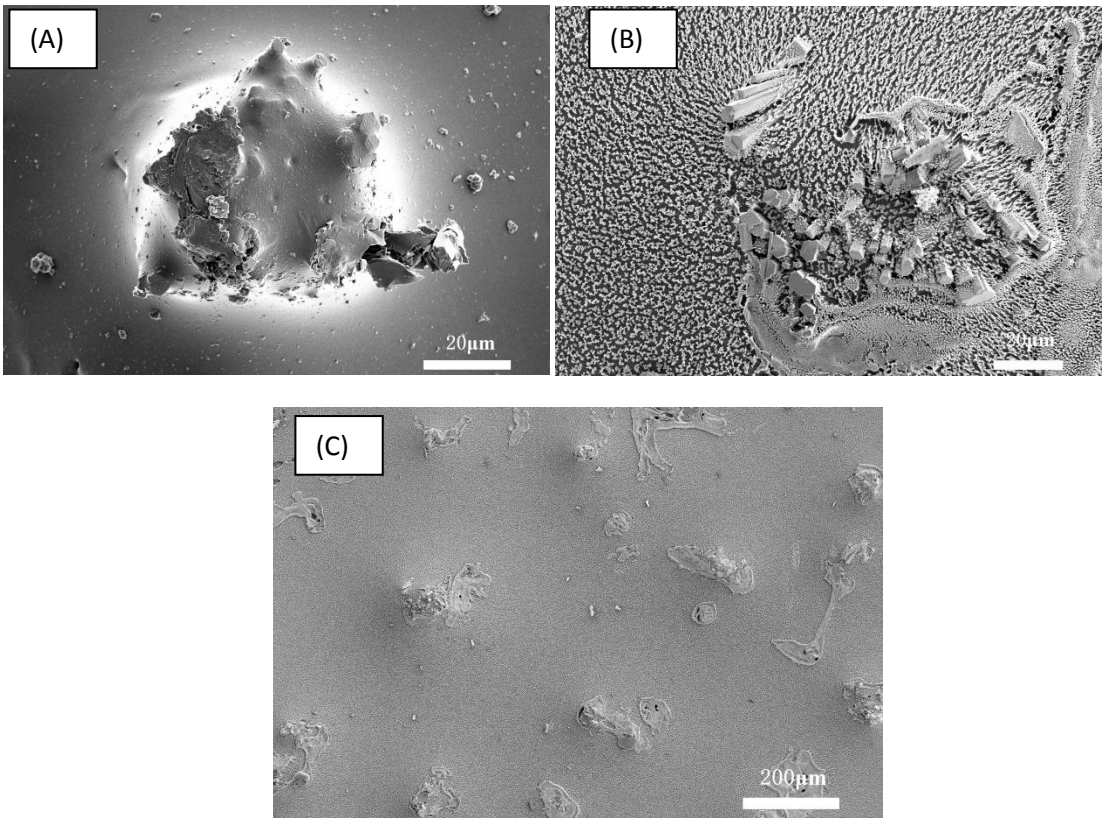

Figure 2.14 $AlPO_4$-5 spin coated with epoxy, (A) before etching (B) after O_2 RIE etching (C) lower magnification of RIE etched sample

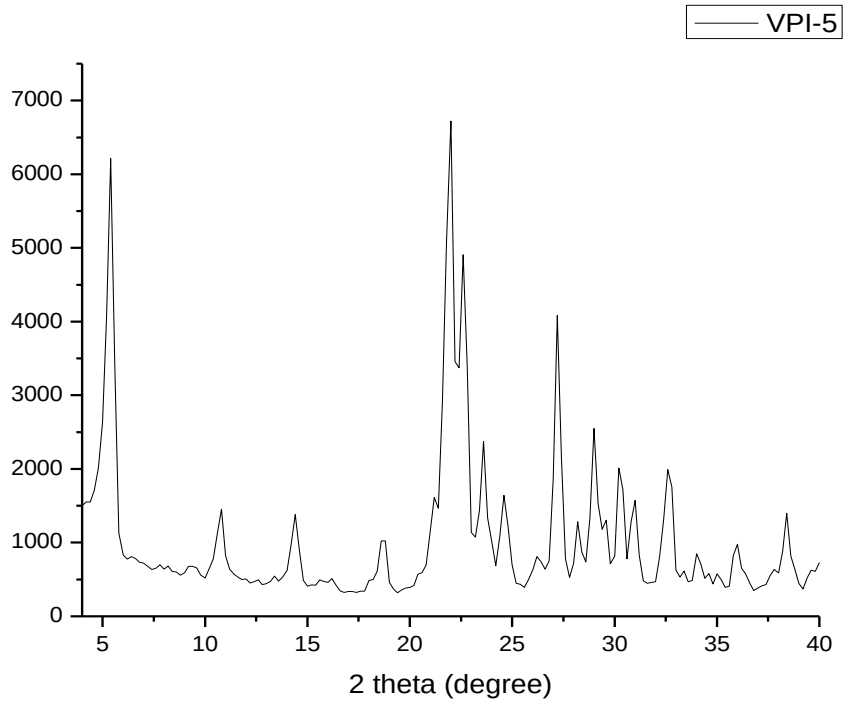

Figure 2.15 XRD of VPI-5

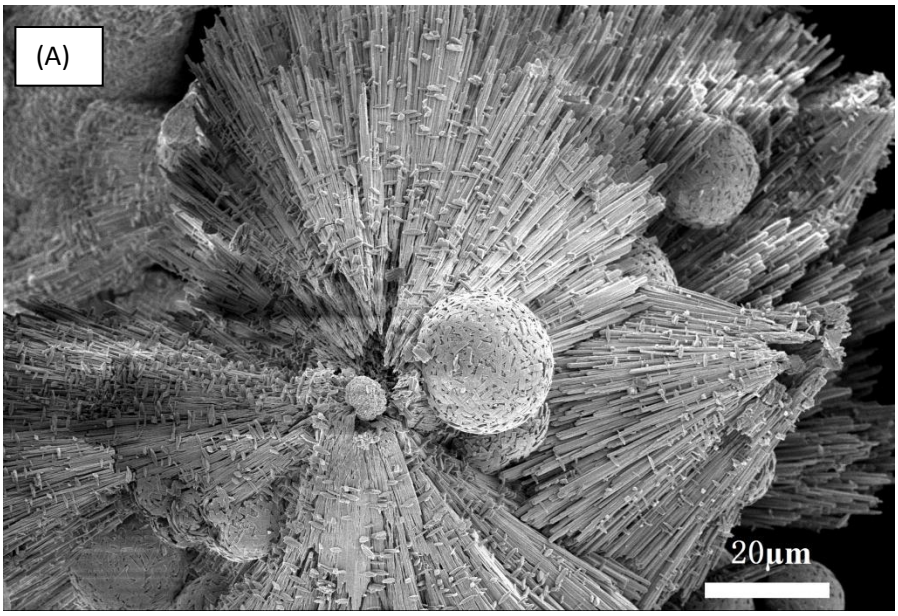
(A)
20μm

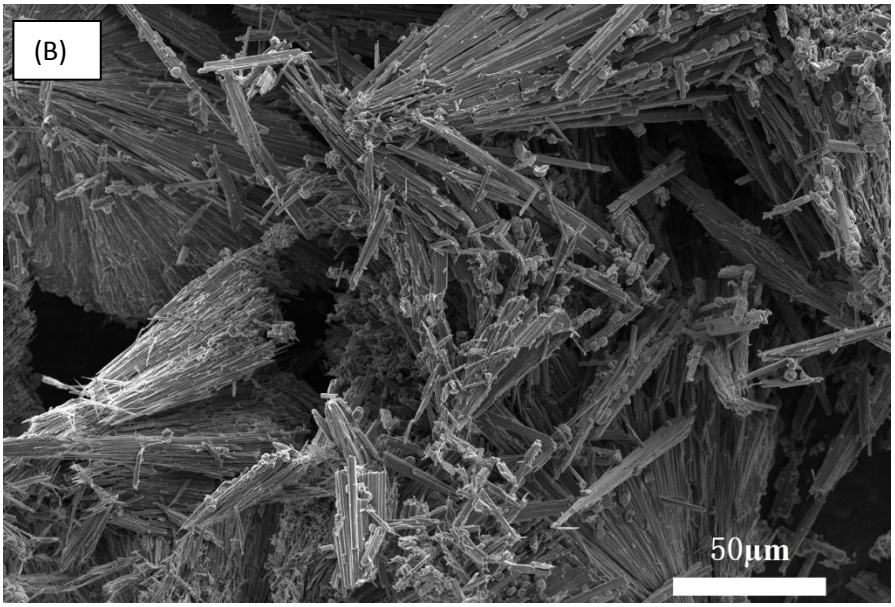
(B)
50μm

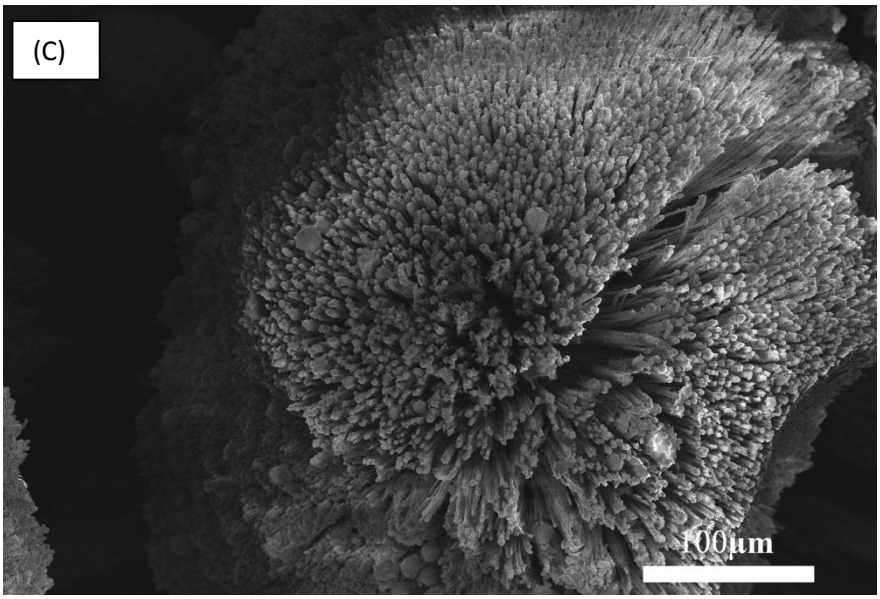

Figure 2.16 SEM images of (A) VPI-5 crystals (B) same sample with different magnification (c) same sample showing the needles radiating from a center point

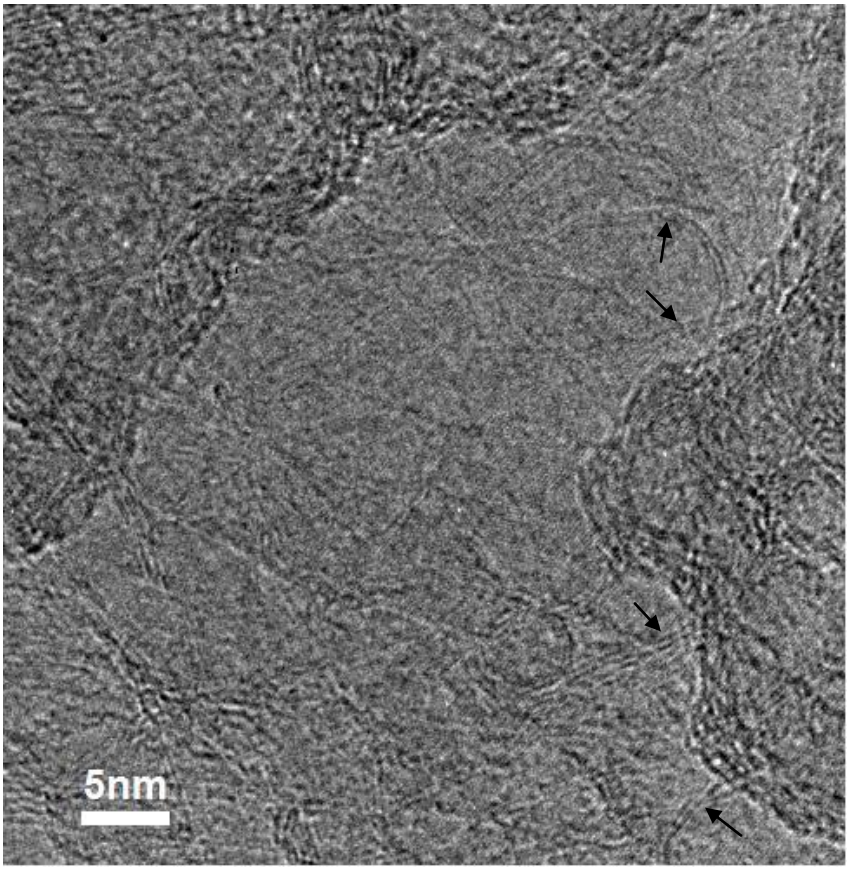

Figure 2.17 TEM image of VPI-5/sugar/Co sample after removal of zeolite with HCl solution

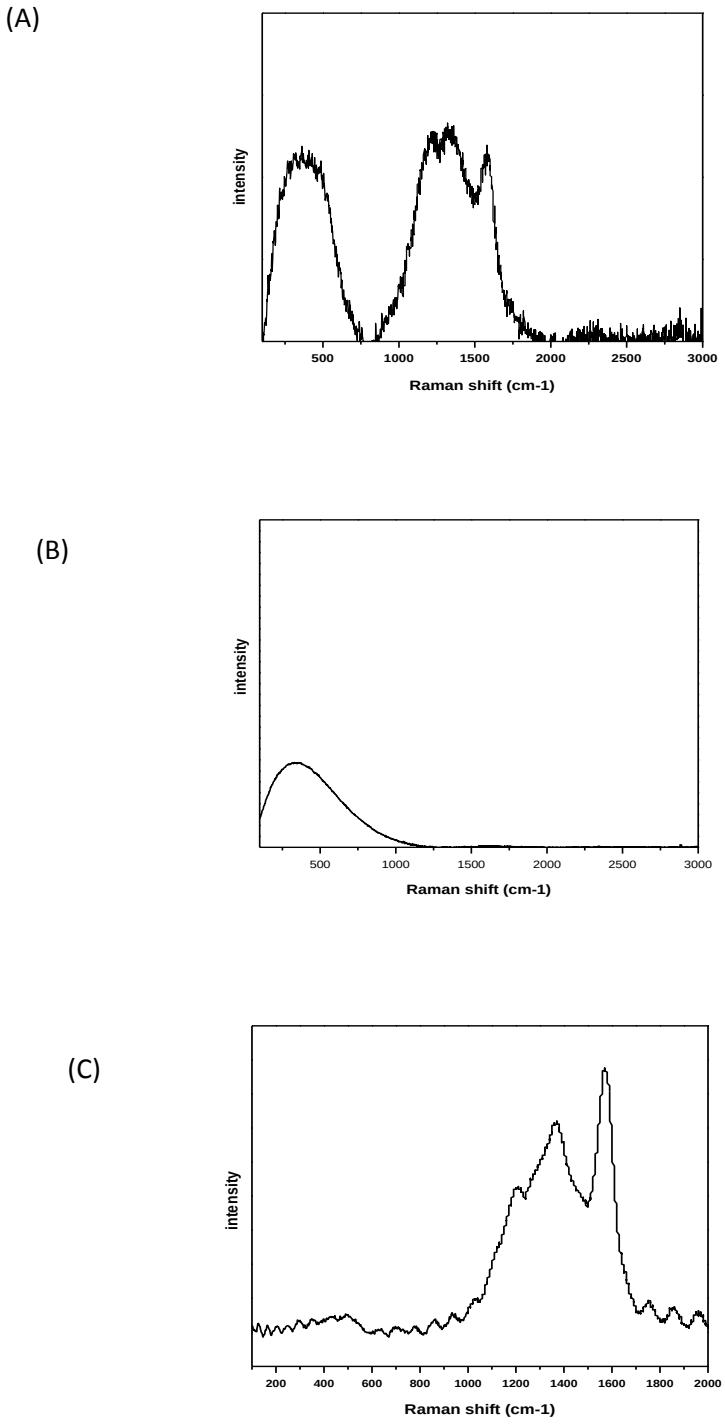

Figure 2.18 Micro Raman spectra measured by Thermo Scientific 780nm laser excitation at room temperature (A) SWNTs inside the channels of VPI-5 crystals (B) VPI-5/sucrose before pyrolysis (C) after removal of zeolite template.

(A)

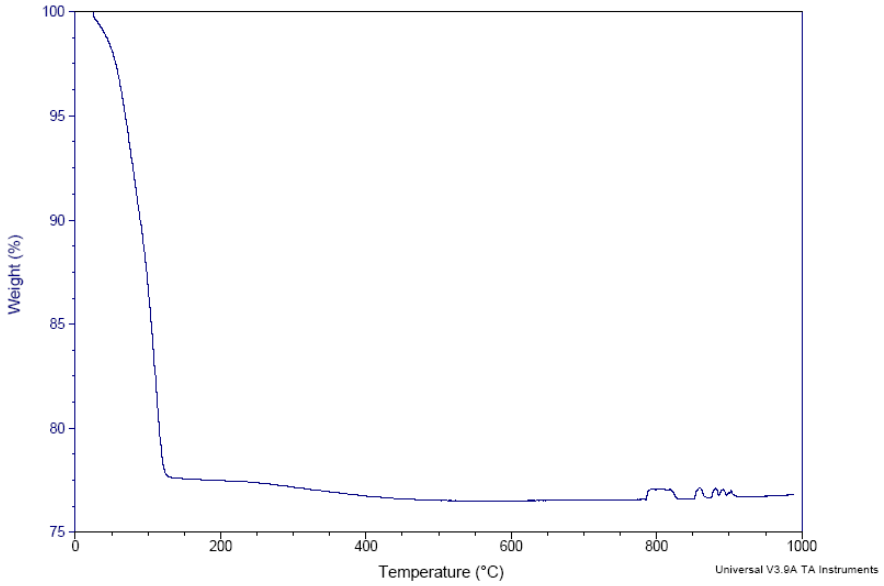

(B)

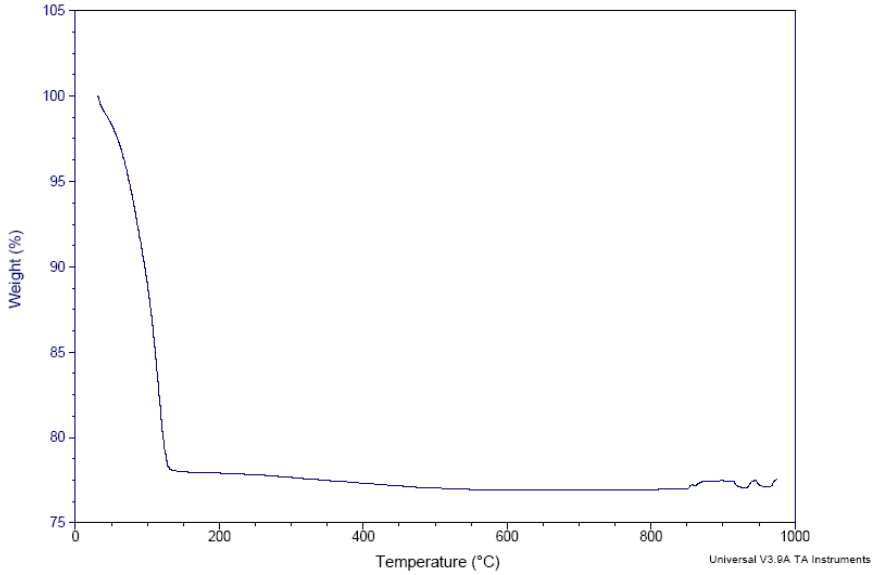

Figure 2.19 TGA of as synthesized VPI-5 crystal with water inside the channels (A) pyrolysis in N_2 gas. (B) TGA of as synthesized VPI-5 crystal burn at 1000◦C in air.

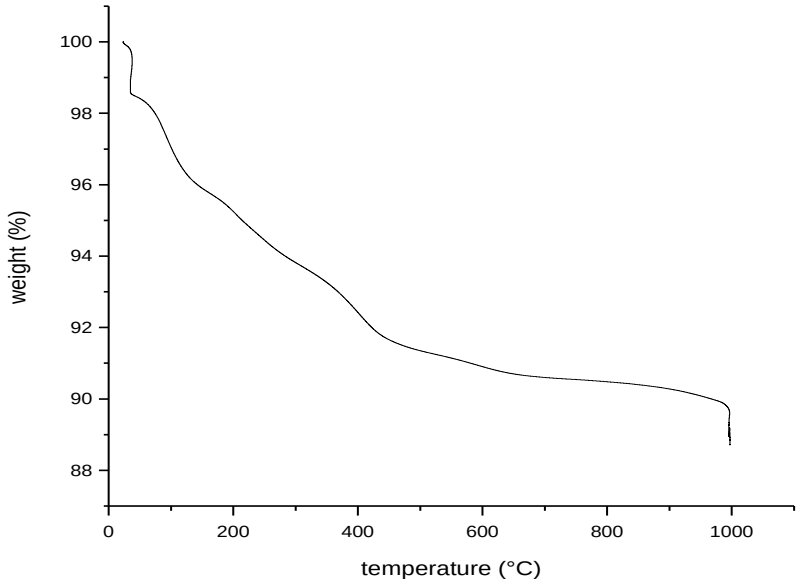

Figure 2.20 The TG curve of VPI-5 crystal with sugar inside the channels pyrolysis in N_2 gas, and then burn at 1000◦C in air.

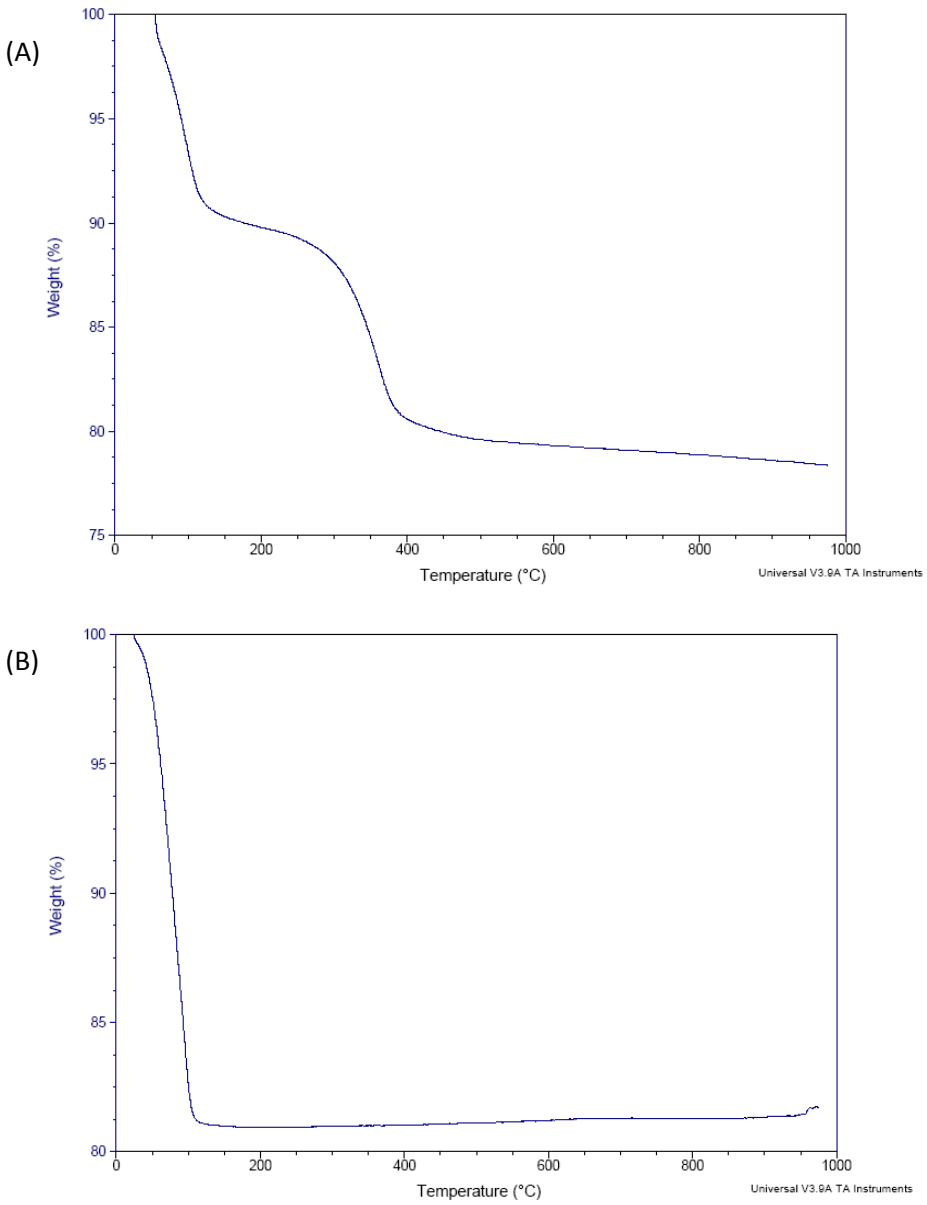

Figure 2.21 The TG curve of VPI-5 crystal with PEG (A) pyrolysis in N_2 gas, (B) the pyrolyzed sample burnt at 1000◦C in air.

(A)

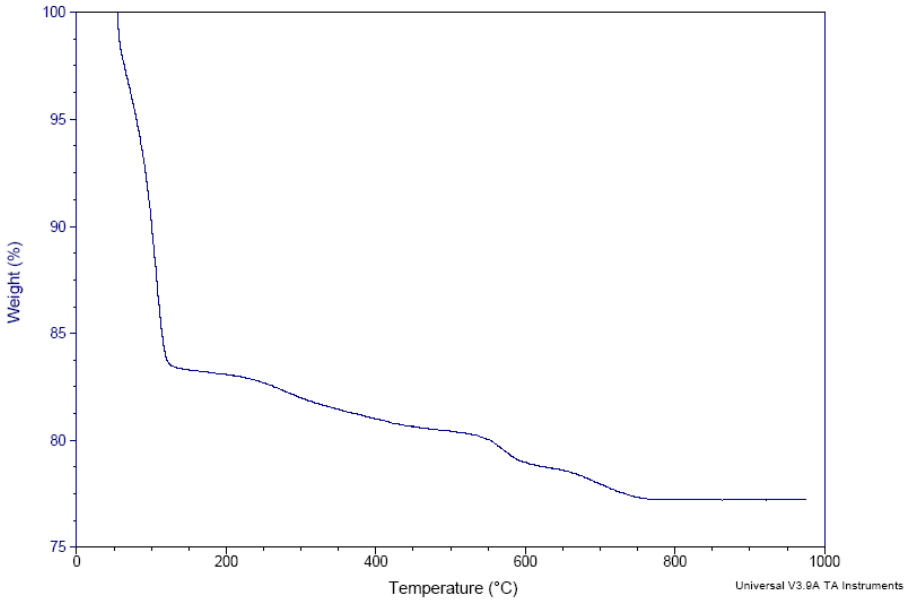

(B)

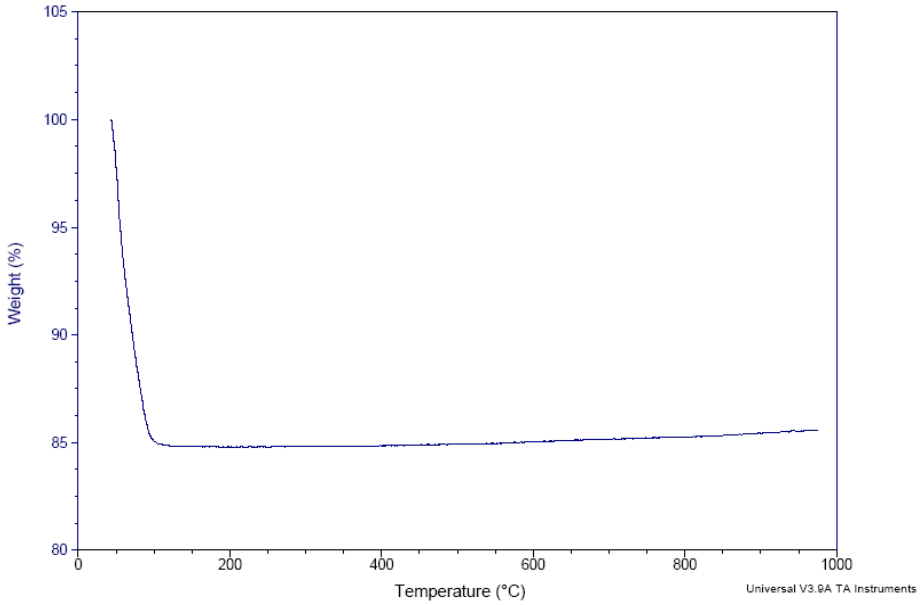

Figure 2.22 The TG curve of VPI-5 crystal with Ni phthalocyanines (A) pyrolysis in N_2 gas, (B) the pyrolyzed sample burnt at 1000◦C in air.

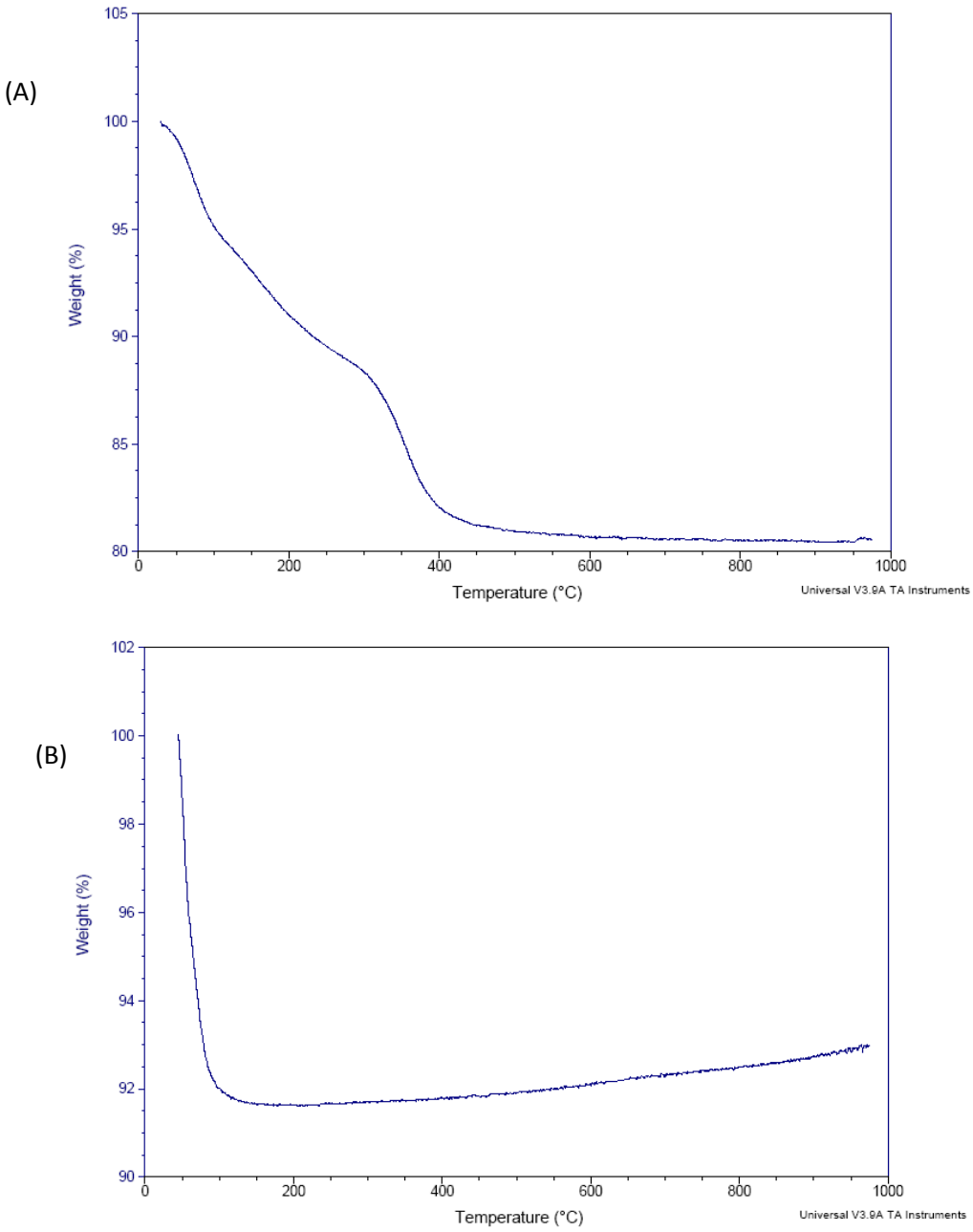

Figure 2.23 The TG curve of VPI-5 crystal with triton (A) pyrolysis in N_2 gas, (B) the pyrolyzed sample burnt at 1000◦C in air.

(A)

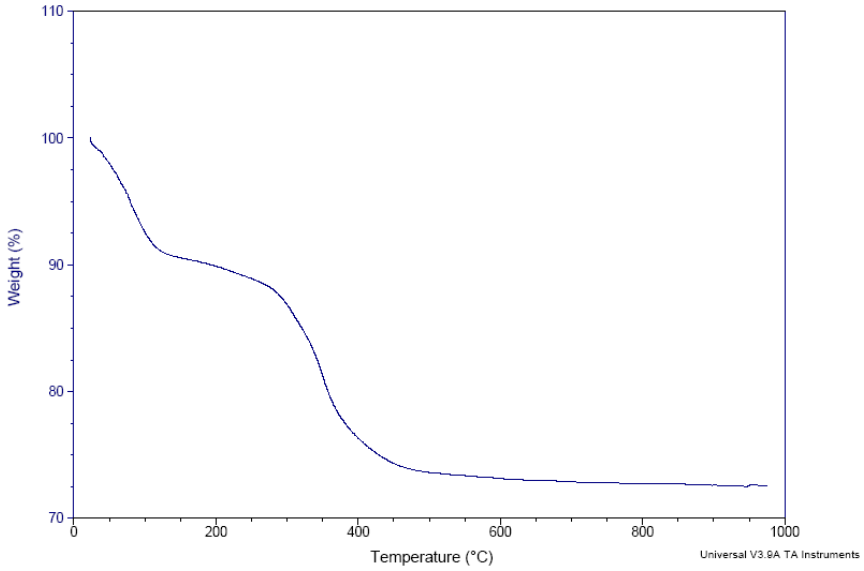

(B)

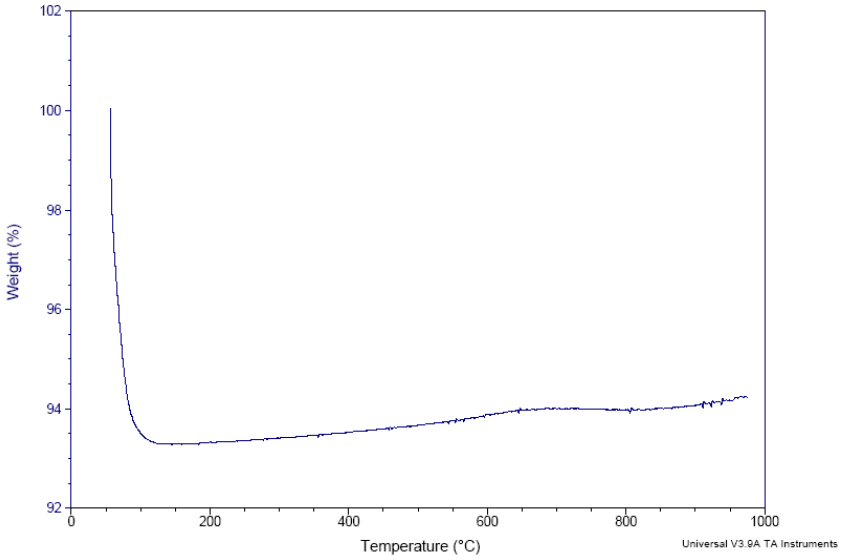

Figure 2.24 The TG curve of VPI-5 crystal with ionic liquid sample #1 (A) pyrolysis in N_2 gas, (B) the pyrolyzed sample burnt at 1000◦C in air.

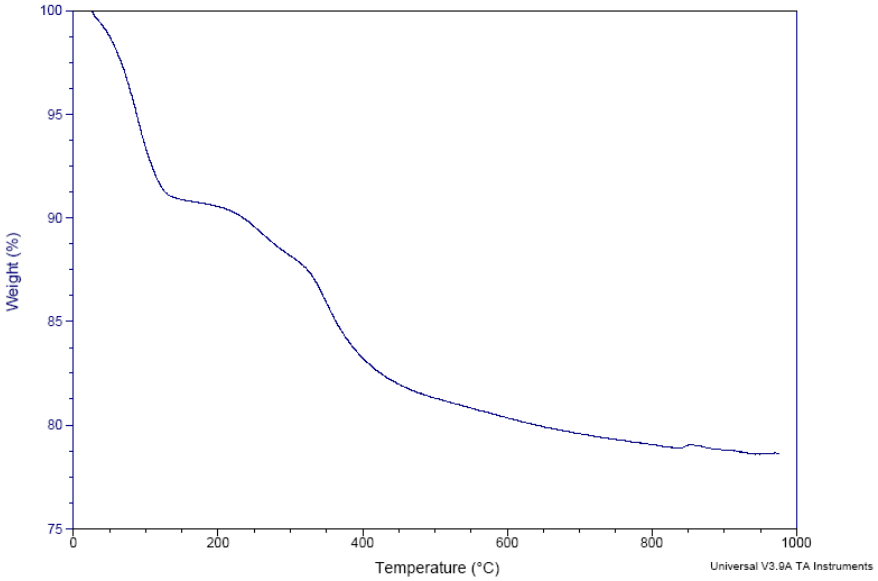

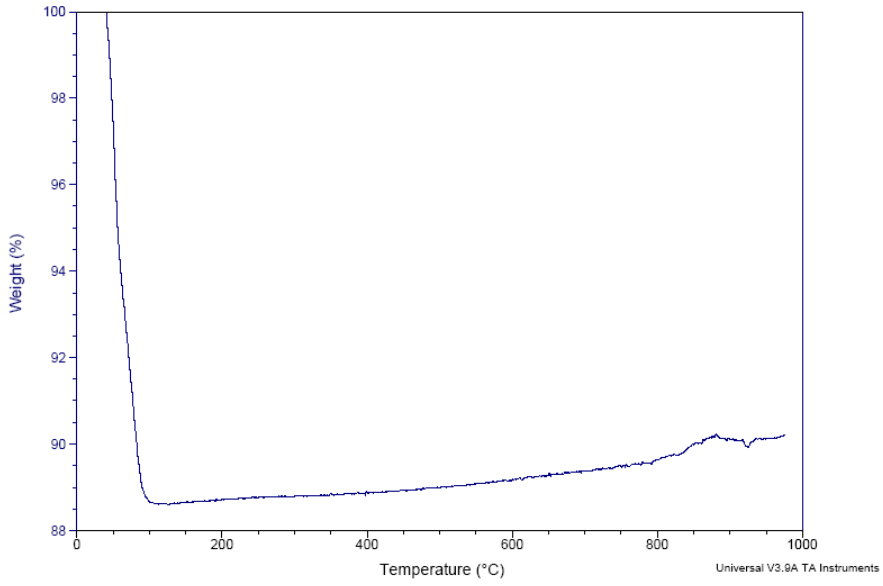

Figure 2.25 The TG curve of VPI-5 crystal with ionic liquid sample #2 (A) pyrolysis in N_2 gas, (B) the pyrolyzed sample burnt at 1000◦C in air.

(a)

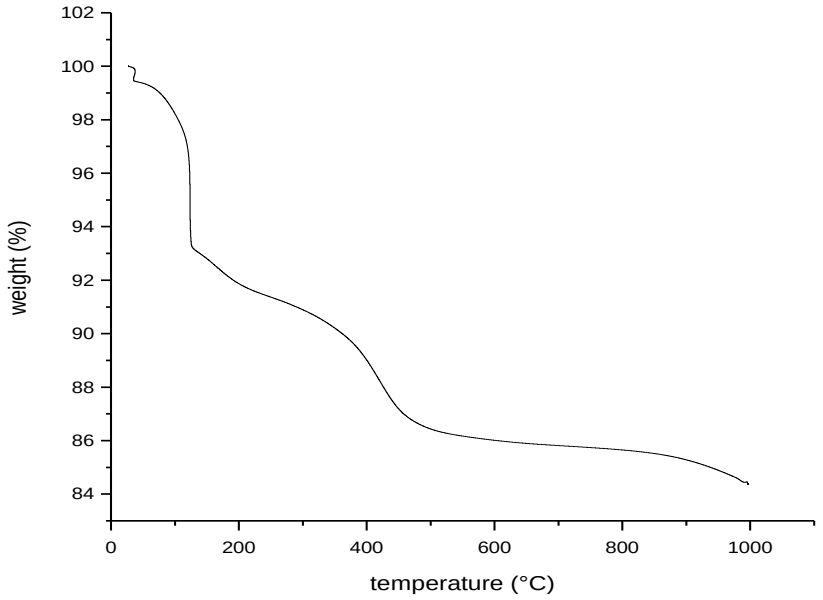
102
100
98
96
94
92
90
88
86
84
weight (%)
0
200
400
600
800
1000
temperature (°C)

(b)

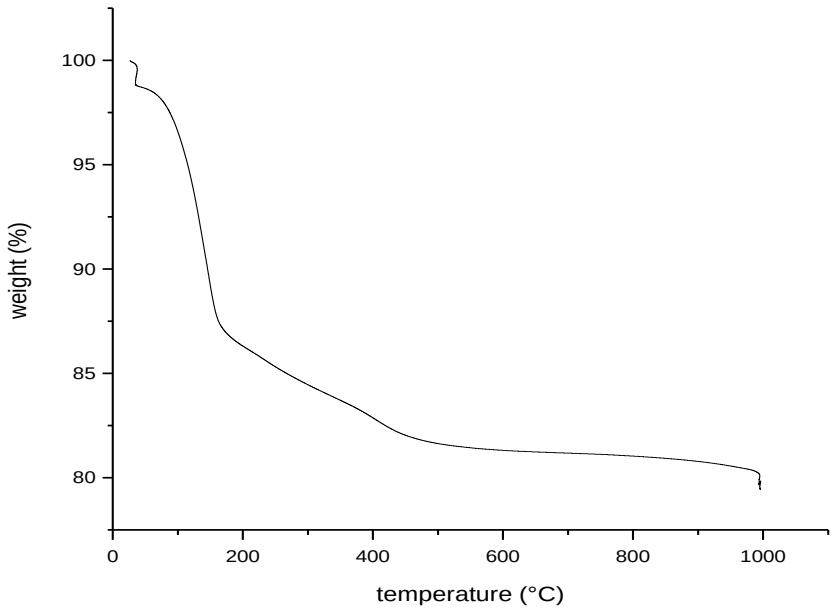
100
95
90
85
80
weight (%)
0
200
400
600
800
1000
temperature (°C)

(c)

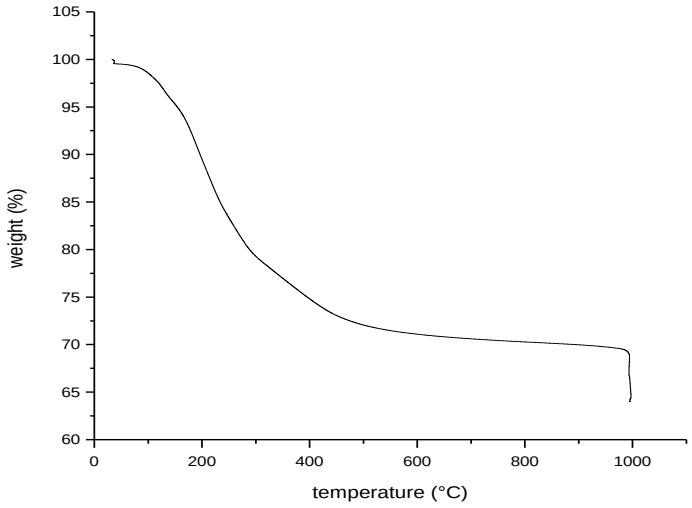

Figure 2.26 The TG curve of VPI-5 crystal with fructose inside the channels pyrolysis in N_2 gas, and then burn at 1000◦C in air. (a) fructose-sample #1 (b) fructose-sample #2 (c) fructose-sample #3

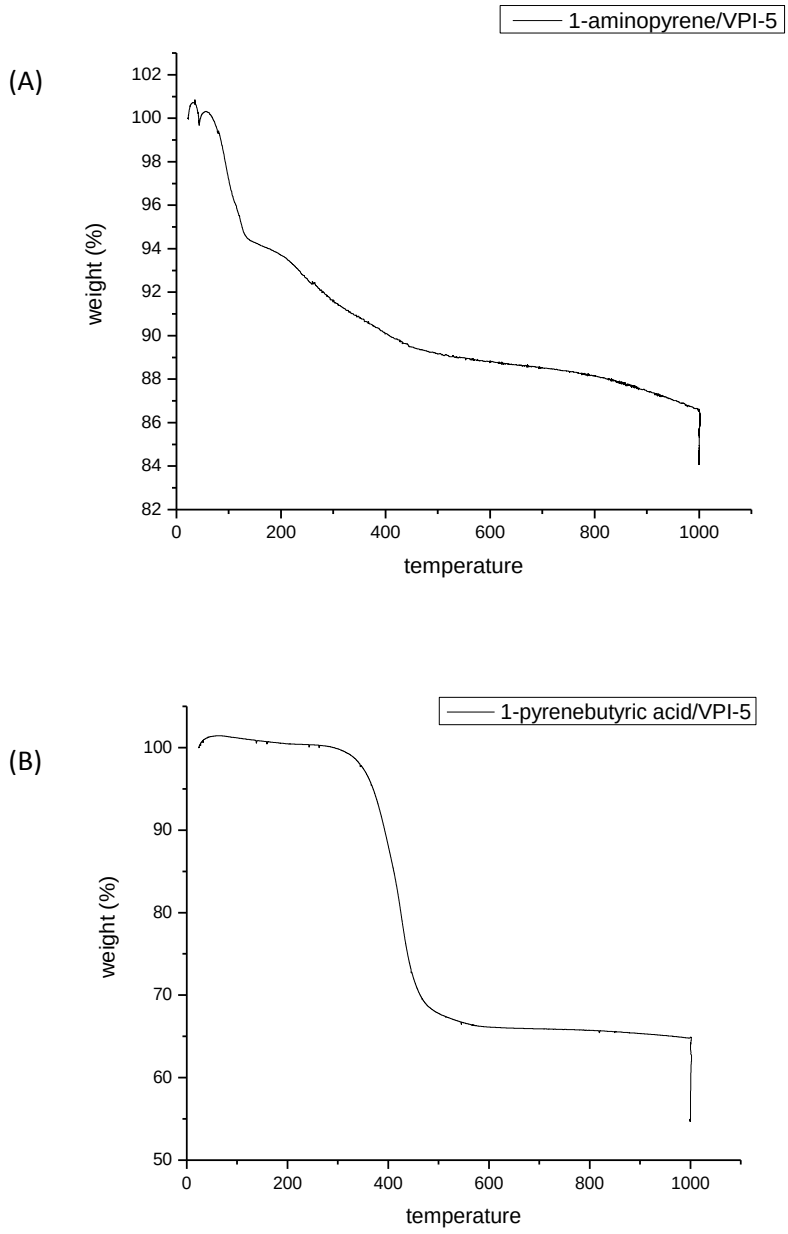

Figure 2.27 The TG curve of VPI-5 crystal with (A) 1-aminopyrene inside the channels pyrolysis in N_2 gas, and then burn at 1000◦C in air. (B) with 1-pyrenebutyric acid inside the channels pyrolysis in N_2 gas, and then burn at 1000◦C in air.

Chapter 3 Fabrication of conductor/insulator/conductor multilayer structures for DNA sequential reactions

3.1 Introduction

Nanopore analytics is an attractive area which can be used for biomolecule sensing, such as peptides, proteins and DNA strands. It is because that the amount of current is very sensitive to the size and shape of nanopore. If nanoparticles pass through the nanopore, it can create a change of the current and corresponding transmembrane voltage through the nanopore. In this way, signal data is obtained, and each current pulse is due to a single molecular translocation.

Many techniques have been developed to fabricate this nanopore sensing device, such as natural protein pores[4, 5], nanopores in silicons [6-13] , organic polymer [14-21], graphene[26-30], and individual carbon nanotube pores[22-24]. Most of these nanopores just have only a single layer, but not multilayer structure.

For better control of DNA translocation, and make it more readable, we tried to fabricate multilayer structure. There are three advantages, firstly, in this structure each layer is several nanometers thick and can be individually addressed with voltage. Secondly, the conductive layer can be chemically functionalized to control a DNA strand passing through the nanopore. Finally, voltage between the conductive layers can change the

electric field inside the nanopore. This interaction between the electric field and the DNA molecule might trap DNA in the nanopore. [45-47]

A critical point for DNA sequencing is that both the diameter of the pore must be controlled for straight DNA passage and the interaction length (in flow direction) at the constriction point must be within the length of nucleic acid sequence length (~1nm). The latter point has largely been ignored or not controlled. Graphene nanopore might be an ideal electrode because of its atomic thick property. Recently, Bashir et al. drilled nanohole in graphene/Al_2O_3 multilayer structure by focus ion beam (FIB). [30] In this thesis, we propose to control this interaction length by using a thin lipid bilayer film in multilayer structure to avoid of using the high cost of FIB.

Two system of conductor/insulator/conductor system and conductor/lipid bilayer system were chosen to produce the nanopore structure. In conductor/insulator/conductor multilayer structure, one is carbon conductor and S1813 insulator, the other is copper conductor and S1813 insulator. Carbon materials have been employed due to a number of advantageous properties, such as low-cost, disposable, easy to etch with reactive ion etching (RIE). [110, 111] However, the conductivity of carbon materials is not good for further pore functionalization. Copper is employed due to its excellent electrical conductivity, which widely used in electronic industry. The second system has lipid bilayer formed in the pores of silicon oxide membrane. This structure has monolayer thick ‘interrogation’ chemistry at pore exits necessary to resolve DNA units.

3.2 Experimental

3.2.1 Chemicals

Table 3.1 Chemicals used and manufacturers

Chemical	Manufacturer
Carbon graphite target	Kurt J. Lesker (99.999%)
Cu target	Kurt J. Lesker (99.999%)
Ni target	Kurt J. Lesker (99.999%)
S1813 (positive photoresist)	Rohm and Haas Electronic materials LLC
PMMA (positive photoresist)	Microchem
(100) SiO_2 wafer	University Wafer
Oxalic acid	Aldrich (99%)

3.2.2 Experimental details

3.2.2.1 Carbon/photoresist/carbon structure

3.2.2.1.1 SiO_2 as mask

As shown in Figure 3.2, silicon oxide wafer is used. In step 1, a Si wafer with 100 nm SiO_2 layer was ultrasonically cleaned with acetone, isopropanol (IPA), deionized (DI) water, and nitrogen drying. S1813 was diluted in the Thinner P solvent with the volume ratio of 1:10. Then appropriate diluted Shipley 1813 positive photo resist solution is spun coated on a silicon wafer. The sample is baked at 115 ℃ for 1min.

In step 2, thin flat carbon film is prepared by sputtering method. The sputtered films have been deposited from a 50mm diameter graphite target in an atmosphere of high purity argon. Argon of 99.99% purity at constant pressure of 3.6 mtorr was used as a sputtering gas in the experiment. Carbon was RF magnetron-sputtered at a power of 100W and the film with a thickness of 15nm was deposited in the constant rate of 0.2 Å/s. The quartz crystal used to monitor the rate of deposition was also used to determine the final thicknesses of the deposited carbon films. Step one and two are repeated for obtaining a multilayer structure.

In step 3, 100nm thick SiO_2 is deposited by RF sputtering at a power of 100W, followed by spin coating with 2% PMMA at 5000rpm. E beam lithography is used for creating nanopore structures in PMMA which can subsequently be transferred to the substrate materials.

Finally, in order to pattern a SiO_2 layer, a RIE process in C_4F_8/O_2 was used to transfer the image from the PMMA layer to SiO_2 layer. It uses chemically reactive plasma to remove material. The etching rate of SiO_2 is about 100nm/min. Then porous SiO_2 membrane is used as a template during the O_2 reactive ion etching (RIE) process. Oxygen is used to etch through the polymer/carbon multilayer.

3.2.2.1.2 Anodic Aluminum Oxidation (AAO) as mask

AAO preparation

Anodic oxidation was carried out on 1μm thick aluminum films in 0.3M oxalic acid solution at room temperature using Pt as a counter electrode (Fig.3.3). The anodization was conducted under a constant voltage mode (40 V) for approximately 4 min. Then the aluminum samples were etched in 0.3M phosphoric acid in order to enlarge the pore depth.

3.2.2.2 Copper/photoresist/copper structure

Our fabrication process is shown schematically in Figure 3.4. On the back side of the wafer, the SiO_2 was patterned using standard photolithography techniques to form an etch mask. We use a 2μm-thick layer of SiO_2 on both sides of a (100) silicon wafer as the substrate. Appropriate S1813 photoresist solution is spun coated on a silicon wafer. After baking at 115 ℃ for 1min, the sample is exposed at UV light for 6sec, and then put into MF319 developer for 30sec. Nickel was RF magnetron-sputtered at a power of 75W and the film with a thickness of 50nm was deposited in the constant rate of 1.2 Å/s. Then a lift-off step was employed to define the bottom electrode pattern via Shipley 1165 resist remover for 2h. The back oxide SiO_2 layer was then removed by RIE dry etching in C_4F_8/O_2 to transfer the image from the Ni layer to SiO_2 layer.

The backside of the wafer was exposed to a highly selective silicon etchant, KOH, which removes Si preferentially in the (100) plane. The back etching method is widely used in pattern silicon nanopores structure. [112], [113] The back etched pores serve as the mechanical support for the thin multilayer structure. The SiO_2 serves as the protective layer during the Si etching process, because the etching rates for SiO_2 and Si in 20%

KOH at 70 ℃ are 50μm/h and 100nm/h, respectively. The window area was etched down to around 200μm.

On the top side, 20nm Ni layer is obtained by sputtering. Appropriate S1813 photo resist solution is spun coated above the Ni layer. Then standard photolithography technique is used in order to obtain the nanopore structure. The nickel layer is then patterned in an aqueous solution of $FeCl_3$ and HCl mixture by wet etching method. Wet etching use liquid chemicals or etchants to remove materials, which is generally isotropic. Finally, the oxide layer pore is opened by RIE etching.

We electroplated Cu nano-particles at the edge of conductive layer using the procedure outlined in Figure 3.5. 20nm Cu thin layer is sputtered on the SiO_2 wafer, and then e beam lithography is employed to fabricate nanopore structure in PMMA layer. Then we use $FeCl_3$ (6×10^{-5}M) and HCl (1×10^{-3}M) to etch Cu and get 2 μm Cu nanopores. The etching time is about 15sec. The reaction is set up on three electrode system in a U tube as shown in Figure 3.6. Ag/AgCl is the reference electrode, Pt is the counter electrode, the wafer is the working electrode, and the electrolyte is 1mM $CuSO_4$ solution.

3.3 Results and discussion

3.3.1 Carbon/photoresist/carbon system

RF magnetron sputtering has been used to obtain thin carbon layer. The result shows that the carbon film prepared by sputtering method has the properties of thickness reproducible and controllable with subnanometer precision. The interface roughness is

about 0.5nm. The rougness of carbon on the photoresist layer increased slightly because the roughness of PR (~1.5nm) is a little higher than the SiO_2 wafer (~0.3nm).

In order to obtain vertical pore structure, RIE dry etching method is employed. RIE process in C_4F_8/O_2 mixture is used to transfer the image from the PMMA layer to the SiO_2. The SiO_2 serves as the protective layer, since carbon and photoresist can be easily removed by oxygen, while the SiO_2 still remains. The etch rates have been determined as 100nm/min with pressure at 30mtorr. The carbon film can be finely patterned by O_2 RIE. The etching rate of carbon and photoresist in O_2 are 30nm/min and 340nm/min, respectively. The detailed condition of RIE etching is shown in Table 3.2.

The property of RIE controlled oxygen etched holes is investigated by SEM as shown in Figure 3.7. The SEM images show that both the 2μm and 200nm pores have very uniform, orientationally aligned, nanometer sized pores with vertical sides. It is important to note that we use RIE to produce gaseous byproducts that leave the pore structure. If physical sputtering/ion-milling were used, the back sputtering would short out or cover the multilayer structure. However, the carbon layer is not conductive enough for the Cu electroplating step, which may due to the formation of sp^3 clusters. Several other methods have also been used for the fabrication of thin carbon film including flash evaporation, e beam evaporation and thermal evaporation, but the carbon layer is still not so conductive.

Table 3.2 RIE etching rate and pressure

materials	Etching rate	RIE gas flow and pressure
PMMA	260nm/min	C_4F_8 gas flow = 45sccm; O_2 gas flow=5 sccm; Pressure=30mtorr
SiO_2	100nm/min	
S1813	340nm/min	O_2 gas flow = 30 sccm; Pressure = 35 mtorr
carbon	30nm/min	

Anodic aluminum oxide, which has high pore density and high level of ordering, might also be an excellent mask material for the fabrication one-dimensional pores. In 1995, Masuda and Fukuda reported the two-step anodization process, in which they obtained self- ordered alumina structures [114]. Here, anodic porous alumina is fabricated by one step method because of the thin Al layer. Different etching time and phosphoric acid concentration are used to find the best etching condition.

The growth of porous aluminum oxide is as following step. Firstly, hydrogen ions are reduced to hydrogen gas at cathode and aluminum is oxidized into aluminum oxide. Then a barrier oxide layer forms. The anodic reaction is given in (1) and (2) [115]

$$6OH^- - 6e^- \rightarrow 3H_2O^{2-} \qquad (1)$$

$$2Al + 3O^{2-} \rightarrow Al_2O_3 \qquad (2)$$

The cathodic reaction is given as (3)

$$6H^+ + 6e^- \rightarrow 3H_2 \qquad (3)$$

Secondly, part of the aluminum oxide is dissolved into the electrolyte and some small paths start to grow. The electric field is focused at the bottom of paths and enhances its

dissolution. Then the pores continue growing and become enlarged. Finally, a steady state pore structure is formed. [115], [116]

Compared the results of figure 3.8(a) with figure 3.9(c), the Al is etched with same time (60min) but with different phosphoric acid concentration. The pores are much larger of 0.3M phosphoric acid etching than 0.1M one. It also shows from both figures that longer etching time will make the pores larger. The optimum condition of AAO membrane fabrication in our system is etching the aluminum sample in 0.3M phosphoric acid for 40min. In this condition, uniform 50nm pore structure is obtained. (Fig.3.9b)

In figure 3.10, with thin carbon layer as substrate, 500nm thick free- standing AAO membrane is obtained, which may because the carbon is oxidized to CO_2 gas when the aluminum is anodized.

We tried to prepare AAO membrane on polymer because AAO might be a good protective layer in the multilayer structure. We tried both S1813 (fig.3.11(a)) and PMMA (fig.3.11(b)) as the substrate layer, however, it does not show very uniform pore structure. It maybe because the polymer layer is not conductive, which influences the electrical field during AAO formation process.

3.3.2 Copper/photoresist/copper system

Aqueous $FeCl_3$ solution is widely used as an etchant in producing printed circuit of copper. HCl is added to dissolve the CuCl precipitate. The reaction equation is shown as below,[117]

$$FeCl_3(aq) + Cu(s) \rightarrow FeCl_2(aq) + CuCl(s)$$

$$CuCl\,(s) + 3Cl^-(aq) \rightarrow [CuCl_4]^{3-}\,(aq)$$

Since $FeCl_3$/HCl solution only dissolve copper but not PMMA, we can use PMMA as the wet etching mask.

Figure 3.12 shows SEM images of patterns of copper pores that were fabricated by photolithography, followed by etching of samples in the solution of $FeCl_3$ (6×10^{-5}M) and HCl (1×10^{-3}M) mixture. In order to find the optimum etching time, sample is etched from 5sec to 15sec. After 15sec, most Cu materials are completely etched. Only some copper nanoparticles are left at the center of the pore, which can be removed during RIE opening SiO_2 pores.

Then copper nanoparticles are deposited at the edge of etched copper layer to prove the edge conductivity. The Cu electroplating in our system is a process where Cu^{2+} in solution are reduced on to the surface of conductive layer. Different copper electroplating time is used in order to find the best condition. Figure 3.14 shows after 60sec electroplating, there is a uniform ring formed at the edge of copper pore, and 120sec maybe is too long for this deposition.

In order to completely open the pores, Ni layer serves as the etching mask during RIE C_4F_8/O_2 etch. Because there is a thin layer of NiO formed on Ni surface after sputtering, the sample is immersed in HCl solution for 2min to remove the oxide layer. Then the nickel nanopores can be obtained by $FeCl_3$ etching with S1813 as mask. The etching rate of nickel is much slower than copper. It takes about 2min to completely remove nickel with the same concentration of $FeCl_3$ in copper etching. Figure 3.14 shows the RIE etching process of SiO_2. In Figure 3.14(c), SiO_2 pore has been completely opened, and from its cross section, the thickness is only about 1.4 μm.

3.4 Conclusion

In carbon/insulator/carbon system, reproducible and controllable thin-film carbon electrode has been fabricated with sputtering deposition. 200nm vertical multilayer pore structure has been prepared with RIE etching and thin AAO membrane with 50nm pore diameter has been synthesized by one step anodization. However, sputtered carbon layer is not conductive enough. Therefore, copper/insulator/copper system is established to improve the conductivity. 2 μm copper nanopores have been successfully etched by $FeCl_3$/HCl solution. Nanopore pattern on SiO_2 wafer with Ni as protective layer has been opened by RIE method.

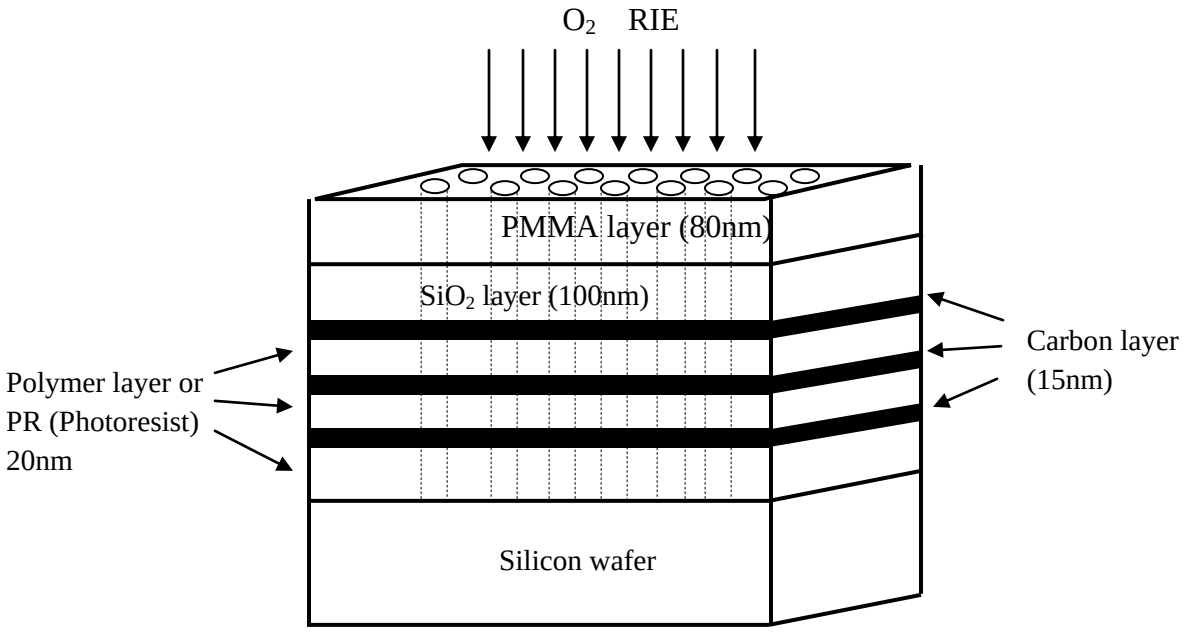

Figure 3.1 Schematic of the SiO_2/carbon/PR multilayer structure.

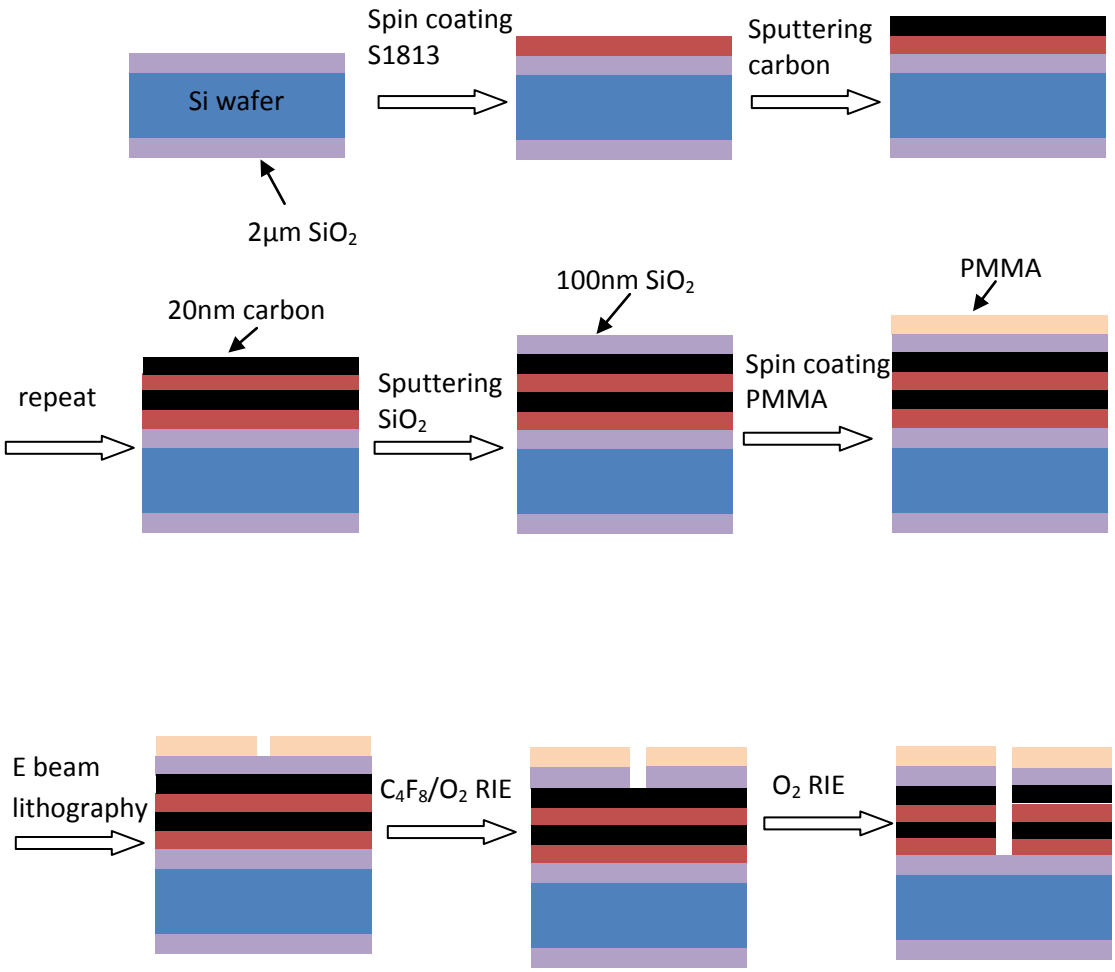

Figure 3.2 Schematic drawing of the fabrication process of the SiO_2/carbon/PR multilayer structure.

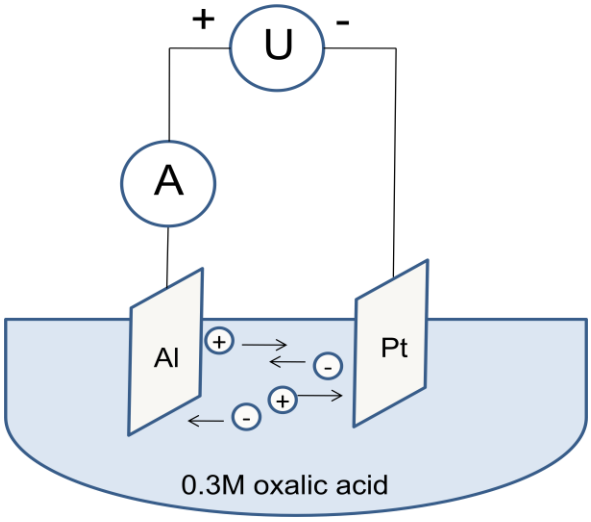

Figure 3.3 Schematic of AAO anodization

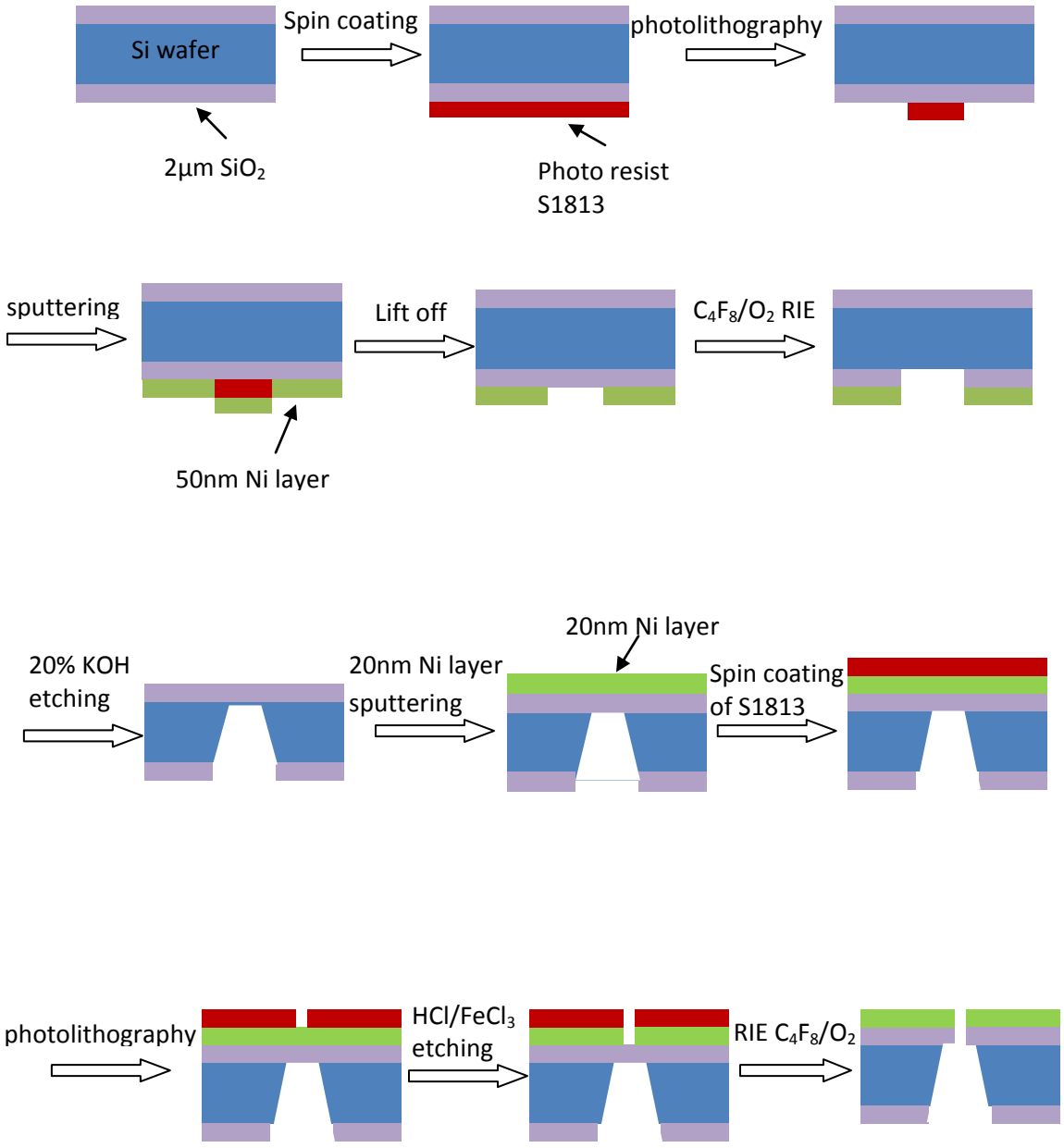

Figure 3.4 A schematic of the fabrication procedure for single layer back etching

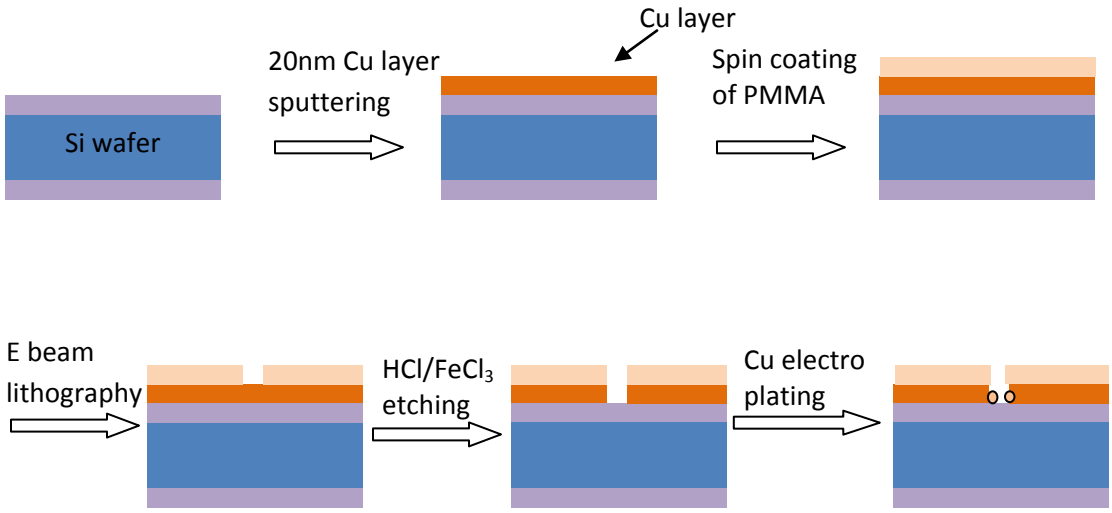

Figure 3.5 A schematic of the fabrication procedure for copper nanopore wet etch and electroplating

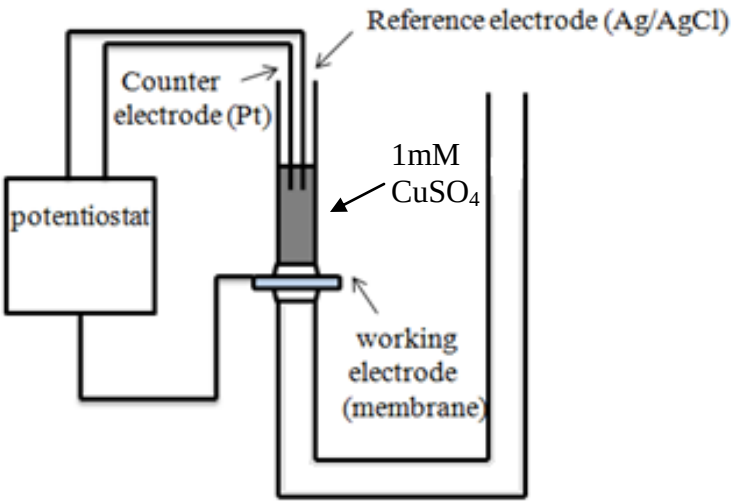

Figure 3.6 Schematic of the Cu electroplating.

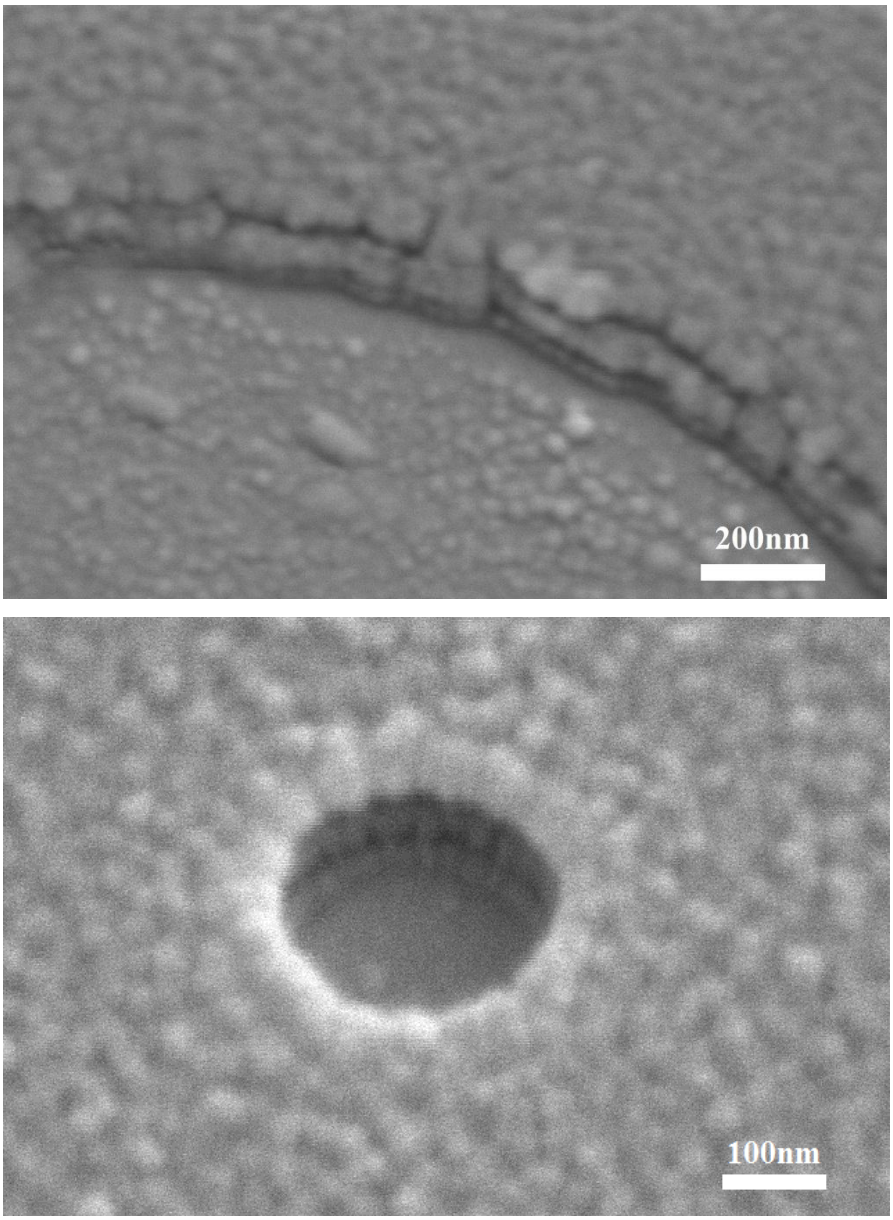

Figure 3.7 SEM image of the multilayer pore. (A) 2μm pore (B) 200nm pore

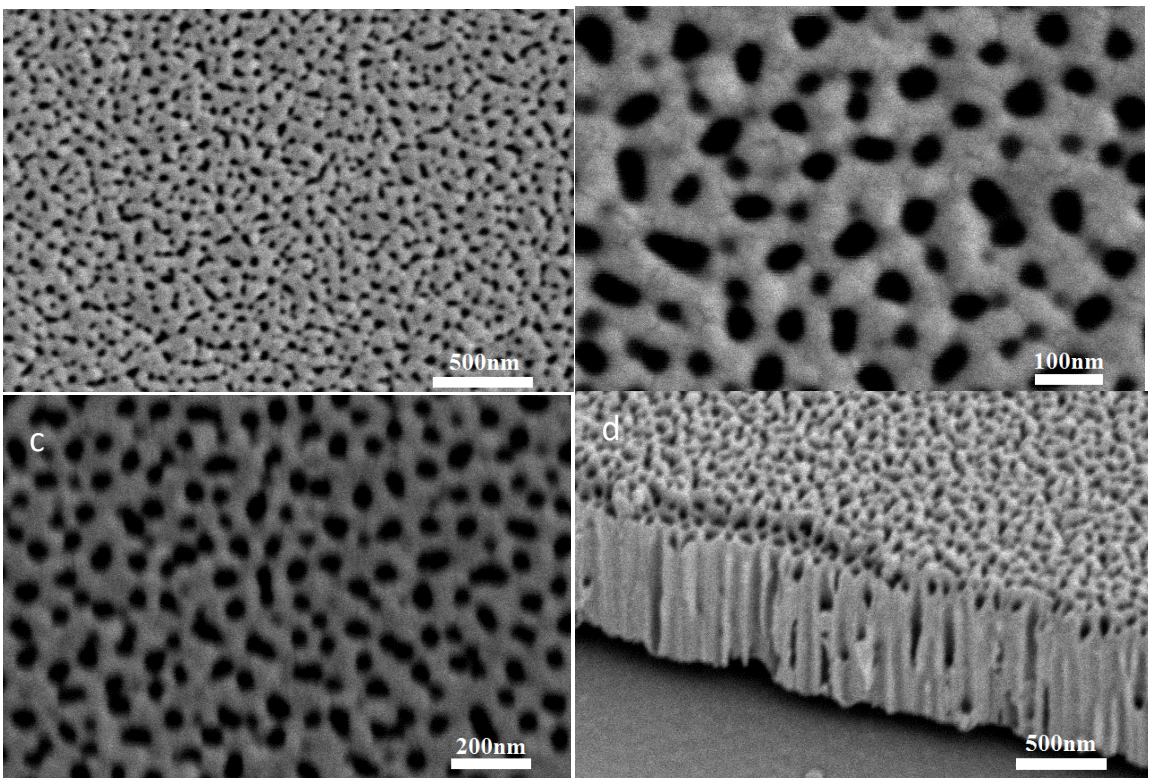

Figure 3.8 SEM image of the AAO membrane with 0.1M H_3PO_4 at different etching time. (A) 60min (B)75min (C)90min (D) cross section of c

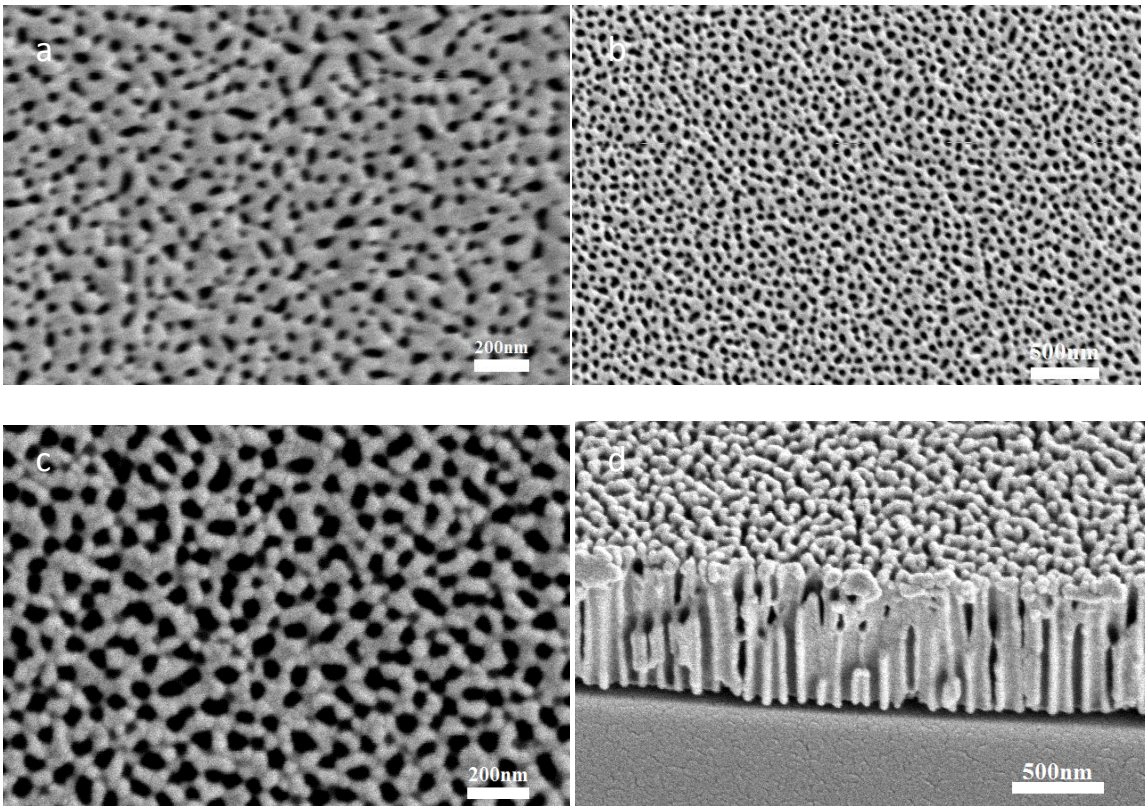

Figure 3.9 SEM image of the AAO membrane with 0.3M H_3PO_4 at different etching time. (A) 30min (B)40min (C)60min (D) cross section of c

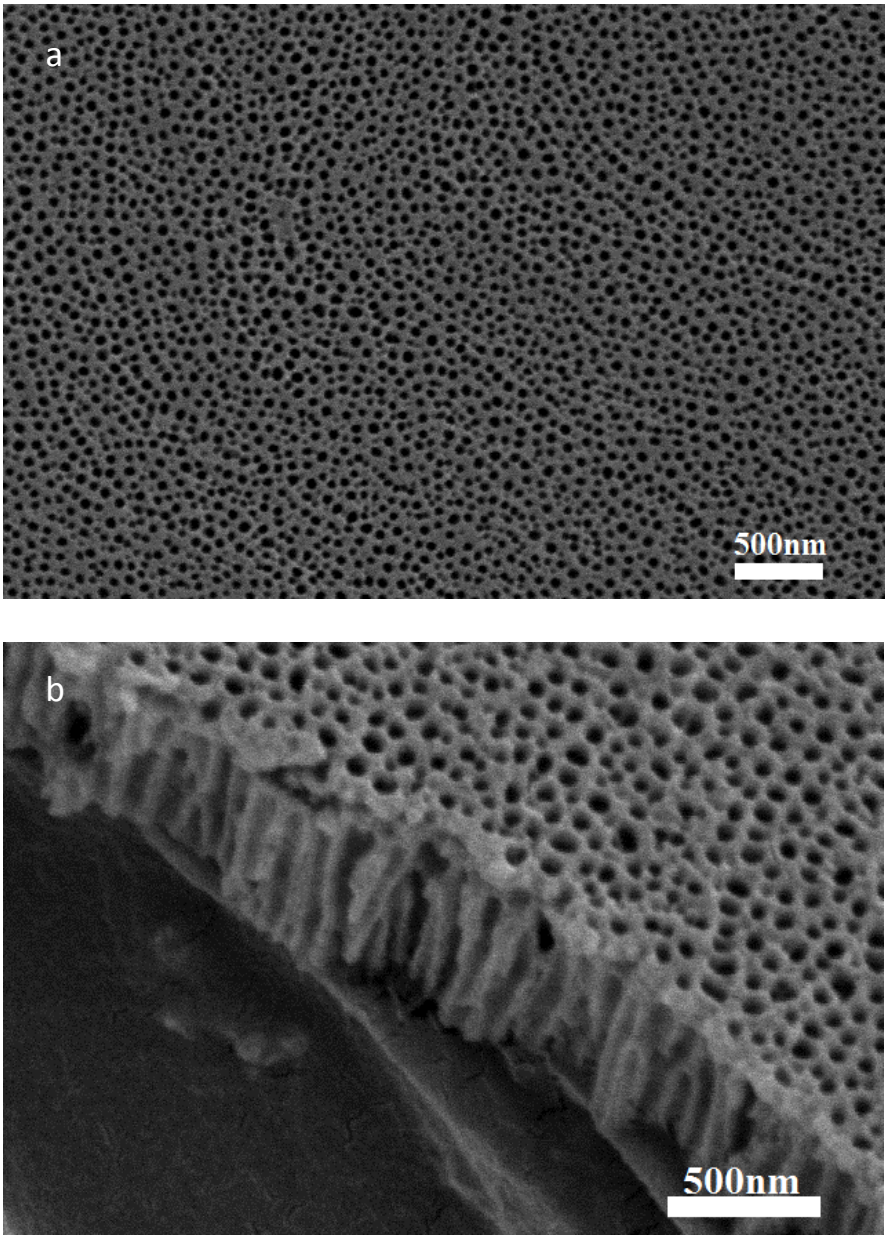

Figure 3.10 SEM image of the freestanding AAO membrane (A) top surface (B) cross section

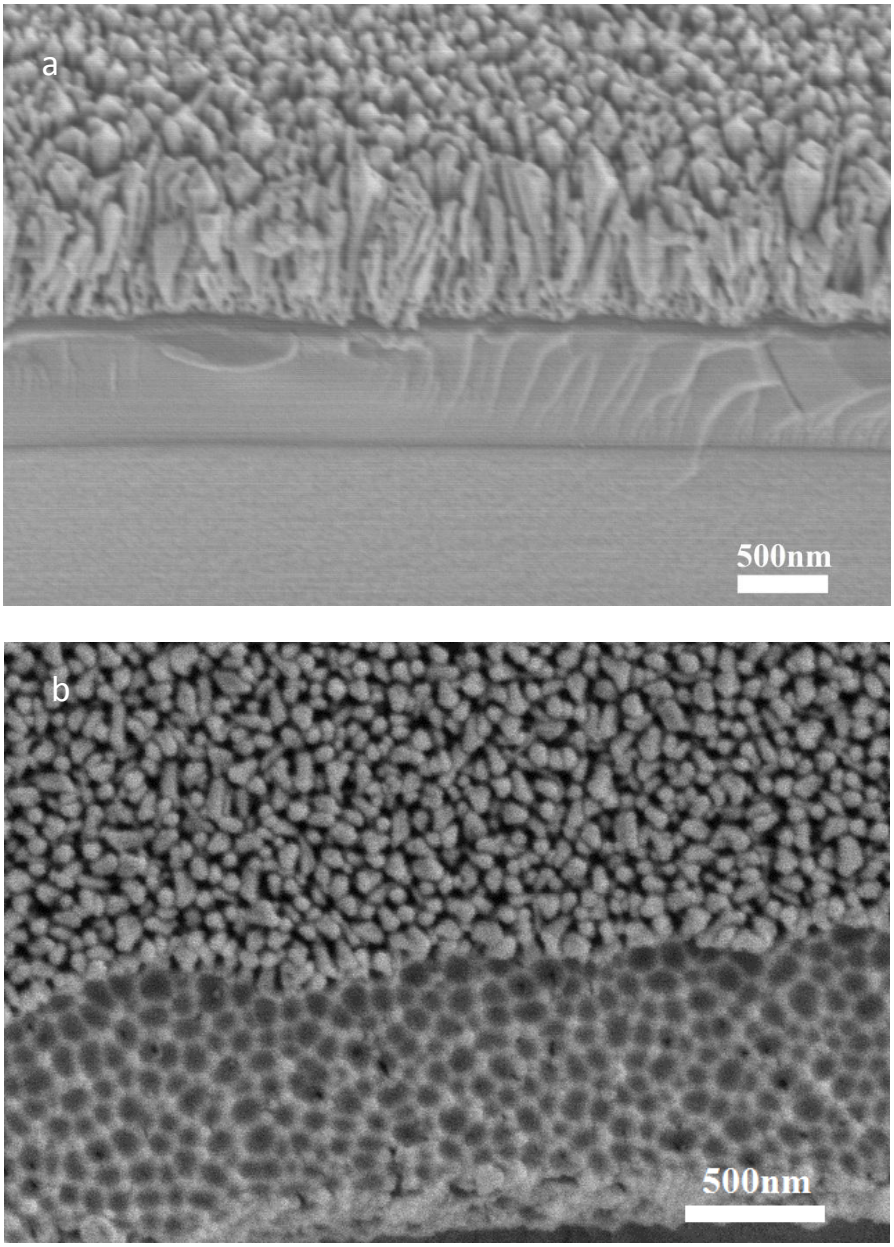

Figure 3.11 SEM image of the freestanding AAO membrane (A) on S1813 layer (B) on PMMA layer

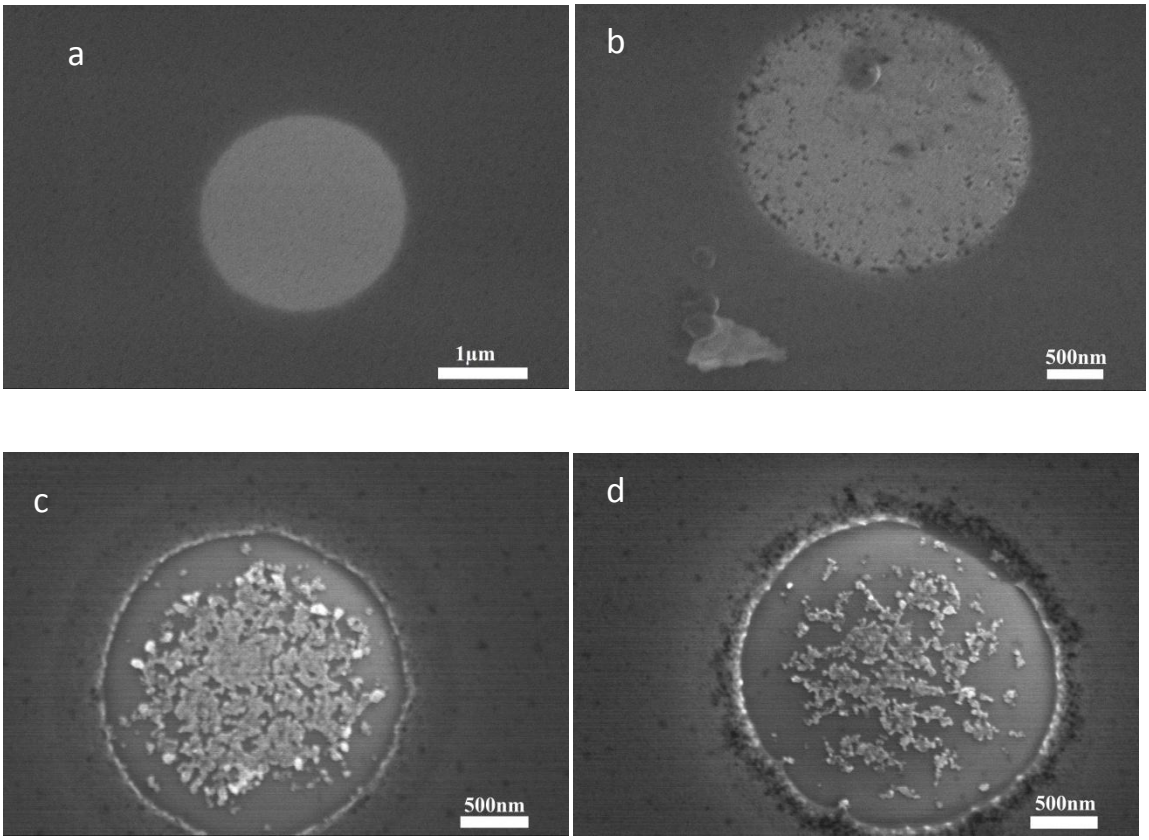

Figure 3.12 SEM images of the PMMA/Cu structure (A) after e beam lithography (B) after $FeCl_3$ etch 5sec (C) after $FeCl_3$ etch 12sec (D) after $FeCl_3$ etch 15sec

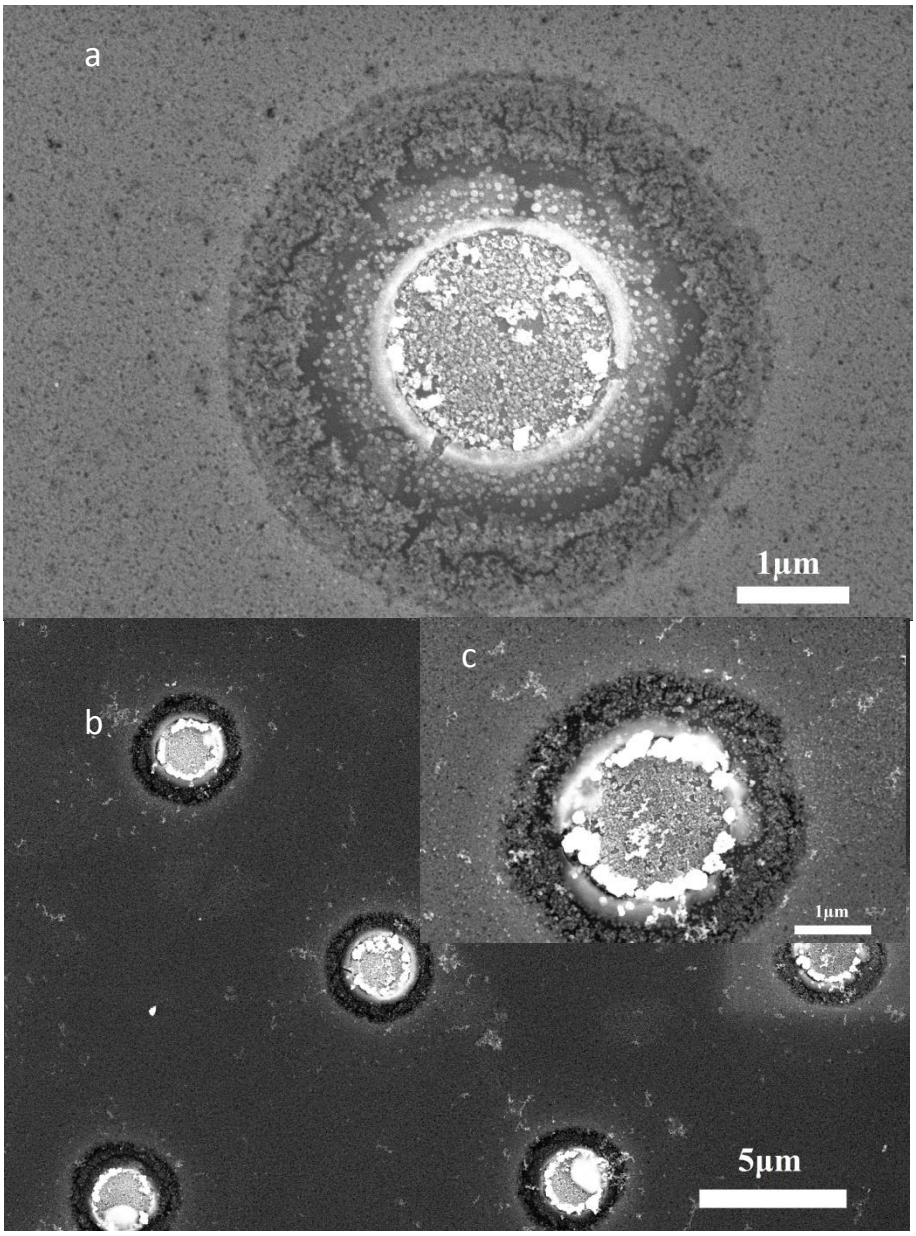

Figure 3.13 SEM image of PMMA/Cu $FeCl_3$ etch 12sec sample after (A) -0.1V 60sec Cu electroplating (B) -0.1V 120sec Cu (higher lower magnification) (C) -0.1V 120sec Cu (lower magnification)

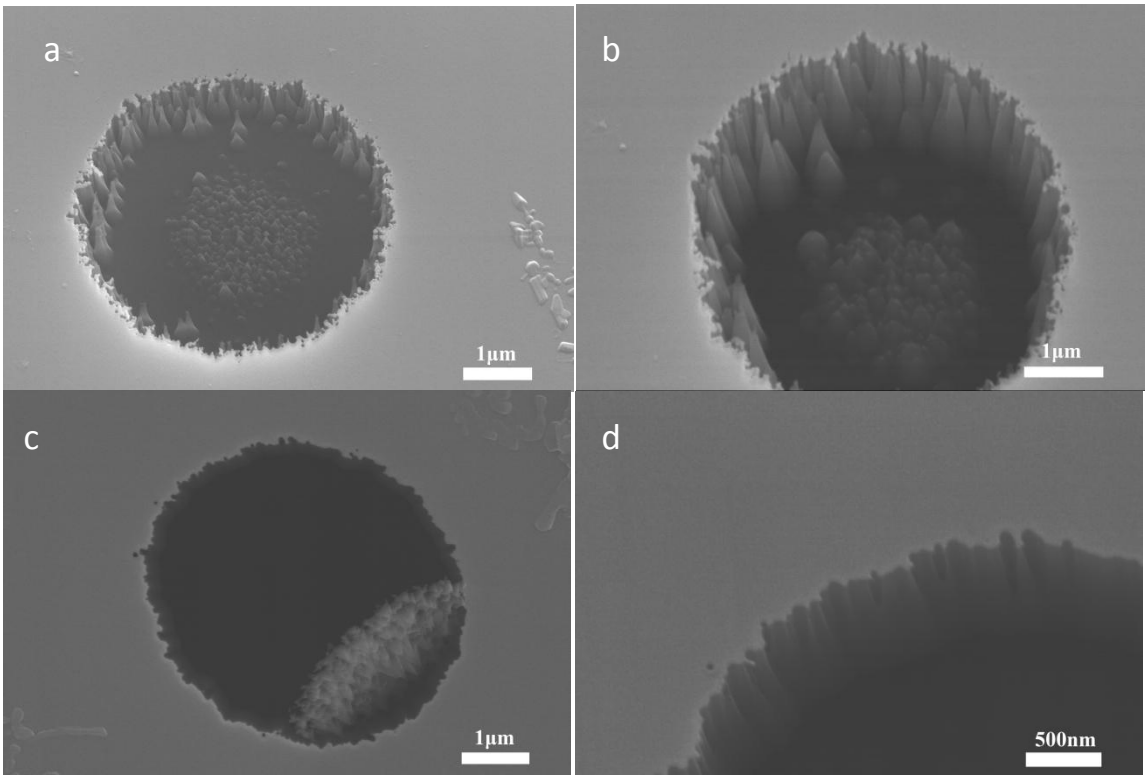

Figure 3.14 SEM images of single layer back etching (a) after 10min RIE etching (b) after RIE 20min (c) top view of the pore (d) cross section of the pore

Chapter 4 Conclusions and future work

4.1 Conclusions

4.1.1 Carbon nanotube membrane for water desalination

High quality $AlPO_4$-5 crystals without F^- had been fabricated in order to produce high quality 0.4nm SWNTs in their channels. Thermogravimetric analysis is used to explore the thermal decomposition of TPA within AFI crystals. It has been found that the carbon yield is about 2% after pyrolysis at 1000◦C. Micro raman data also shows peaks at 510 and 550cm^{-1} in RBMs zone, which are attributed to chiral (4, 2) and zigzag (5, 0) nanotubes, respectively.

Larger single wall carbon nanotubes with 0.7nm in diameter were synthesized from sucrose by a pyrolytic technique using VPI-5 zeolite as template. The diameter of SWNTs is confirmed by a high resolution transmission electron microscopy. In order to study the adsorption effect of VPI-5 crystals and have higher filling density, we have traced various organic precursor decomposition processes during heating by TG. However, the challenge is the poor repeatability of SWNTs synthesis. Although we succeed once to produce CNTs with sucrose as a precursor we haven't been able to repeat the result after 6 tries at the same condition and 10 attempts with variations of precursor and catalyst. The two areas to focus on are the incorporation of metal catalyst that can be reduced to the metalic state within the template and effective incorporation of non volatile organic precursors.

4.1.2 Multilayer project

Nanopore sequencing is an attractive field since it is a possible solution to reduce the price of genome test. Our goal is to fabricate conductor/insulator/conductor multilayer structure for the DNA sequence, because the similar structure as metal-oxide-semiconductor (MOS) capacitor forming in a nanoscale artificial membrane may trap DNA into the pores and reduce the speed of DNA translocating. [45] At the same time, the conductive layer can be independently functionalized in order to control a DNA strand as it travels through the nanopore.

Till now, reproducible and controllable thin-film carbon electrode has been fabricated with sputter deposition. 200nm vertical multilayer pore structure with carbon/S1813/carbon structure has been prepared by RIE etching with SiO_2 as etching mask. Hexagonally well-ordered AAO template with uniform 50nm pores has been fabricated by one step anodization. However, carbon layer is not conductive enough for further copper electroplating. 20nm thick copper electrode has been fabricated with sputter method. 2μm pores have been obtained by using $FeCl_3$ as an etchant and photo resist as protective layer. Copper nanoparticles are deposited at the edge of conductive layer by electroplating method.

4.2 Future work

4.2.1 Water desalination project

In the future, SWCNT made by precise zeolite templates may bring new opportunity for water desalination because of its uniform diameter and atomically smooth inner wall structure. Different organic precursors and pyrolysis conditions will be employed to fabricate uniform 0.7nm SWNTs. The obtained carbon nanotubes can be embedded in epoxy matrix, microtome cut to form 5μm thick carbon nanotube membranes. With these carbon nanotubes, it is possible to separate water molecules and salt ions with associate hydration sphereby size exclusion. The entrance of carbon nanotubes can also be diazonium grafted with charged groups to demonstrate molecular selectivity.

4.2.2 multilayer project

This structure with single nanopore in the lipid bilayer might be a good platform for DNA translocation and biosensing. The edge of the conductive layer can be functionalized with long chain alkane primary amine molecule (i.e. $CH_3(CH_2)_{10}NH_2$) which will demonstrate hydrophobic property. Free standing planar lipid layers can be formed automatically in the pores. Biological protein α-haemolysin can form nanopores that spontaneously insert themselves into the lipid bilayer membrane. The passage of molecule through nanopore can be monitored by ionic current. Different proteins can be incorporated in the lipid layer, and it will show different selectivity.

Reference

1. Branton, D., et al., *The potential and challenges of nanopore sequencing.* Nat Biotech, 2008. **26**(10): p. 1146-1153.
2. Pushkarev, D., N.F. Neff, and S.R. Quake, *Single-molecule sequencing of an individual human genome.* Nat Biotech, 2009. **27**(9): p. 847-850.
3. Greenlee, L.F., et al., *Reverse osmosis desalination: Water sources, technology, and today's challenges.* Water Research, 2009. **43**(9): p. 2317-2348.
4. Bayley, H. and P.S. Cremer, *Stochastic sensors inspired by biology.* Nature, 2001. **413**(6852): p. 226-230.
5. Bayley, H., O. Braha, and L.Q. Gu, *Stochastic Sensing with Protein Pores.* Advanced Materials, 2000. **12**(2): p. 139-142.
6. Li, J., et al., *Ion-beam sculpting at nanometre length scales.* Nature, 2001. **412**(6843): p. 166-169.
7. Stein, D., J. Li, and J.A. Golovchenko, *Ion-Beam Sculpting Time Scales.* Physical Review Letters, 2002. **89**(27): p. 276106.
8. Gershow, M. and J.A. Golovchenko, *Recapturing and trapping single molecules with a solid-state nanopore.* Nat Nano, 2007. **2**(12): p. 775-779.
9. Li, J., et al., *DNA molecules and configurations in a solid-state nanopore microscope.* Nat Mater, 2003. **2**(9): p. 611-615.
10. Chen, P., et al., *Probing Single DNA Molecule Transport Using Fabricated Nanopores.* Nano Letters, 2004. **4**(11): p. 2293-2298.
11. Storm, A.J., et al., *Fabrication of solid-state nanopores with single-nanometre precision.* Nat Mater, 2003. **2**(8): p. 537-540.
12. Storm, A.J., et al., *Translocation of double-strand DNA through a silicon oxide nanopore.* Physical Review E, 2005. **71**(5): p. 051903.
13. Park, S.R., H. Peng, and X.S. Ling, *Fabrication of Nanopores in Silicon Chips Using Feedback Chemical Etching.* Small, 2007. **3**(1): p. 116-119.
14. Siwy, Z., et al., *Preparation of synthetic nanopores with transport properties analogous to biological channels.* Surface Science, 2003. **532–535**(0): p. 1061-1066.
15. Siwy, Z.S. and S. Howorka, *Engineered voltage-responsive nanopores.* Chemical Society Reviews, 2010. **39**(3): p. 1115-1132.
16. Howorka, S. and Z. Siwy, *Nanopore analytics: sensing of single molecules.* Chemical Society Reviews, 2009. **38**(8): p. 2360-2384.
17. Kalman, E.B., I. Vlassiouk, and Z.S. Siwy, *Nanofluidic Bipolar Transistors.* Advanced Materials, 2008. **20**(2): p. 293-297.
18. Vlassiouk, I. and Z.S. Siwy, *Nanofluidic Diode.* Nano Letters, 2007. **7**(3): p. 552-556.
19. Sexton, L.T., L.P. Horne, and C.R. Martin, *Developing synthetic conical nanopores for biosensing applications.* Molecular BioSystems, 2007. **3**(10): p. 667-685.
20. Mukaibo, H., et al., *Controlling the Length of Conical Pores Etched in Ion-Tracked Poly(ethylene terephthalate) Membranes.* Small, 2009. **5**(21): p. 2474-2479.
21. Paolo, S., et al., *Conical nanopore membranes: solvent shaping of nanopores.* Nanotechnology, 2006. **17**(15): p. 3951.
22. Sun, L. and R.M. Crooks, *Single Carbon Nanotube Membranes: A Well-Defined Model for Studying Mass Transport through Nanoporous Materials.* Journal of the American Chemical Society, 2000. **122**(49): p. 12340-12345.
23. Henriquez, R.R., et al., *The resurgence of Coulter counting for analyzing nanoscale objects.* Analyst, 2004. **129**(6): p. 478-482.

24. Haitao Liu, J.H., Jinyao Tang, Hao Liu, Pei Pang, Di Cao, Predrag Krstic, Sony Joseph, Stuart Lindsay, and Colin Nuckolls, *Translocation of Single-Stranded DNA Through Single-Walled Carbon Nanotubes.* Science, 2010. **327**: p. 64.
25. Geim, A.K. and K.S. Novoselov, *The rise of graphene.* Nat Mater, 2007. **6**(3): p. 183-191.
26. Garaj, S., et al., *Graphene as a subnanometre trans-electrode membrane.* Nature, 2010. **467**(7312): p. 190-193.
27. Merchant, C.A., et al., *DNA Translocation through Graphene Nanopores.* Nano Letters, 2010. **10**(8): p. 2915-2921.
28. Postma, H.W.C., *Rapid Sequencing of Individual DNA Molecules in Graphene Nanogaps.* Nano Letters, 2010. **10**(2): p. 420-425.
29. Schneider, G.g.F., et al., *DNA Translocation through Graphene Nanopores.* Nano Letters, 2010. **10**(8): p. 3163-3167.
30. Venkatesan, B.M., et al., *Stacked Graphene-Al2O3 Nanopore Sensors for Sensitive Detection of DNA and DNA–Protein Complexes.* ACS Nano, 2011. **6**(1): p. 441-450.
31. Ivan Vlassiouk, P.Y.A., Sergey N. Dmitriev, Ken Healy, and Zuzanna S. Siwy, *Versatile ultrathin nanoporous silicon nitride membranes.* PNAS, 2009. **106**(50): p. 21039-21044.
32. Menon, V.P. and C.R. Martin, *Fabrication and Evaluation of Nanoelectrode Ensembles.* Analytical Chemistry, 1995. **67**(13): p. 1920-1928.
33. Bahr, J.L., et al., *Functionalization of Carbon Nanotubes by Electrochemical Reduction of Aryl Diazonium Salts: A Bucky Paper Electrode.* Journal of the American Chemical Society, 2001. **123**(27): p. 6536-6542.
34. Delamar, M., et al., *Modification of carbon fiber surfaces by electrochemical reduction of aryl diazonium salts: Application to carbon epoxy composites.* Carbon, 1997. **35**(6): p. 801-807.
35. Majumder, M., et al., *Enhanced electrostatic modulation of ionic diffusion through carbon nanotube membranes by diazonium grafting chemistry.* Journal of Membrane Science, 2008. **316**(1–2): p. 89-96.
36. Majumder, M., N. Chopra, and B.J. Hinds, *Effect of Tip Functionalization on Transport through Vertically Oriented Carbon Nanotube Membranes.* Journal of the American Chemical Society, 2005. **127**(25): p. 9062-9070.
37. Allongue, P., et al., *Covalent Modification of Carbon Surfaces by Aryl Radicals Generated from the Electrochemical Reduction of Diazonium Salts.* Journal of the American Chemical Society, 1997. **119**(1): p. 201-207.
38. Allen J. Bard, L.R.F., *Electrochemical Methods, 1st Edition*1980.
39. Srinivasan, V. and W.I. Higuchi, *A model for iontophoresis incroporating the effect of convective solvent flow.* International Journal of Pharmaceutics, 1990. **60**(2): p. 133-138.
40. Szymański, J.d., et al., *Net Charge and Electrophoretic Mobility of Lysozyme Charge Ladders in Solutions of Nonionic Surfactant.* The Journal of Physical Chemistry B, 2007. **111**(19): p. 5503-5510.
41. Kshama B. Jirage, J.C.H., and Charles R. Martin, *Nanotubule-Based Molecular Filtration Membranes.* Science, 1997. **278**: p. 655-658.
42. Striemer, C.C., et al., *Charge- and size-based separation of macromolecules using ultrathin silicon membranes.* Nature, 2007. **445**(7129): p. 749-753.
43. Tong, H.D., et al., *Silicon Nitride Nanosieve Membrane.* Nano Letters, 2004. **4**(2): p. 283-287.
44. Sang Bok Lee, D.T.M., Lacramioara Trofin, Tarja K. Nevanen, Hans Söderlund, and Charles R. Martin, *Antibody-Based Bio-Nanotube Membranes for Enantiomeric Drug Separations.* Science. **296**: p. 2198-2200.

45. Luan, B., et al., *Base-By-Base Ratcheting of Single Stranded DNA through a Solid-State Nanopore.* Physical Review Letters, 2010. **104**(23): p. 238103.
46. S. Polonsky, S.R., and G. Stolovitzky, *Nanopore in metal-dielectric sandwich for DNA position control.* APPLIED PHYSICS LETTERS, 2007. **91**: p. 153103.
47. Maria, E.G., et al., *Simulation of the electric response of DNA translocation through a semiconductor nanopore–capacitor.* Nanotechnology, 2006. **17**(3): p. 622.
48. Mueller, P., et al., *Reconstitution of Cell Membrane Structure in vitro and its Transformation into an Excitable System.* Nature, 1962. **194**(4832): p. 979-980.
49. Kitta, M., H. Tanaka, and T. Kawai, *Rapid fabrication of Teflon micropores for artificial lipid bilayer formation.* Biosensors and Bioelectronics, 2009. **25**(4): p. 931-934.
50. Im, H., et al., *Membrane protein biosensing with plasmonic nanopore arrays and pore-spanning lipid membranes.* Chemical Science, 2010. **1**(6): p. 688-696.
51. Li, B. and K.K. Sirkar, *Novel Membrane and Device for Direct Contact Membrane Distillation-Based Desalination Process.* Industrial & Engineering Chemistry Research, 2004. **43**(17): p. 5300-5309.
52. Sherwood, T.K., et al., *Salt Concentration at Phase Boundaries in Desalination by Reverse Osmosis.* Industrial & Engineering Chemistry Fundamentals, 1965. **4**(2): p. 113-118.
53. Hassan, A.M., et al., *A new approach to membrane and thermal seawater desalination processes using nanofiltration membranes (Part 1).* Desalination, 1998. **118**(1–3): p. 35-51.
54. Kimura, S. and S. Sourirajan, *Analysis of data in reverse osmosis with porous cellulose acetate membranes used.* AIChE Journal, 1967. **13**(3): p. 497-503.
55. Singh, P.S., et al., *Probing the structural variations of thin film composite RO membranes obtained by coating polyamide over polysulfone membranes of different pore dimensions.* Journal of Membrane Science, 2006. **278**(1–2): p. 19-25.
56. Li, L., et al., *Influence of counter ions on the reverse osmosis through MFI zeolite membranes: implications for produced water desalination.* Desalination, 2008. **228**(1–3): p. 217-225.
57. Li, L., et al., *Desalination by reverse osmosis using MFI zeolite membranes.* Journal of Membrane Science, 2004. **243**(1–2): p. 401-404.
58. Jeong, B.-H., et al., *Interfacial polymerization of thin film nanocomposites: A new concept for reverse osmosis membranes.* Journal of Membrane Science, 2007. **294**(1–2): p. 1-7.
59. Majumder, M., et al., *Nanoscale hydrodynamics: Enhanced flow in carbon nanotubes.* Nature, 2005. **438**(7064): p. 44-44.
60. Hummer, G., J.C. Rasaiah, and J.P. Noworyta, *Water conduction through the hydrophobic channel of a carbon nanotube.* Nature, 2001. **414**(6860): p. 188-190.
61. Fornasiero, F., et al., *Ion exclusion by sub-2-nm carbon nanotube pores.* Proceedings of the National Academy of Sciences, 2008. **105**(45): p. 17250-17255.
62. T.V. Ratto, J.K.H., A.W. Szmodis, , *Membranes with Embedded Nanotubes for Selective Permeability*, 2010.
63. Guo, T., et al., *Catalytic growth of single-walled manotubes by laser vaporization.* Chemical Physics Letters, 1995. **243**(1–2): p. 49-54.
64. Ebbesen, T.W. and P.M. Ajayan, *Large-scale synthesis of carbon nanotubes.* Nature, 1992. **358**(6383): p. 220-222.
65. Li, Y.-L., I.A. Kinloch, and A.H. Windle, *Direct Spinning of Carbon Nanotube Fibers from Chemical Vapor Deposition Synthesis.* Science, 2004. **304**(5668): p. 276-278.

66. Nessim, G.D., et al., *Tuning of Vertically-Aligned Carbon Nanotube Diameter and Areal Density through Catalyst Pre-Treatment.* Nano Letters, 2008. **8**(11): p. 3587-3593.
67. Wang, N., et al., *Materials science: Single-walled 4 A carbon nanotube arrays.* Nature, 2000. **408**(6808): p. 50-51.
68. Tang, Z.K., et al., *Superconductivity in 4 Angstrom Single-Walled Carbon Nanotubes.* Science, 2001. **292**(5526): p. 2462-2465.
69. Lortz, R., et al., *Superconducting characteristics of 4-Å carbon nanotube–zeolite composite.* Proceedings of the National Academy of Sciences, 2009. **106**(18): p. 7299-7303.
70. Zhai, J.P., et al., *Thermal Decomposition of Carbon Precursors in Decorated AFI Zeolite Crystals.* The Journal of Physical Chemistry B, 2006. **110**(39): p. 19285-19290.
71. Zhai, J.P., et al., *Carbonization Mechanism of Tetrapropylammonium-hydroxide in Channels of AlPO4-5 Single Crystals.* Chemistry of Materials, 2006. **18**(6): p. 1505-1511.
72. Zhai, J.P., et al., *Catalytic effect of metal cations on the formation of carbon nanotubes inside the channels of AlPO4-5 crystal.* Carbon, 2006. **44**(7): p. 1151-1157.
73. Zhai, J.P., et al., *Catalyst effect of metal cations on pyrolysis of hydrocarbon molecules and formation of carbon nanotubes in the channels of AlPO4-5 crystals.* Journal of Porous Materials, 2006. **13**(3-4): p. 291-295.
74. Ye, J.T., J.P. Zhai, and Z.K. Tang, *Raman characterization of 0.4 nm single-walled carbon nanotubes formed in the channels of AlPO 4 -5 zeolite single crystals.* Journal of Physics: Condensed Matter, 2007. **19**(44): p. 445003.
75. Zhai, J.P., et al., *Fabrication of smallest single-walled carbon nanotubes in molecular sieves: A comparison between SAPO-11 and AlPO4-11.* Microporous and Mesoporous Materials, 2009. **124**(1–3): p. 15-19.
76. Kazemimoghadam, M. and T. Mohammadi, *Synthesis of MFI zeolite membranes for water desalination.* Desalination, 2007. **206**(1–3): p. 547-553.
77. Davis, M.E., et al., *VPI-5: The first molecular sieve with pores larger than 10 Ångstroms.* Zeolites, 1988. **8**(5): p. 362-366.
78. Davis, M.E., et al., *Physicochemical properties of VPI-5.* Journal of the American Chemical Society, 1989. **111**(11): p. 3919-3924.
79. Li, Z.M., et al., *Polarized Absorption Spectra of Single-Walled 4 Å Carbon Nanotubes Aligned in Channels of an AlPO4-5 Single Crystal.* Physical Review Letters, 2001. **87**(12): p. 127401.
80. Qiu, S., et al., *Synthesis and structure of the [AlPO4]12 Pr4NF molecular sieve with AFI structure.* Zeolites, 1989. **9**(5): p. 440-444.
81. Iijima, S., *Helical microtubules of graphitic carbon.* Nature, 1991. **354**: p. 56-58.
82. Dalton, A.B., et al., *Super-tough carbon-nanotube fibres.* Nature, 2003. **423**(6941): p. 703-703.
83. Kyotani, T., L.-f. Tsai, and A. Tomita, *Preparation of Ultrafine Carbon Tubes in Nanochannels of an Anodic Aluminum Oxide Film.* Chemistry of Materials, 1996. **8**(8): p. 2109-2113.
84. Ryoo, R., S.H. Joo, and S. Jun, *Synthesis of Highly Ordered Carbon Molecular Sieves via Template-Mediated Structural Transformation.* The Journal of Physical Chemistry B, 1999. **103**(37): p. 7743-7746.
85. Meng, Y., et al., *A Family of Highly Ordered Mesoporous Polymer Resin and Carbon Structures from Organic−Organic Self-Assembly.* Chemistry of Materials, 2006. **18**(18): p. 4447-4464.

86. Kim, T.-W., I.-S. Park, and R. Ryoo, *A Synthetic Route to Ordered Mesoporous Carbon Materials with Graphitic Pore Walls.* Angewandte Chemie, 2003. **115**(36): p. 4511-4515.
87. Tarek Abdel-Fattah, E.J.S., Roy E. Crooks, *Pyrolytic Synthesis of Carbon Nanotubes from Sucrose on a Mesoporous Silicate.* Fullerenes, Nanotubes, and carbon nanostructures, 2006. **14**: p. 585-594.
88. Balogh, Z., et al., *CVD-synthesis of multiwall carbon nanotubes over potassium-doped supported catalysts.* Applied Catalysis A: General, 2008. **344**(1–2): p. 191-197.
89. Kumar, M. and Y. Ando, *Controlling the diameter distribution of carbon nanotubes grown from camphor on a zeolite support.* Carbon, 2005. **43**(3): p. 533-540.
90. Li, G.D., et al., *Structural study of the 0.4-nm single-walled carbon nanotubes aligned in channels of AlPO4-5 crystal.* Carbon, 2002. **40**(6): p. 917-921.
91. Tang, Z.K., et al., *Resonant Raman Scattering of the Smallest Single-Walled Carbon Nanotubes.* Physical Review Letters, 2008. **101**(4): p. 047402.
92. Sun, H.D., et al., *Synthesis and Raman characterization of mono-sized single-wall carbon nanotubes in one-dimensional channels of AlPO4-5 crystals.* Applied Physics A: Materials Science & Processing, 1999. **69**(4): p. 381-384.
93. Zhai, J.P., et al., *Catalytic growth of 0.4 nm single-walled carbon nanotubes aligned inside porous zeolite crystals.* physica status solidi (b), 2006. **243**(13): p. 3082-3086.
94. Parton, R.F., et al., *Stacked phthalocyanines in VPI-5 pores as evidenced by CPDOR 1H 瑿 27Al NMR.* Journal of Molecular Catalysis A: Chemical, 1995. **97**(3): p. 183-186.
95. Jacobs, P., et al., *Synthesis of zeolite crystals and formation of carbon nanostructures in patterned structures*, 2009.
96. García Carmona, J., R. Rodriguez Clemente, and J. Gómez Morales, *Comparative preparation of microporous VPI-5 using conventional and microwave heating techniques.* Zeolites, 1997. **18**(5–6): p. 340-346.
97. Finger, G., et al., *On synthesis conditions for tailoring AlPO4-5 crystal dimensions.* Zeolites, 1991. **11**(5): p. 443-448.
98. Jiang, F.Y., et al., *Synthesis of AlPO4-5 crystals using TBAOH as template.* Microporous and Mesoporous Materials, 2006. **92**(1–3): p. 129-133.
99. Jiang, F.Y., et al., *Synthesis of large optically clear AlPO4-5 single crystals.* Journal of Crystal Growth, 2005. **283**(1–2): p. 108-114.
100. Wöhrle, D., et al., *Nanoporous Networks of Si-, Al-, P-Oxygen Tetrahedra with Encapsulated Dyes as New Composite Materials.* Macromolecular Symposia, 2008. **270**(1): p. 123-134.
101. King, L.J., *Aligned Nanorods of AlPO4-5 Within the Pores of Anodic Alumina*, in *Master of Science*2010, Victoria University ofWellington.
102. Wu, J., et al., *Electrophoretically induced aqueous flow through single-walled carbon nanotube membranes.* Nat Nano, 2012. **7**(2): p. 133-139.
103. Schmidt, W., et al., *VPI-5 and related aluminophosphates: Preparation and thermal stability.* Zeolites, 1992. **12**(1): p. 2-8.
104. de Oñate Martinez, J., et al., *Synthesis of large single crystals of the large-pore aluminophosphate molecular sieve VPI-5.* Microporous and Mesoporous Materials, 1999. **28**(2): p. 261-269.
105. Davis, M.E., *Ordered porous materials for emerging applications.* Nature, 2002. **417**(6891): p. 813-821.
106. Li, H.-X. and M.E. Davis, *Chapter 4 Phosphate-based molecular sieves with pores comprised of greater than 12-rings.* Catalysis Today, 1994. **19**(1): p. 61-106.

107. Prasad, S. and R. Vetrivel, *Interaction of Water Molecules with the VPI-5 Lattice.* The Journal of Physical Chemistry, 1994. **98**(6): p. 1579-1583.
108. Vogt, E.T.C. and J.W. Richardson Jr, *The reversible transition of the molecular sieve VPI-5 into ALPO−84 and the structure of ALPO−84.* Journal of Solid State Chemistry, 1990. **87**(2): p. 469-471.
109. Martens, J.A., et al., *Structure and effective pore size of the dehydrated forms of the molecular sieve VPI-5.* The Journal of Physical Chemistry, 1991. **95**(24): p. 10025-10031.
110. Masami Kakuchi, M.H., and Toshiaki Tamamura, *Amorphous carbon films as resist masks with high reactive ion etching resistance for nanometer lithography.* Applied Physics Letters, 1986. **48**(13): p. 835.
111. Popova, K., *Reactive ion etching of ion-plated carbon films.* Vacuum, 1997. **48**(7–9): p. 681-684.
112. G. Wang, W.C., K. Chang, *A two-step etching method to fabricate nanopores in silicon.* Microsystem Technologies 2008. **14**(7): p. 925-929.
113. Osmanbeyoglu, H.U., T.B. Hur, and H.K. Kim, *Thin alumina nanoporous membranes for similar size biomolecule separation.* Journal of Membrane Science, 2009. **343**(1–2): p. 1-6.
114. Masuda, H. and K. Fukuda, *Ordered Metal Nanohole Arrays Made by a Two-Step Replication of Honeycomb Structures of Anodic Alumina.* Science, 1995. **268**(5216): p. 1466-1468.
115. Taşaltın, N., et al., *Simple fabrication of hexagonally well-ordered AAO template on silicon substrate in two dimensions.* Applied Physics A: Materials Science & Processing, 2009. **95**(3): p. 781-787.
116. V. Parkhutik, V.S., *Theoretical modelling of porous oxide growth on aluminium.* J. Phys. D: Appl. Phys. , 1992. **25**: p. 1258.
117. Xia, Y., et al., *Microcontact Printing of Alkanethiols on Copper and Its Application in Microfabrication.* Chemistry of Materials, 1996. **8**(3): p. 601-603.

Vita

Jingyuan Yao obtained a bachelor degree of engineering from Beijing University of Chemical Technology in year 2005 and a master degree of science in Beijing University of Chemical Technology in 2008.

Selected Publications

1. Bing Hu, **Jingyuan Yao**, Bruce J. Hinds, "Nano-gap electrodes formed at the exposed edge of Au/SAM/Al_2O_3/Au tunnel structures grown by atomic layer deposition, " *Applied Physics Letters*, 2010, 97, 203111.
2. Bing Hu, Xin Zhan, **Jingyuan Yao**, Bruce J. Hinds, "Molecular transport at the exposed edge of Au/SAM/Al_2O_3/Au tunnel junctions, " *Jounal of Applied Physics*, ready for submission.
3. Jonathan M. Wagner, Ji Wu, **Jingyuan Yao**, David W. Rodgers, Bruce. J. Hinds, "Nano test tubes for therapeutic enzyme immobilization," in preparation.
4. **Jingyuan Yao**, Lixia Li, Huaihe Song, Changyi Liu, Xiaohong Chen, "In situ synthesis of magnetically separable ordered mesoporous carbons from F127/$[Ni(H_2O)_6](NO_3)_2$/resorcinol-formaldehyde composites, " *Carbon*, 2009, 47, 436.
5. Lixia Li, Huaihe Song, Qincang Zhang, **Jingyuan Yao**, Xiaohong Chen, "Effect of compounding process on the structure and electrochemical property of ordered mesoporous carbon/polyaniline composites as electrodes for supercapacitors, " *J. Power Sources*, 2009, 187, 268.